

UNCLASSIFIED

AD NUMBER

AD267502

LIMITATION CHANGES

TO:

Approved for public release; distribution is unlimited.

FROM:

Distribution authorized to U.S. Gov't. agencies and their contractors; Specific Authority; JUL 1961. Other requests shall be referred to Aeronautical Systems Division, Wright-Patterson AFB, OH 45433.

AUTHORITY

ASD ltr, 6 Aug 1974

THIS PAGE IS UNCLASSIFIED

UNCLASSIFIED

AD 267 502

*Reproduced
by the*

ARMED SERVICES TECHNICAL INFORMATION AGENCY
ARLINGTON HALL STATION
ARLINGTON 12, VIRGINIA



UNCLASSIFIED

NOTICE: When government or other drawings, specifications or other data are used for any purpose other than in connection with a definitely related government procurement operation, the U. S. Government thereby incurs no responsibility, nor any obligation whatsoever; and the fact that the Government may have formulated, furnished, or in any way supplied the said drawings, specifications, or other data is not to be regarded by implication or otherwise as in any manner licensing the holder or any other person or corporation, or conveying any rights or permission to manufacture, use or sell any patented invention that may in any way be related thereto.

ASD TECHNICAL REPORT 61-186

267 502

**STUDY OF PARACHUTE PERFORMANCE
AT LOW SUPERSONIC DEPLOYMENT SPEEDS;
EFFECTS OF CHANGING SCALE AND CLUSTERING**

PAUL E. PEDERSEN

COOK RESEARCH LABORATORIES
A DIVISION OF COOK ELECTRIC COMPANY
CHICAGO, ILLINOIS

JULY 1961

This report is not to be announced
or distributed automatically
to foreign governments
(AFR 205-43A, paragraph 6d).

NOX

AERONAUTICAL SYSTEMS DIVISION

NO OTS

267 502

CATALOGED BY ASTIA
AS AD NO.

**STUDY OF PARACHUTE PERFORMANCE
AT LOW SUPERSONIC DEPLOYMENT SPEEDS;
EFFECTS OF CHANGING SCALE AND CLUSTERING**

PAUL E. PEDERSEN

*COOK RESEARCH LABORATORIES
A DIVISION OF COOK ELECTRIC COMPANY
CHICAGO, ILLINOIS*

JULY 1961

AERODYNAMICS DECELERATOR BRANCH
FLIGHT ACCESSORIES LABORATORY
CONTRACT No. AF 33(616)-5991
PROJECT No. 5775
TASK No. 57993

AERONAUTICAL SYSTEMS DIVISION
AIR FORCE SYSTEMS COMMAND
UNITED STATES AIR FORCE
WRIGHT-PATTERSON AIR FORCE BASE, OHIO

FOREWORD

This report was prepared by the Cook Research Laboratories, a division of Cook Electric Company, Chicago, Illinois, in compliance with USAF Contract No. AF 33(616)-5991. The contract was initiated under USAF Project No. 5775, Task No. 57993 by the Parachute Branch, Aeronautical Accessories Laboratory, Wright Air Development Center with Mr. Alfons Hegele as Project Officer. The Project Officer in the later phases of the program was Capt. L. H. Latham.

The work at the Cook Research Laboratories on Project P-1513 was conducted under the supervision of Dr. J. R. Downing, Director; and Paul E. Pedersen, Project Engineer.

Work on the program was initiated on 1 July 1958 and was completed on 31 August 1959.

Staff members who contributed to the project included Dr. H. V. Hawkins, Assistant Director and Technical Head, Aerodynamics Section; R. O. Fredette, Assistant Director of Research; L. J. Lorenz, Administrative Head, Aerodynamics Section; F. A. Ruprecht, Supervisor, Parachute Section; G. B. Neill, Engineer-in-charge, Field Test Section; and N. T. Guttenberger, Data-Analysis Engineer, Aerodynamics Section.

ABSTRACT

Parachute design and operational data were collected on a series of rocket powered sled tests conducted on the Air Force Flight Test Center Track at Edwards Air Force Base, California. Parachute deployment velocities ranged between Mach 0.76 and 1.57. Parachute types that were investigated included Guide Surface Ribless, FIST Ribbon, Conical Ribbon, Equiflo and Hemisflo designs. The majority of the test parachutes were designed to have a drag area of approximately 15 square feet. Limited testing was accomplished with some configurations of reduced drag area to investigate effects of changing scale. Results of this were not conclusive. Clustering of parachutes was also investigated with triple clusters of FIST Ribbon parachutes.

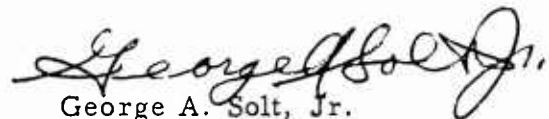
The data obtained during the program included inflation characteristics, opening shock factors, drag forces, inflated area relationships, and stability of the parachutes through the velocity ranges investigated.

Associated systems, such as the deployment and release system, test vehicles and instrumentation system are also discussed.

PUBLICATION REVIEW

This report has been reviewed and is approved.

FOR THE COMMANDER:



George A. Solt, Jr.

Chief, Aerodynamic Decelerator Branch
Flight Accessories Laboratory

TABLE OF CONTENTS

	<u>Page</u>
I INTRODUCTION	1
II TEST CONDITIONS.	2
A. Test Facility.	2
B. Test Program	2
C. Parachutes	4
D. Instrumentation	5
III CONCLUSIONS AND RECOMMENDATIONS	6
IV PARACHUTE PERFORMANCE CHARACTERISTICS	8
A. General.	8
B. Guide Surface Ribless Parachute	8
C. FIST Ribbon Parachutes	11
D. Conical Ribbon Parachutes	16
E. Equiflo Parachute	20
F. Hemisflo Parachute	21
V TEST RESULTS	22
A. Guide Surface Ribless Parachute	22
1. General	22
2. Test Program	22
3. Parachute Performance.	24
a. Guide Surface Ribless, Type GS-201 (4 foot diameter, 12 gore)	24
b. Guide Surface Ribless, Type GS-202 (2 foot diameter, 6 gore).	30

TABLE OF CONTENTS (cont'd)

	<u>Page</u>
B. FIST Ribbon Parachute	31
1. General	31
2. Test Program	32
3. Parachute Performance	33
a. FIST Ribbon Type FR-127	33
b. FIST Ribbon Type FR-130	38
c. FIST Ribbon Type FR-130 Triple Cluster.	43
C. Conical Ribbon Parachute	48
1. General	51
2. Test Program	51
3. Parachute Performance	52
a. 15 Degree Conical Ribbon Type 15CR134	52
b. 20 Degree Conical Ribbon Type 20CR128	59
c. 30 Degree Conical Ribbon Type 30CR129	63
d. 45 Degree Conical Ribbon Type 45CR131	68
D. Equiflo Parachute	71
1. General	71
2. Test Program	72
3. Parachute Performance	72
a. Equiflo Type ESR-132, ESR-133	75
E. Hemisflo Parachute	80
1. General	80
2. Test Program	80
3. Parachute Performance	83

LIST OF APPENDICES

	<u>Page</u>
I PARACHUTE DEPLOYMENT AND RELEASE SYSTEMS	86
A. Deployment System	86
B. Release System	90
C. Deployment and Release System Circuitry	91
II TEST VEHICLES	94
III INSTRUMENTATION	100
A. Recording System	100
B. Playback System	104
C. Sled Borne Camera Calibration	104

LIST OF ILLUSTRATIONS

<u>Figure No.</u>	<u>Title</u>	<u>Page</u>
1	Typical Dynamic Characteristics, Guide Surface Ribless Type GS-201 Parachute.	11
2	Typical Dynamic Characteristics, Triple Cluster FIST Ribbon Type FR-130 Parachute.	13
3	Variation of Drag Coefficient with Mach Number, Triple Cluster FIST Ribbon Type FR-130 Parachutes . . .	14
4	Variation of Angular Displacement with Mach Number, Triple Cluster FIST Ribbon Type FR-130 Parachutes . . .	14
5	Variation of Area Ratio as a Function of Mach Number, Triple Cluster FIST Ribbon Type FR-130 Parachutes . . .	15
6	Variation of Drag Coefficient as a Function of Area Ratio, Triple Cluster FIST Ribbon Type FR-130 Parachutes.	16
7	Drag Coefficient as a Function of Cone Angle	18
8	Area Ratio as a Function of Cone Angle	18
9	Average Angular Displacement as a Function of Cone Angle.	19
10	Typical Panel Shape Layout and Basic Dimensions for the 6 and 12 Gore Modified Guide Surface Ribless Parachute	22
11	Sequence of Guide Surface Ribless Parachute in Operation	23
12	Abnormal Inflation Characteristics, Guide Surface Ribless Parachute - Test No. 2.	28
13	Performance Curves, Guide Surface Ribless Parachute - Test No. 3	29

LIST OF ILLUSTRATIONS (cont'd)

<u>Figure No.</u>	<u>Title</u>	<u>Page</u>
14	Performance Curves, Guide Surface Ribless Parachute - Test No. 9	30
15	Performance Curves - Guide Surface Ribless Parachute	31
16	Typical FIST Ribbon Parachute Gore Assembly	32
17	FIST Ribbon Parachute in Operation	32
18	Deployment and Inflation Sequence, FIST Ribbon Type FR-127 Parachute - Test No. 1.	37
19	Performance Curves - FIST Ribbon Type FR-127 Parachute	39
20	Deployment and Inflation Sequence, FIST Ribbon Type FR-130 Parachute - Test No. 24	41
21	Performance Curves - FIST Ribbon Type FR-130 Parachute	42
22	Performance Curves (Expanded) - FIST Ribbon Type FR-130 Parachutes	43
23	Geometry of Triple Cluster Configuration	44
24	Performance Curves - Triple Cluster, FIST Ribbon Type FR-130 Parachutes	45
25	Shock Waves on Clustered Parachutes - Test No. 15	47
26	Collapsed Parachute Cluster on Test No. 15	48
27	Subsonic Deployment and Inflation Sequence on Cluster Test No. 7.	49
28	Supersonic Deployment and Inflation Sequence on Cluster Test No. 11.	50

LIST OF ILLUSTRATIONS (cont'd)

<u>Figure No.</u>	<u>Title</u>	<u>Page</u>
29	Typical Geometry and Gore Layout - Conical Ribbon Parachute	51
30	15 Degree Conical Ribbon Type 15CR128 Parachute in Operation	52
31	Deployment and Inflation Sequence, 15 Degree Conical Ribbon Type 15CR134 Parachute - Test No. 25	56
32	Deployment and Inflation Sequence, 15 Degree Conical Ribbon Type 15CR134 Parachute - Test No. 26	57
33	Performance Curves - 15 Degree Conical Ribbon Type 15CR134 Parachutes.	58
34	20 Degree Conical Ribbon Type 20CR128 Parachute in Operation	59
35	Deployment and Inflation Sequence, 20 Degree Conical Ribbon Type 20CR128 Parachute - Test No. 21	60
36	Performance Curves - 20 Degree Conical Ribbon Type 20CR128 Parachutes.	62
37	30 Degree Conical Ribbon Type 30CR128 Parachute in Operation	63
38	Deployment and Inflation Sequence, 30 Degree Conical Ribbon Type 30CR129 Parachute - Test No. 5	64
39	Deployment and Inflation Sequence, 30 Degree Conical Ribbon Type 30CR129 Parachute - Test No. 8	65
40	Deployment and Inflation Sequence, 30 Degree Conical Ribbon Type 30CR129 Parachute - Test No. 22	66
41	Performance Curves - 30 Degree Conical Ribbon Type 30CR129 Parachutes.	67

LIST OF ILLUSTRATIONS (cont'd)

<u>Figure No.</u>	<u>Title</u>	<u>Page</u>
42	45 Degree Conical Ribbon Type 45CR131 Parachute in Operation	68
43	Deployment and Inflation Sequence, 45 Degree Conical Ribbon Type 45CR131 Parachute in Operation	69
44	Performance Curves - 45 Degree Conical Ribbon Type 45CR131 Parachutes.	70
45	Typical Gore Assembly, Equiflo Parachute	72
46	Performance Curves - Equiflo Type ESR-132, 133 Parachutes.	77
47	Equiflo Type ESR-132 Parachute in Operation - Test No. 17	78
48	Deployment and Inflation Sequence, Equiflo Type ESR-133 Parachute - Test No. 20	79
49	Typical Gore Assembly - Hemisflo Parachute	80
50	Performance Curves - Hemisflo Type EHR-135 Parachute	84
51	Hemisflo Type EHR-135 Parachute in Operation - Test No. 27	85
52	Pictorial Diagram of Deployment System.	87
53	Components of Deployment System on Table Prior to Packing	88
54	Parachute Compartment - Tomahawk Sled	88
55	Parachute Compartment - LOX-I Sled	88
56	Deployment Gun Details	89

LIST OF ILLUSTRATIONS (cont'd)

<u>Figure No.</u>	<u>Title</u>	<u>Page</u>
57	Acceleration Lock and Stowage Strap Arrangement	90
58	Parachute Attachment and Release Device	90
59	Schematic Diagram - Deployment and Release System	92
60	Pictorial Sketch of Knife Electrodes and Screen Box Arrangements.	92
61	Knife Electrodes Mounted on Tomahawk Sled.	92
62	Screen Boxes Attached to Track	92
63	Tomahawk Parachute Test Vehicle with X-15 Pusher Sled	94
64	Basic Dimensions (3 view) of Tomahawk Parachute Test Vehicle.	96
65	Damage to Tomahawk Sled - Test No. 17.	98
66	LOX-I Parachute Test Vehicle	98
67	Basic Dimensions (3 view) of LOX-I Parachute Test Vehicle.	99
68	Block Diagram of Instrumentation System	101
69	Sled Mounted Space-Time Magnet.	102
70	Sled Mounted Space-Time Inductance Coil	103
71	Block Diagram of Playback System.	105

LIST OF TABLES

<u>Table No.</u>	<u>Title</u>	<u>Page</u>
I	Schedule of Tests Conducted on Program.	3
II	General Parachute Characteristics	9
III	Average Performance Characteristics - Guide Surface Ribless Type GS-201 Parachute	10
IV	Average Performance Characteristics - Triple Cluster-FIST Ribbon Type FR-130 Parachutes.	12
V	Average Performance Characteristics - Conical Ribbon Parachutes.	17
VI	Average Performance Characteristics - Equiflo Type ESR-132, 133 Parachute.	20
VII	Performance Characteristics - Hemisflo Type EHR-135 Parachute	21
VIII	Physical Details and Dimensions of Guide Surface Ribless Parachutes	25
IX	Materials Used in Guide Surface Ribless Parachutes. . .	26
X	Performance Summary Data - Guide Surface Ribless Parachutes	27
XI	Physical Details and Dimensions of FIST Ribbon Parachutes.	34
XII	Materials Used in FIST Ribbon Parachutes.	35
XIII	Performance Summary Data - FIST Ribbon Parachutes.	36
XIV	Average Performance Characteristics - Triple Cluster-FIST Ribbon Type FR-130 Parachutes.	46
XV	Physical Details and Dimensions of Conical Ribbon Parachutes.	53

LIST OF TABLES (cont'd)

<u>Table No.</u>	<u>Title</u>	<u>Page</u>
XVI	Materials Used in Conical Ribbon Parachutes	54
XVII	Performance Summary Data - Conical Ribbon Parachutes	55
XVIII	Average Performance Characteristics - 15 Degree Conical Ribbon Type 15CR134 Parachutes	56
XIX	Average Performance Characteristics - 20 Degree Conical Ribbon Type 20CR128 Parachutes	61
XX	Average Performance Characteristics - 30 Degree Conical Ribbon Type 30CR129 Parachutes	65
XXI	Average Performance Characteristics - 45 Degree Conical Ribbon Type 45CR131 Parachutes	69
XXII	Physical Details and Dimensions of Equiflo Parachutes	73
XXIII	Materials Used in Equiflo Parachutes.	74
XXIV	Performance Summary Data - Equiflo Parachutes	76
XXV	Average Performance Characteristics - Equiflo Type ESR-132, 133 Parachutes	78
XXVI	Physical Details and Dimensions of Hemisflo Parachutes	81
XXVII	Materials Used in Hemisflo Parachutes.	82
XXVIII	Performance Summary Data - Hemisflo Parachutes . . .	83
XXIX	Test Vehicles, Propulsion and Performance	95

LIST OF SYMBOLS

A_R^*	Area Ratio - Ratio of instantaneous projected area of inflated canopy (S_{p1}) to nominal design surface area (S_o) or theoretical projected area (S_p), whichever is applicable - %
A_{VR}	Vertical ribbon width - in.
a	Speed of sound in air - ft/sec
B_{HR}	Horizontal ribbon width - in.
b_{HR}	Distance between horizontal ribbons - in.
C	Radial ribbon width - in.
C_{D_o}	Drag coefficient of parachute canopy based on total cloth area, S_o - dimensionless
C_{D_p}	Drag coefficient of parachute canopy based on inflated (projected) canopy area - dimensionless
D_b	Diameter, base (conical parachutes)
D_c	Diameter, constructed - ft
D_o	Diameter, nominal: equal to $\sqrt{\frac{4S_o}{\pi}}$ - ft
D_p	Projected or inflated canopy diameter - ft
e_g	Base width of gore - in.
e_{gv}	Gore width at vent - in.
e_{gm}^*	Maximum gore width - in.
F	Drag force of parachute as transmitted to sled - lbs
F_c	Constant force on fully inflated canopy - lbs
F_o	Peak opening shock force - lbs
F_s	Peak snatch force - lbs

LIST OF SYMBOLS (cont'd)

f	Cyclic frequency - cycles/sec
h_g	Height of gore - in.
l_s	Length of suspension lines from canopy skirt to confluence point - ft
M	Mach number = V/a
n_g	Number of gores
q	Dynamic pressure = $\frac{\rho}{2} V^2$ - lbs/ft ²
q_c	Impact pressure, compressible
q_s	Dynamic pressure corresponding to the velocity at peak snatch force - lbs/ft ²
q_o	Dynamic pressure corresponding to the velocity at peak opening shock force - lbs/ft ²
S_o	Total cloth area of canopy, or design surface area including slots and vent - ft ²
S_p	Theoretical projected area of inflated canopy - ft ²
S_{p1}^*	Instantaneous (measured) projected area of inflated canopy - ft ²
X	Opening shock factor - dimensionless, denotes the relationship between peak opening shock force, F_o , and constant force, F_c , at equivalent velocity
α^*	Conical angle (conical parachutes) = $\cos^{-1} \frac{D_b}{D_c}$
λ_g	Geometric canopy porosity - %, considered equal to total porosity, (λ_t), for parachutes of heavy construction
\emptyset	Angular displacement (stability) of parachute or parachute system from reference axis

* Denotes that the definition is not included in the Parachute Handbook (Reference 1) or that the definition in the Handbook had been modified.

SECTION I

INTRODUCTION

The use of rocket powered track borne parachute test vehicles for the detailed study of parachute behavior and operational characteristics has been well established as a means of obtaining structural data and performance information not otherwise available.

To further the knowledge obtained on previous test programs of a similar nature (Reference 2), a comprehensive research program was initiated. This program, the subject of this report, concerned the study and evaluation of the operational and aerodynamic characteristics of fabric parachutes when operated at transonic and low supersonic velocities in a high dynamic pressure environment.

A total number of 27 tests were conducted with parachutes of the Guide Surface Ribless, FIST Ribbon, Conical Ribbon, Equiflo, and Hemisflo type. Most of these tests were made with single test parachutes with drag areas of approximately 15 square feet. Some variation of this parameter was introduced in a limited number of tests. Clustered configurations were also investigated with one parachute design.

Manuscript released by the author May 1961 for publication as an ASD Technical Report.

SECTION II

TEST CONDITIONS

A. Test Facility

All of the tests that were made on this program were conducted on the 20,000 foot Experimental Track Facility at the Air Force Flight Test Center, Edwards Air Force Base, California. The parachutes were tested by deploying them from rocket powered test vehicles at preselected velocities and locations along the track. Complete descriptions of the test vehicle systems which were utilized in the conduct of these tests are given in Appendix II.

B. Test Program

A total of 27 tests were conducted with 11 configurations of five basic parachute types. Deployment velocities ranged from Mach 0.76 to Mach 1.57. A tabulation of the individual tests giving test number, test date, parachute type, and deployment Mach number is presented in Table I.

Parameters such as deployment velocity, structural details and parachute geometric properties were varied in the program to determine effects on operational characteristics and limits of the parachutes.

The program was limited by certain factors which are more or less inherent to this type of testing. These are not necessarily detrimental but should be considered when reference is made to the data. The major limitations are listed below:

- (1) Parachute size - Individual parachutes were limited to a drag area of approximately 15 square feet maximum.
- (2) Deployment velocity was limited to a range from the low transonic to the low supersonic.
- (3) Altitude was limited to ground elevation at the test facility (approximately 2,300 feet mean sea level).
- (4) Parachute stability was measured with respect to a fixed (one degree of freedom) attachment point on the test vehicle.
- (5) Infinite mass - The mass of the test vehicle was so great in comparison to the parachutes being tested that little velocity change occurred during the deployment and inflation process.

TABLE I
SCHEDULE OF TESTS CONDUCTED ON PROGRAM

Test No.	Test Date	Test Parachute			Deployment Mach No.
		Dia. (ft)	Type	Type No.	
1	12/9/58	6.17	FIST Ribbon	FR-127	1.368
2	1/7/59	4.0	Guide Surface Ribless	GS-201	0.959
3	1/29/59	4.0	Guide Surface Ribless	GS-201	0.911
4	2/5/59	6.24	20 Degree Conical Ribbon	20CR128	1.045
5	2/17/59	6.07	30 Degree Conical Ribbon	30CR129	1.044
6	3/6/59	6.24	20 Degree Conical Ribbon	20CR128	1.300
7	3/10/59	4.78	Triple Cluster-FIST Ribbon	FR-130	0.812
8	3/12/59	6.07	30 Degree Conical Ribbon	30CR129	1.480
9	3/17/59	4.0	Guide Surface Ribless	GS-201	1.410
10	3/25/59	4.78	Triple Cluster-FIST Ribbon	FR-130	1.042
11	4/1/59	4.78	Triple Cluster-FIST Ribbon	FR-130	1.528
12	4/9/59	6.18	45 Degree Conical Ribbon	45CR131	1.026
13	4/17/59	6.18	45 Degree Conical Ribbon	45CR131	1.081
14	4/27/59	2.0	Guide Surface Ribless	GS-202	1.393
15	5/4/59	4.78	Triple Cluster-FIST Ribbon	FR-130	1.503
16	5/6/59	6.20	Equiflo	ESR-132	1.052
17	5/12/59	6.20	Equiflo	ESR-132	1.567
18	6/18/59	6.18	45 Degree Conical Ribbon	45CR131	0.979
19	6/25/59	4.78	Triple Cluster-FIST Ribbon	FR-130	0.873
20	6/30/59	6.20	Equiflo	ESR-133	1.071
21	7/2/59	6.24	20 Degree Conical Ribbon	20CR128	1.081
22	7/9/59	6.07	30 Degree Conical Ribbon	30CR129	1.043
23	7/14/59	4.78	FIST Ribbon	FR-130	1.054
24	7/22/59	4.78	FIST Ribbon	FR-130	1.012
25	7/28/59	6.24	15 Degree Conical Ribbon	15CR134	1.087
26	7/30/59	6.24	15 Degree Conical Ribbon	15CR134	0.765
27	8/5/59	6.24	Hemisflo	EHR-135	0.765

Detailed results of each test operation were included in the Cook Research Laboratories' progress reports (Reference 3) and in data reports submitted to the contracting agency. A summary of the characteristics and performance of the parachute types tested are presented in Section IV of this report. Detailed test results are included by parachute type and configuration in Section V.

C. Parachutes

The majority of the parachutes investigated in the program were designed to have a drag area of approximately 15 square feet with ultimate structural quality able to withstand deployment and operation at low supersonic velocities. Limited configurations were designed with lower drag areas. The general types and configuration variations which were investigated are listed below:

- (1) Modified Guide Surface Ribless
 - (a) 4 foot diameter, 12 gore, $C_{DA} = 10$
 - (b) 2 foot diameter, 6 gore, $C_{DA} = 2.5$
- (2) FIST Ribbon
 - (a) 6.17 foot diameter, 16 gore, $C_{DA} = 15$
 - (b) 4.78 foot diameter, 16 gore, $C_{DA} = 9$
- (3) Conical Ribbon
 - (a) 15 degree, 6.24 foot diameter, 16 gore, $C_{DA} = 15$
 - (b) 20 degree, 6.24 foot diameter, 16 gore, $C_{DA} = 15$
 - (c) 30 degree, 6.07 foot diameter, 16 gore, $C_{DA} = 15$
 - (d) 45 degree, 6.18 foot diameter, 16 gore, $C_{DA} = 15$
- (4) Equiflo (extended skirt FIST Ribbon)
 - (a) 6.20 foot diameter, 16 gore, $C_{DA} = 15$
- (5) Hemisflo (extended skirt hemispherical)
 - (a) 6.24 foot diameter, 16 gore, $C_{DA} = 15$

In addition to these single parachute configurations, the 4.78 foot diameter FIST Ribbon parachute was also tested in a triple cluster configuration on a single suspension system.

Complete descriptions of the parachute configurations are presented in Section V together with test data obtained for these particular types.

D. Instrumentation

Complete instrumentation was carried on the test vehicle during each test operation.

A magnetic tape recording system provided records of the following parameters:

- (1) Drag force
- (2) Impact pressure
- (3) Acceleration
- (4) Time
- (5) Position.

From these parameters other pertinent information, such as opening shock force, inflation time and velocity, was determined.

Measurements of parachute area and stability were obtained from sled borne high speed motion picture camera film. These were synchronized to tape recorded information by common time and position impulses.

Additional operational information was obtained with stationary high speed motion picture, sequence and still photography.

A detailed description of the instrumentation and playback equipment employed on the tests appears in Appendix III.

SECTION III

CONCLUSIONS AND RECOMMENDATIONS

After examination and analysis of the data collected on this series of tests, the following conclusions and recommendations were reached:

- (1) Current configurations of Guide Surface Ribless parachutes appear to have reached their maximum operational capability in the Mach 1.0 to 1.5 region. This limitation is, within the current state of the art, structural. There was, however, no evidence of deteriorating performance characteristics at the maximum velocities at which this parachute type was successfully operated.
- (2) With the exception of severe undamped buffeting, the FIST Ribbon parachutes in single configuration exhibited normal subsonic performance characteristics. Because such buffeting is known to significantly affect the structural integrity of a parachute and appears to be related to parachute suspension system combinations, further investigation should be undertaken to determine limiting canopy-suspension system design parameters.
- (3) On the basis of equivalent drag area, no apparent advantage was obtained by clustering parachutes. Much longer filling times were required by the clustered arrangement than would be required by a single parachute of equivalent drag area. More volume was required to contain these parachutes and deployment and inflation characteristics were unpredictable.
- (4) Conical Ribbon parachute configurations showed a slight decrease in drag coefficient with increasing conical angle. Stability characteristics, although not so conclusive, showed some tendency to diverge as the cone angles increased. The most marked variations were evident in the relationship of steady state area ratios to cone angle. This illustrated that significant reductions in normal area ratios occurred between the 30 and 45 degree configurations. Since this is basically a geometric property, the effect on aerodynamic characteristics is not evident.
- (5) Because of the limited data obtained with Equiflo and Hemisflo parachutes, no conclusions in regard to these designs can be reached.
- (6) In the tests where low supersonic data were obtained, the information was, as a rule, found to be within the ranges of generally accepted theory. Mach number effects on the behavior of parachutes were

noticed. A relationship between steady state area ratio and drag coefficient was also demonstrated.

(7) Data points for filling time vs velocity did not follow any pattern suggested or supported by either theoretical or empirical data.

(8) Because of the limited variation of parachute sizes during the program, no significant information was obtained on the effects of changing scale.

SECTION IV

PARACHUTE PERFORMANCE CHARACTERISTICS

A. General

This section of the report presents a summary and analysis of the major aerodynamic performance characteristics of the parachute types which were investigated during the program. Detailed summaries of test results of the individual tests are presented, according to parachute type, in Section V of the report.

The parachute test program provided general design information and parachute performance characteristics in the velocity ranges in which each configuration was investigated and established preliminary designs for the parachutes which were deployed and operated successfully in the transonic and low supersonic speed ranges. Performance characteristics which were obtained included drag coefficients, opening shock factors, inflation behavior, area ratios and stability. Values of these parameters for each parachute configuration which yielded sufficient characteristic information are presented in Table II.

Typical performance curves for each type of parachute tested have been included in the summary paragraphs that follow. Such curves have been derived from the average results of those tests of particular parachute types which exhibited conclusive operational characteristics. Corresponding tabular data is also presented to show basic geometric properties as well as pertinent performance parameters.

Where possible, curves and data have been included to show the effects and relationships of geometric and aerodynamic characteristics on the performance of the parachute configurations or systems as they were investigated on this program.

B. Guide Surface Ribless Parachute

Of the four tests conducted with guide surface ribless parachutes, three were with a four foot diameter, 12 gore design and one test was with a two foot diameter, six gore version. Satisfactory performance was obtained on only two of the tests, both of those being with the four foot diameter parachute. In the other two tests the parachutes suffered severe structural damage during inflation resulting in complete collapse of the canopies.

TABLE II
GENERAL PARACHUTE CHARACTERISTICS

Guide Surface Type	No. of Gores	Projected Diameter D_p (ft)	Projected Area S_p (ft ²)	Drag Coefficient C_D	Opening Shock Factor X	Area Ratio AR (%)	Stability Angular Displacement θ (deg.)	Deployment Mach No. Range
Ribless - GS-201	12	4.0	12.57	0.80	1.58	84	2.0 \pm 2.0	0.91 - 1.41
Ribbon Type	Geometric Porosity λ_g (%)	Nominal Diameter D_o (ft)	Nominal Area S_o (ft ²)	Drag Coefficient C_{D_o}	Opening Shock Factor X	Area Ratio AR (%)	Stability Angular Displacement θ (deg.)	Deployment Mach No. Range
FIST Ribbon FR-127	26.2	6.17	29.90	0.47 0.30*	---- 1.31*	36.9.	3.0 \pm 1.0	1.37
FIST Ribbon FR-130	19.3	4.78	17.95	0.52	1.00	42.6	2.0 \pm 1.0	1.01 - 1.05
FIST Ribbon-Cluster FR-130	19.3	4.78(3)	53.85	0.52 0.28*	---- 0.78*	43.5 28.0*	2.0 \pm 1.0 7.0 \pm 3.5*	0.81 - 1.53
15° Conical Ribbon 15CR134	25.2	6.24	30.58	0.52	0.94	46.0	3.5 \pm 1.0	0.76 - 1.09
20° Conical Ribbon 20CR128	25.8	6.24	30.58	0.51	0.97	45.4	2.3 \pm 1.3	1.04 - 1.30
30° Conical Ribbon 30CR129	25.7	6.07	28.94	0.48	1.09	44.8	2.8 \pm 2.5	1.04 - 1.48
45° Conical Ribbon 45CR131	25.6	6.18	30.00	0.47	0.98	38.8	4.0 \pm 2.0	0.98 - 1.08
Equiflo ESR 132, 133	25.8	6.20	30.19	0.50	1.00	45.50	1.5 \pm 1.2	1.05 - 1.57
Hemisflo EHR-135	25.4	6.24	30.60	0.51	1.23	37.5	3.0 \pm 2.0	0.765

*Supersonic

Because complete performance information was obtained on only one of the tests, and partial information on the other test, the average performance characteristics, shown in Table III, and the typical dynamic characteristics, shown in Figure 1, are based to a large extent on information from only the one successful test.

TABLE III
AVERAGE PERFORMANCE CHARACTERISTICS -
GUIDE SURFACE RIBLESS TYPE GS-201 PARACHUTE

Projected Diameter, D_p (ft)	4.0
Projected Area, S_p (ft ²)	12.57
Weight (lbs)	14.40
Bulk (ft ³)	0.72
Drag Coefficient, C_D	0.80
Opening Shock Factor (X)	1.58
Area Ratio, A_R (%)	84
Stability, ϕ (deg.)	2.0 \pm 2.0

Since it is not apparent in the average performance characteristics, it should be noted that some abnormalities were present in the operation of the parachutes in the otherwise successful tests. In both cases initial inflation of the parachutes was poor. Several adjacent gores in the parachutes were not inflated to the normal gore widths and the guide surface portions of some gores were concave rather than convex.

Usable data indicated a drag coefficient of 0.80 for the guide surface ribless parachute. Based on this drag coefficient, the average opening shock factor was 1.58. This, however, was the average of a high (1.82) and a low (1.34) value determined from the two tests from which this information could be obtained.

In spite of the inflation deformities noted above, parachute stability was good. Mean displacement averaged two degrees with oscillatory variations of plus or minus two degrees.

No performance data were obtained from the test with the two foot

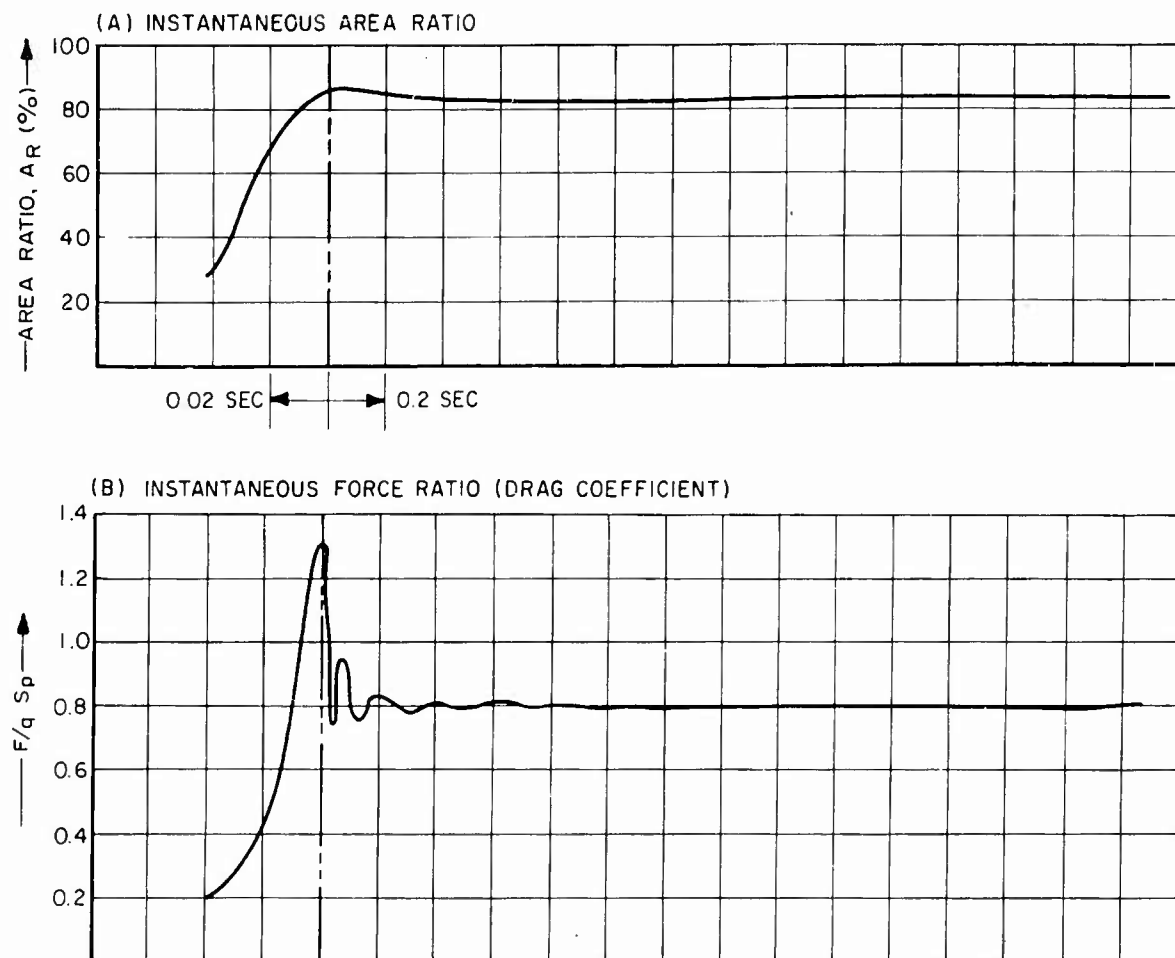


Figure 1. Typical Dynamic Characteristics, Guide Surface Ribless Type GS-201 Parachute

diameter guide surface ribless parachute. This parachute failed structurally and collapsed immediately after inflation.

A presentation of the results of the individual tests conducted with guide surface ribless parachutes appears in Section V-A-3 of this report.

C. FIST Ribbon Parachutes

Two types of FIST Ribbon parachutes were tested in the program. One test was made with the Type FR-127 - a 6.17 foot diameter, 16 gore design - at a deployment velocity of Mach 1.37. Significant amounts of minor damage resulted from the test, consequently further testing of this particular parachute design was not attempted. General details and test results are given in Section V-B-3a of this report.

Seven tests were conducted with a 4.78 foot diameter, 16 gore Type FR-130 parachute design. Five of these tests were with cluster configurations of three parachutes. The remaining two tests were made with single parachutes to provide correlation data to determine differences in characteristics between single and clustered parachute operation.

Unusual behavior, in the manner of high amplitude force oscillations, occurred in both of the single parachute tests. These fluctuations were not prevalent in the tests of the same parachutes in clustered configuration. It is probable that the differences in the aerodynamic and physical properties of the parachute and suspension systems allowed the single parachute configurations to attain natural system frequencies by interaction in the force and inflation modes. Although this is prevalent to some extent in all tests where generally elastic suspension systems are used, such fluctuations are usually damped rapidly to a steady state operational condition.

Test results of the two tests conducted with the single Type FR-130 parachutes are presented in Section V-B-3b of this report.

The FIST Ribbon parachutes which provided the most complete performance information in this program were the cluster configurations consisting of three Type FR-130 parachutes on one suspension system. Two of the five tests with these parachutes were tested at supersonic deployment conditions. Average performance characteristics for the triple cluster configuration are presented in Table IV. Typical dynamic characteristics based on average results of the five tests are presented graphically in Figure 2.

TABLE IV

AVERAGE PERFORMANCE CHARACTERISTICS -
TRIPLE CLUSTER-FIST RIBBON TYPE FR-130 PARACHUTES

Nominal Diameter, D_0 (ft)	Each	4.78	
Nominal Area, S_0 (ft ²)	Each	17.95	
Weight (lbs)		29.0	
Bulk (lbs)		1.45	
Geometric Porosity, λ_g (%)		19.3	
Drag Coefficient, C_{D_0}		0.52	0.28
Opening Shock Factor, X		0.93	0.78
Area Ratio, A_R (%)		43.5	28.0
Stability, ϕ (deg.)		2.0 \pm 1.0 Subsonic	7.0 \pm 3.5 Supersonic

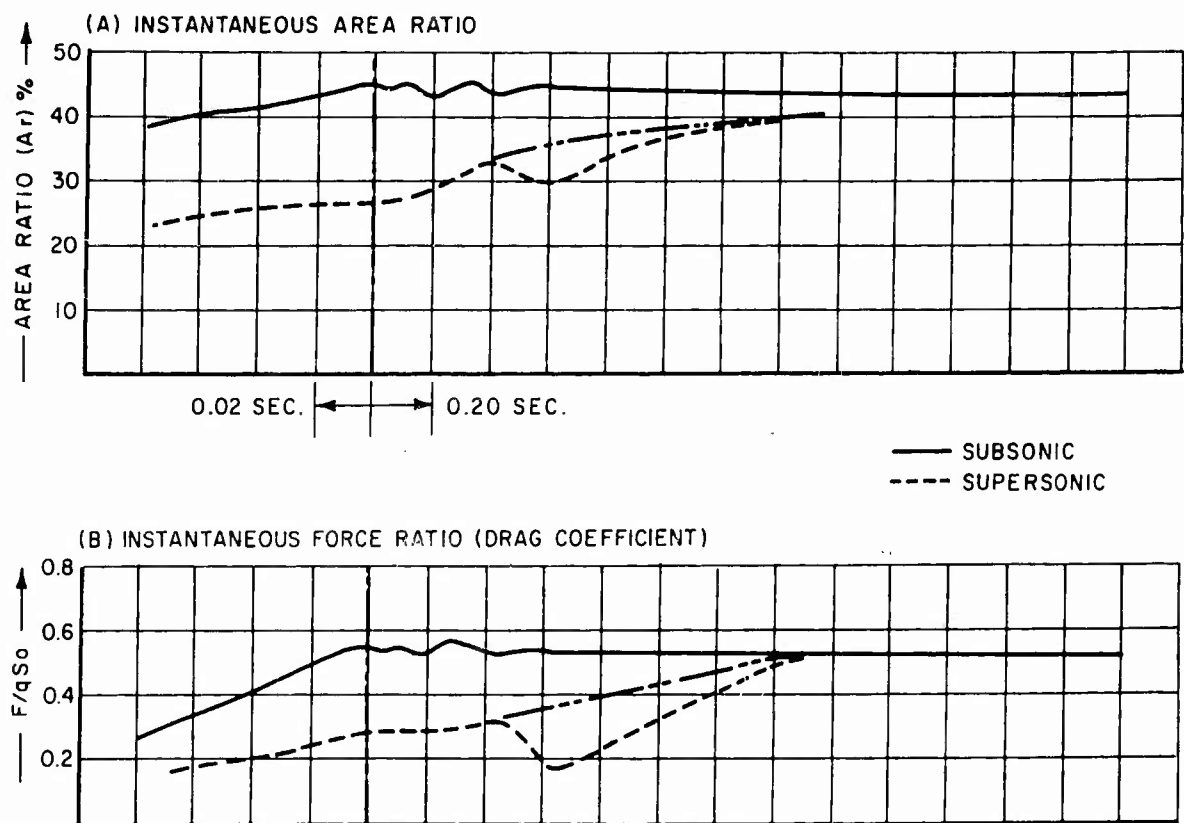


Figure 2. Typical Dynamic Characteristics, Triple Cluster FIST Ribbon Type FR-130 Parachute

A similarity of inflation characteristics was particularly noticeable in the subsonic tests. Inflation times were very long, ranging between 0.165 and 0.195 seconds. Even longer inflation times were evident in the supersonic tests, but these could not be firmly established because of the transitional conditions under which the data were taken. Area ratio relationship was also changing too rapidly during the inflation process to determine an optimum figure for this parameter.

A marked variation in drag coefficient from supersonic to subsonic operation was noted in the cluster tests. Figure 3 shows this variation as averaged from the two tests in which supersonic deployments were obtained. It should be noted that in both of these tests, one or more of the parachutes in the cluster partially collapsed during the transition from supersonic to subsonic operation. This is evident in the dip in the curve in Figure 3 between Mach numbers 1.15 and 0.9. Photographic data show that it was always the lowest parachutes in the clusters that deflated. The significance of this is not completely substantiated but it was noted in the sequence photographs that in the velocity region where this occurred there was what appeared to be a

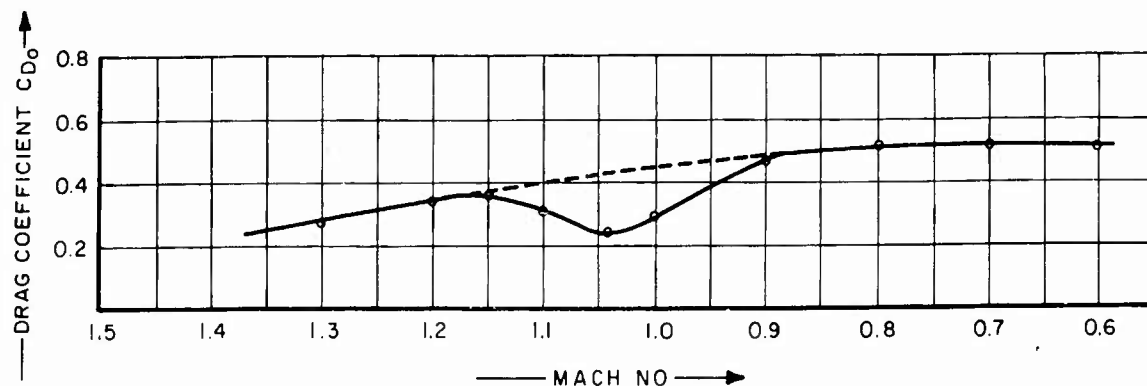


Figure 3. Variation of Drag Coefficient with Mach Number, Triple Cluster FIST Ribbon Type FR-130 Parachutes

reflected shock wave impinging on the parachute. There may also have been some wake effect since the parachutes which were affected were always in the lowest, centerline position behind the test vehicle.

Stability of the clustered parachutes, as a parachute system, showed significant variations through the velocity ranges tested. The curve in Figure 4 shows the average clustered parachute system angular displacement as a function of Mach number. The solid line in the curve shows the mean

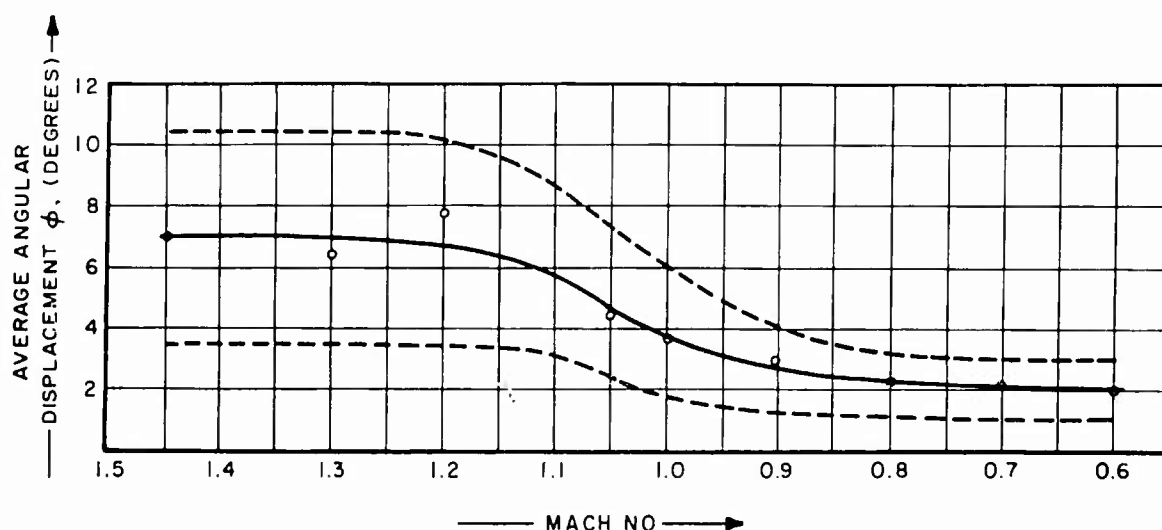


Figure 4. Variation of Angular Displacement with Mach Number, Triple Cluster FIST Ribbon Type FR-130 Parachutes

displacement of the system. Variations from the mean, in the form of oscillations or drift, are shown by the dotted lines on each side of the mean line.

From the information obtained on the supersonic test it is also possible to determine an average area ratio relationship as a function of Mach number. This curve is shown in Figure 5. Although the discrepancy in this curve, due to the deflation or collapse of the parachutes near the sonic velocity point, is shown as a single dip, the actual deviations on the two tests were not of equal magnitude and were not so clearly defined. The typical action is, however, represented by the deviation as shown. When faired through the dip, the curve appears to be almost a linear function. If the curve could be extended on both ends, however, it would undoubtedly plot as an extended "S" curve, becoming asymptotic to a finite upper and lower area ratio limit.

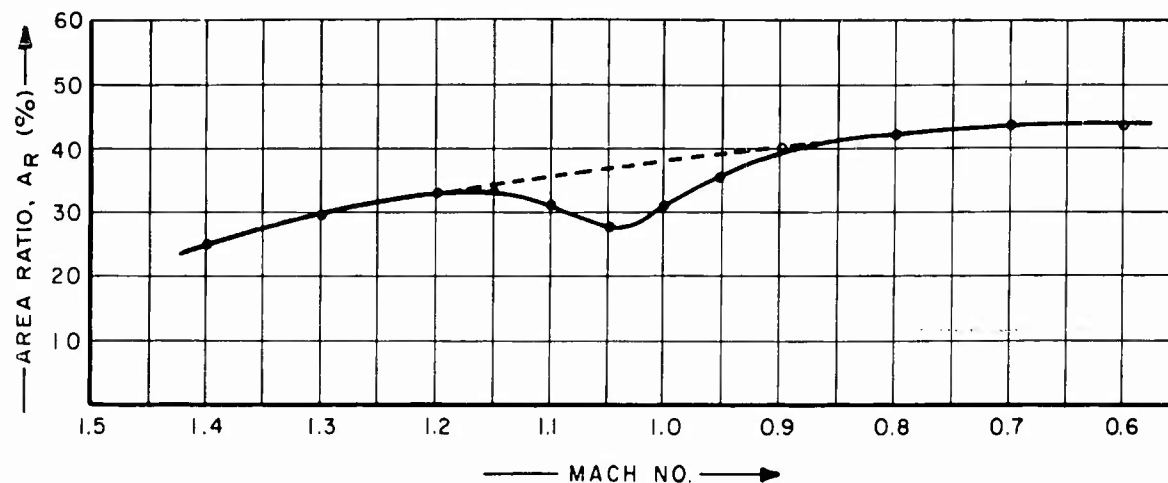


Figure 5. Variation of Area Ratio as a Function of Mach Number, Triple Cluster FIST Ribbon Type FR-130 Parachutes

If the data presented in Figures 3 and 5 are investigated further, a relationship of the drag coefficient as a function of area ratio can be determined. This relationship is shown in Figure 6. Although near linearity is indicated, it is - like the curves it is derived from, "S" shaped - with finite limits of both drag coefficient and area ratios. The upper limit is shown in Figure 6 as the point where the theoretical normal inflation is considered to be 100 percent and the corresponding drag coefficient is the accepted subsonic value. The lower limit cannot be determined from this data.

The dashed line in the curve shows a proportional linear variation based on the known subsonic relationship. This shows that, although the actual variation is nearly linear, it is not proportionally linear.

It is also interesting to note that the area ratio-drag coefficient relationship was maintained through the interim when there was a collapse of one or more of the parachutes. That is, when the parachutes collapsed and reduced the area ratio of the cluster, the drag coefficient dropped correspondingly.

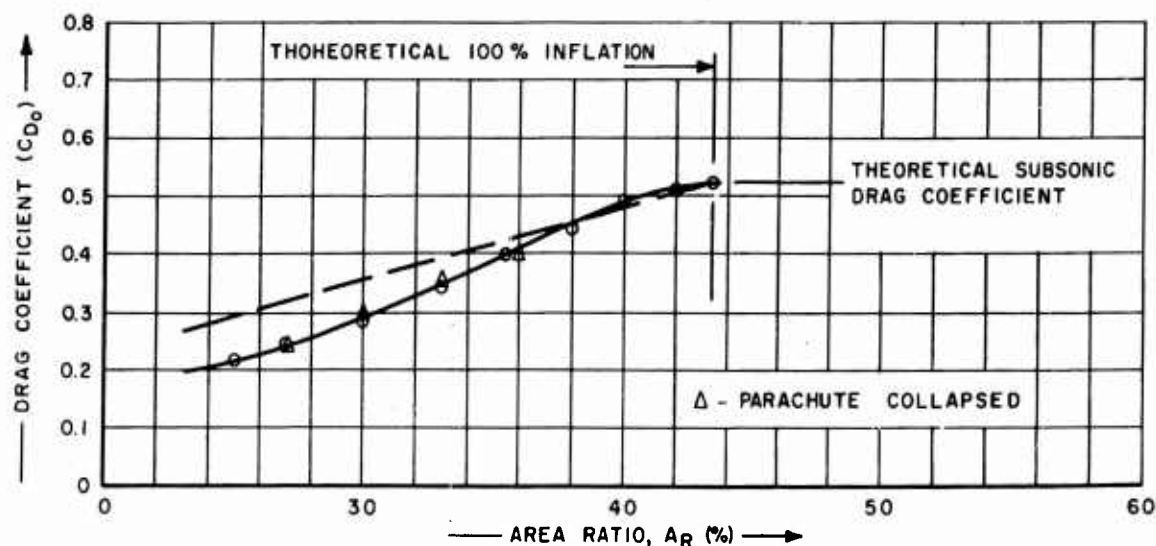


Figure 6. Variation of Drag Coefficient as a Function of Area Ratio, Triple Cluster FIST Ribbon Type FR-130 Parachutes

Details of the individual tests conducted with the clustered configurations are presented in Section V-B-3c of this report.

D. Conical Ribbon Parachutes

Of the total of 11 tests conducted with Conical Ribbon parachute configurations, two were made with the 15 degree design and three each were made with the 20, 30, and 45 degree designs. Satisfactory performance was obtained on all of these tests.

Geometric porosities of the parachutes were nearly identical, ranging between 25.2 and 25.8 percent. Because of this similarity the effects on performance parameters due to porosity change cannot be evaluated for these designs. Materials and fabrication methods were also generally the same for all conical parachute configurations.

Major geometric properties and average performance characteristics for these parachutes are presented in Table V.

Several trends are noticed which appear to be a function of the cone angle of the parachute. The drag coefficient, shown in the curve in Figure 7 as a function of the cone angle, decreases slightly with increasing cone angle. If a linear variation such as that shown in the curve is assumed, the line passes through the average points for the 15, 20, and 45 degree parachutes. The average point for the 30 degree design falls slightly below this line but this is not considered significant since the deviation is within the accuracy

TABLE V

AVERAGE PERFORMANCE CHARACTERISTICS -
CONICAL RIBBON PARACHUTES

Conical Ribbon Type	15CR134	20CR128	30CR129	45CR131
Conical Angle (deg.)	15	20	30	45
Nominal Diameter, D_o (ft)	6.24	6.24	6.07	6.18
Nominal Area, S_o (ft ²)	30.58	30.58	28.94	30.00
Weight (lbs)	20.4	21.3	20.4	20.1
Bulk (ft ³)	1.02	1.06	1.02	1.00
Geometric Porosity, λ_g (%)	25.2	25.8	25.7	25.6
Drag Coefficient, C_{D_o}	0.52	0.51	0.48	0.47
Opening Shock Factor, X	0.94	0.97	1.09	0.98
Area Ratio, A_R (%)	46.0	45.4	44.8	38.8
Stability, ϕ (deg.)	3.5 \pm 1.0	2.3 \pm 1.3	2.8 \pm 2.5	4.0 \pm 2.0

of the data. If a band is drawn, as represented by the dotted lines in Figure 7, boundaries which encompass the extremities of the data obtained in the individual tests are found. This band represents only two percent deviation from the average and now includes some of the data points for the 30 degree conical design. From this it would appear that the drag coefficient for the 30 degree conical should be approximately 0.49. It is also interesting to note that if the curve is continued to a cone angle of 0 degrees, or a flat parachute, the drag coefficient should be about 0.55. This value has been attained with some FIST ribbon designs. It should also be noted that the drag coefficient values shown are for parachutes with geometric porosities of 25 to 26 percent. Some variation in drag coefficient would be effected by significant changes in the porosity.

Figure 8 shows the area ratio as a function of parachute cone angle. As shown, the area ratio is not significantly affected with cone angles as high as 30 degrees. When the cone angle is increased to 45 degrees, however, a marked effect is evident.

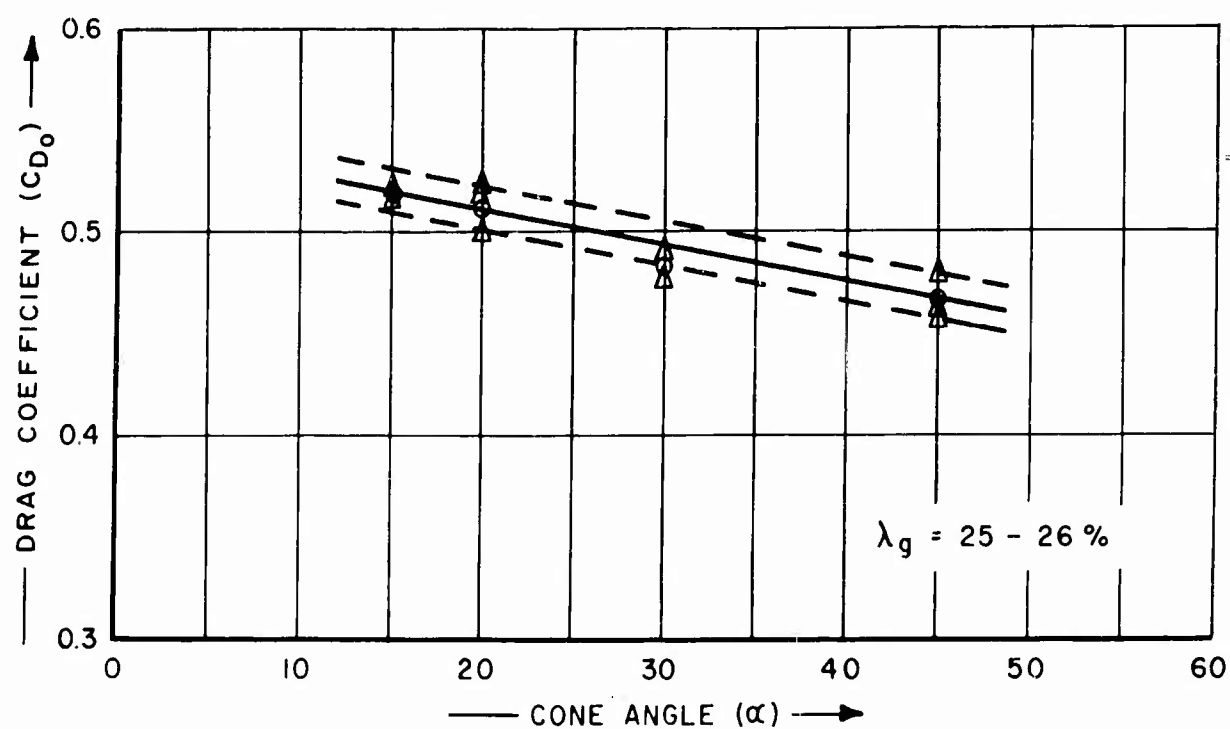


Figure 7. Drag Coefficient as a Function of Cone Angle

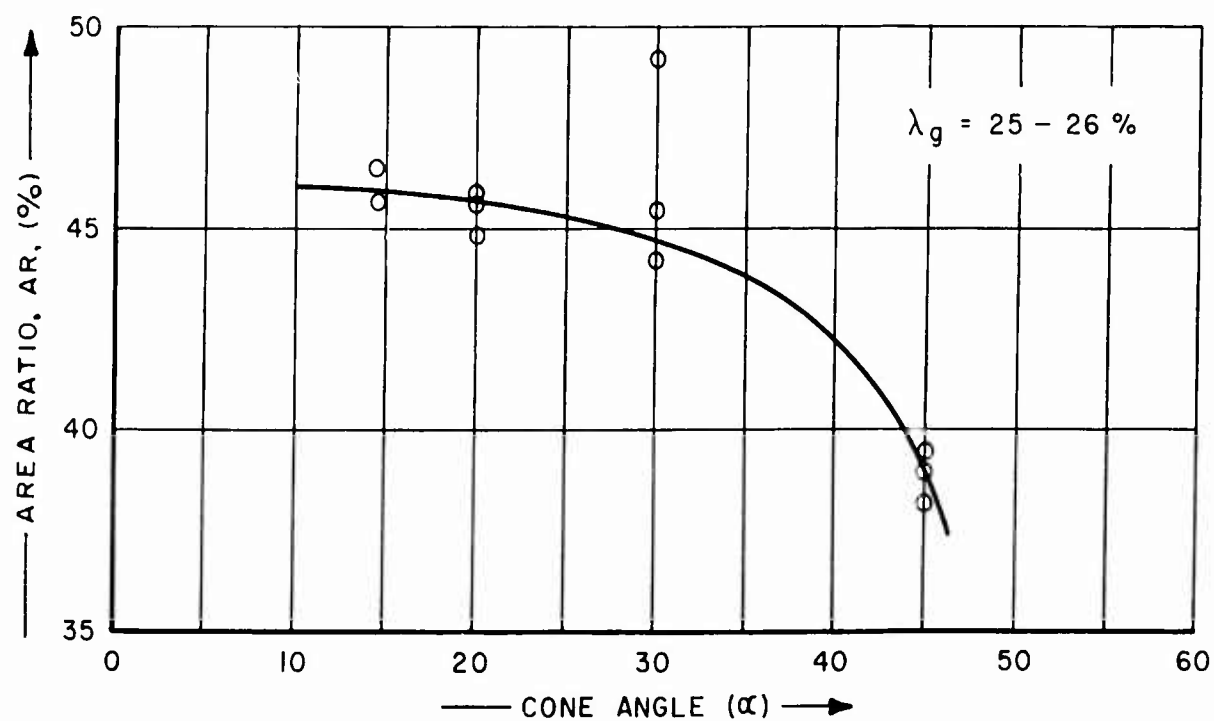


Figure 8. Area Ratio as a Function of Cone Angle

Although the curve appears to be a function of the cosine of the cone angle, this is probably not true through the whole range of angles from zero to 90 degrees. At the smaller cone angles the parachute behaves much like a flat circular design, taking an inflated shape with a diameter which is much less than the design base diameter of the cone. As larger cone angles are used, the parachute becomes increasingly formed or shaped. At some transition point in the conical angle relationship, the restriction of the base diameter becomes the limiting inflation factor.

From the data presented in Figure 8 it appears that this transition point is between 30 and 45 degrees.

With the exception of the 15 degree design, the Conical Ribbon parachutes exhibited stability characteristics that appeared to be related to the cone angle. Figure 9 shows the average angular displacement as a function of cone angle. The average values shown for each configuration represent the average of all tests conducted with that configuration. Average values for the individual tests were within approximately plus or minus one degree of the plotted value.

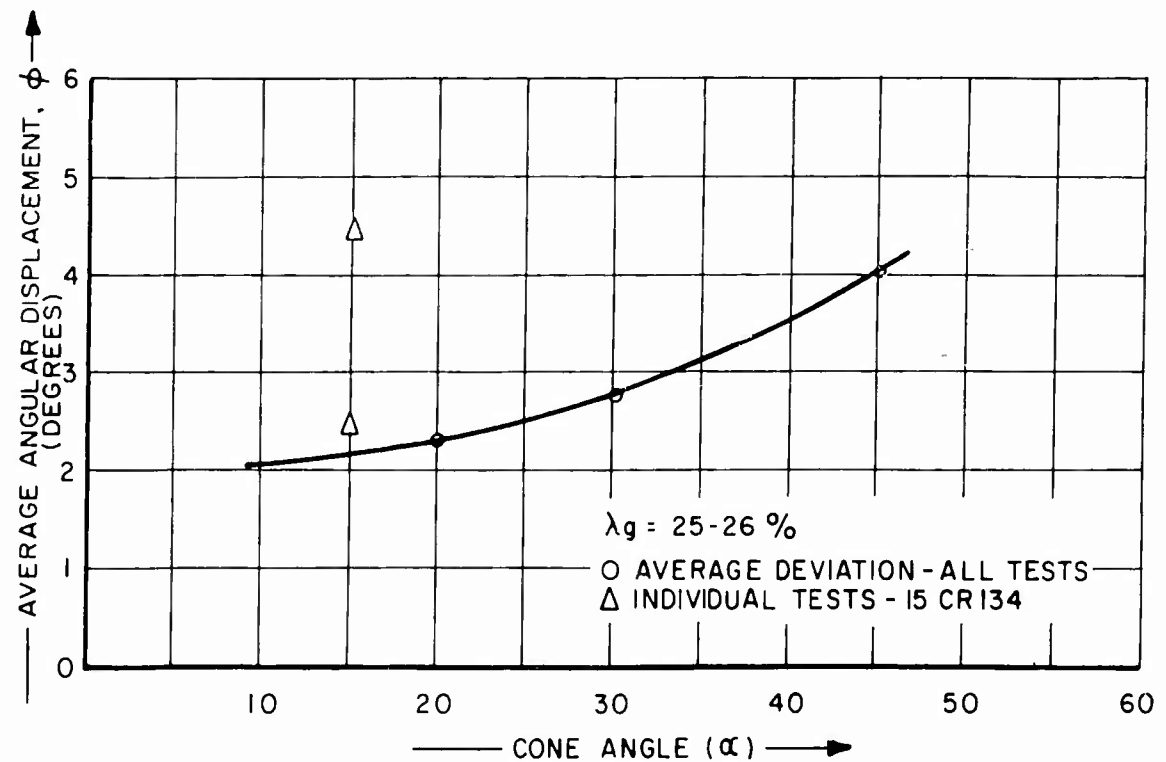


Figure 9. Average Angular Displacement as a Function of Cone Angle

Two test points are shown for the 15 degree configuration. These represent the averages of each of the tests conducted with this parachute, and are presented to illustrate that the excessive average displacement which results was primarily because of the behavior of the parachute on one test.

E. Equiflo Parachute

Three tests, details of which can be found in Section V-D-3, were conducted with Equiflo parachutes. On one of these tests the parachute suffered severe structural damage and was destroyed. In the two tests where satisfactory performance data were obtained, minor damage resulted to the parachute in one of the tests. Typical average performance characteristics for the Equiflo design resulting from these tests are presented in Table VI.

TABLE VI
AVERAGE PERFORMANCE CHARACTERISTICS -
EQUIFLO TYPE ESR-132, 133 PARACHUTE

Nominal Diameter, D_0 (ft)	6.20
Nominal Area, S_0 (ft ²)	30.19
Weight (lbs)	20.70
Bulk (ft ³)	1.03
Geometric Porosity, λ_g (%)	25.80
Drag Coefficient, C_{D_0}	0.50
Opening Shock Factor, X	1.00
Area Ratio, A_R (%)	45.50
Stability, ϕ (deg.)	1.5 \pm 1.2

There was some evidence of skirt flutter during the initial portion of the tests. These damped rapidly as the tests progressed.

Drag coefficient, opening shock factor and area ratio relationships were quite consistent on both of the tests. Over-all stability of this parachute design was very good.

All of the Equiflo parachutes were designed and fabricated with suspension line-diameter ratios of 2.

F. Hemisflo Parachute

Only one test, the last in the program, was conducted with a Hemisflo parachute. Performance curves and characteristics of this configuration are presented in Section V-E-3 of this report.

Generally good operation resulted. Inflation characteristics appeared to be near the optimum design relationship during the steady state portion of the test and general stability of the parachute was good. An opening shock factor of 1.23 was obtained and a steady state drag coefficient of 0.51 was recorded in subsonic operation. Since these values represent only the one test, they cannot be established as optimum averages for the Hemisflo parachute design. The performance characteristics presented in Table VII should therefore be evaluated with this in mind.

TABLE VII

PERFORMANCE CHARACTERISTICS -
HEMISFLO TYPE EHR-135 PARACHUTE

Nominal Diameter, D_o (ft)	6.24
Nominal Area, S_o (ft ²)	30.6
Weight (lbs)	19.4
Bulk (ft ³)	0.97
Geometric Porosity, λ_g (%)	25.4
Drag Coefficient, C_{D_o}	0.51
Opening Shock Factor, X	1.23
Area Ratio, A_R (%)	37.5
Stability, ϕ (deg.)	3.0 \pm 2.0

The Hemisflo parachute which was tested on this program was designed and fabricated with a suspension line-diameter ratio of 2.

SECTION V

TEST RESULTS

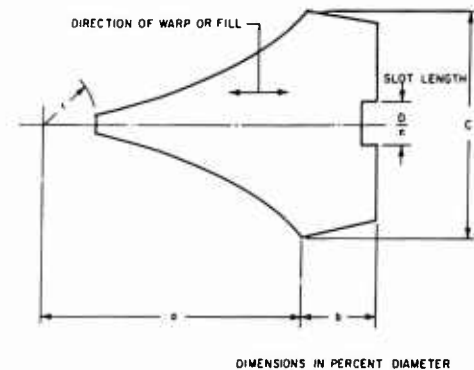
A. Guide Surface Ribless Parachute

1. General

The Guide Surface Ribless parachutes which were tested in this program were a modified version of the basic Guide Surface Ribless design. Instead of the separate guide surface and roof panels of the original parachute of this type, the modified version was of one-piece construction.

Like all ribless type parachutes, the modified design did not have internal cloth ribs to contain and separate the suspension lines from the canopy. The one-piece roof and guide surface panel were designed and fabricated so that the inflated shape of the canopy assumed the geometric form most conducive to good flow separation and stability. The suspension lines were rigidly attached to the exterior of the canopy along the seams which formed the roof panel portion of the parachute.

A typical panel shape layout and basic dimensions for the six and 12 gore modified Guide Surface Ribless parachute is shown in Figure 10. The sequence photographs in Figure 11 illustrate a typical parachute of the Guide Surface Ribless type in operation.



2. Test Program

Four tests were conducted with modified Guide Surface Ribless parachutes during the test program. Three of these tests were with a four foot diameter, 12 gore, Type GS-201 parachute and one test was with a two foot diameter, six gore, Type GS-202 design. Test velocities with the Type GS-201 parachute ranged from Mach 0.91 to Mach 1.41.

DIAMETER D (FT)	NO. OF GORES n	a	b	c	r (INCHES)
4.0	12	44.0	11.0	57.9	4.78
2.0	6	49.8	20.2	71.1	2.33

Figure 10. Typical Panel Shape Layout and Basic Dimensions for the 6 and 12 Gore Modified Guide Surface Ribless Parachute

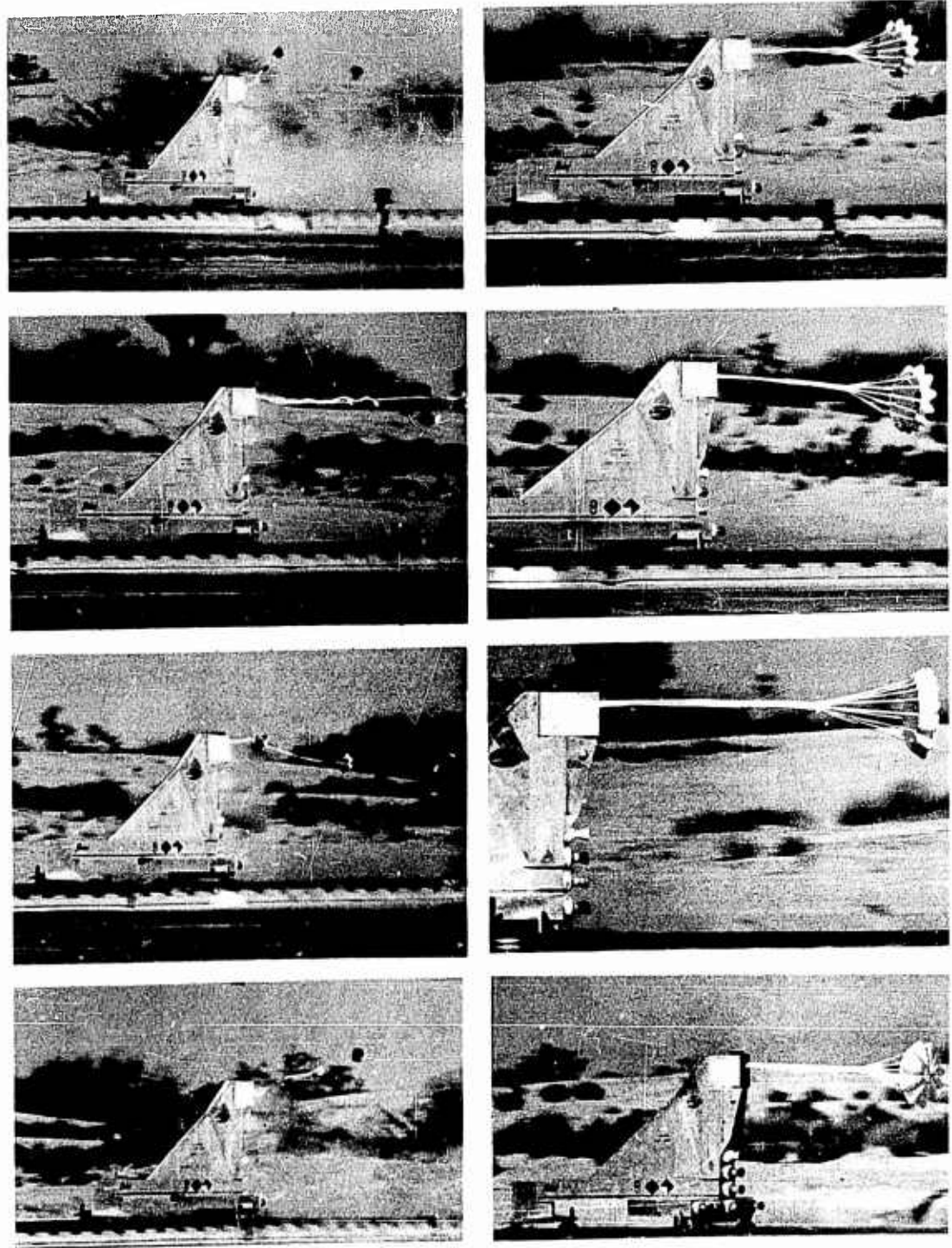


Figure 11. Sequence of Guide Surface Ribless Parachute in Operation

The Type GS-202 parachute was tested at Mach 1.39.

All of the test parachutes in this series were manufactured from MIL-C-8021A, Type III, 600 pound tensile strength nylon drag parachute cloth. Physical details and material specifications are presented in Tables VIII and IX, respectively.

3. Parachute Performance

A summary of performance data of the modified Guide Surface Ribless parachutes, as measured on the sled test program, is presented in Table X and graphically illustrated in the performance curves in Figures 13 through 15.

In the four tests conducted with Guide Surface Ribless parachutes, two basic configurations were used. These varied both in diameter and number of gores. Performance of the parachutes in the tests of each configuration are discussed in the following paragraphs.

a. Guide Surface Ribless, Type GS-201 (4 foot diameter, 12 gore)

Three tests, Nos. 2, 3 and 9 were made with the 4 foot diameter, 12 gore configuration.

In Test No. 2 the parachute was not properly inflated through a major portion of the test period. Some evidence of incomplete inflation was also noted in Test No. 3, but general parachute operation was not seriously affected. In Test No. 9 suspension line and canopy failure resulted in complete collapse of the parachute.

Test No. 2, the initial test with this parachute configuration, was made at a deployment velocity of 1,060 feet per second ($M = 0.96$) although little recorded data are available on this test, trackside and sequence photography shows that the parachute was not properly inflated during the test period. Several adjacent gores appeared to be bunched together and not inflated to the same gore widths exhibited throughout the rest of the parachute. The guide surface portion of another gore was also noted to be pressed inward, i. e., concave rather than the normally inflated convex shape. These abnormal inflation characteristics are shown in Figure 12, a and b, respectively.

Similar tendencies toward partial inflation were noted in Test No. 3. Although the guide surface portions of the canopy

TABLE VIII
PHYSICAL DETAILS AND
DIMENSIONS OF GUIDE SURFACE RIBLESS PARACHUTES

Parachute Type Number	GS-201	GS-202
Design Diameter, D_p (ft)	4.0	2.0
Design Projected Area, S_p (ft ²)	12.57	3.14
No. of Gores and Suspension Lines	12	6
Canopy Material	Type III - 600 lb	Type III - 600 lb
Suspension Line Material	1 x 6000	1 x 6000
Suspension Line Length (ft)	5.0	2.5
Vent Diameter (in.)	9.56	4.66
Vent Line Length (in.)	7.75	4.125
Slot Length (in.)	4.0	4.0
Vent Band Reinforcing	1 x 6000	1 x 4000
Thread Size - Canopy Seams	5 Cord	5 Cord
Thread Size - Line Attachment	5 Cord	5 Cord
Pattern Details	Fig. 10	Fig. 10
Weight (lbs)	14.4	5.5
Bulk (ft ³)	0.72	0.27
Used on Test Nos.	2, 3, 9	14
CRL Specification No.	597-8701	597-9961

TABLE IX
MATERIALS USED IN GUIDE SURFACE RIBLESS PARACHUTES

Part	Material	Specification	Size	Tensile Strength
Canopy	Cloth, Nylon	MIL-C-8021A-III	14 oz/sq yd	600 lb/in.
Suspension Lines	Webbing, Nylon	MIL-W-4088-XVIII	1 in.	6000 lb
Reinforcing	Webbing, Nylon	MIL-W-4088-XVIII	1 in.	6000 lb
	Webbing, Braided Coreless	MIL-C-7215-IX	1 in.	4000 lb
	Webbing, Nylon Tubular	MIL-W-5625	1 in.	3000 lb
	Tape, Nylon	MIL-T-5038-IV	1 in.	1000 lb
Thread	Webbing, Nylon	MIL-W-4088-I	9/16 in.	500 lb
	Nylon	MIL-T-7807	5, 3, FF	40, 24, 16

TABLE X

PERFORMANCE SUMMARY DATA - GUIDE SURFACE RIBLESS PARACHUTES

Parachute Type		GS-201			GS-202
Test Number		2	3	9	14
Velocity, V_s (ft/sec)		1,060	1,009	1,588	1,579
Mach Number (M) at V_s		0.959	0.911	1.410	1.393
Dynamic Pressure, q_s (lb/ft ²)		1,189	1,140	2,741	2,665
Deployment Time, t_d (sec)		0.210	0.225	0.155	0.250
Inflation Time, t_f (sec)		-	0.04	0.04	0.02
Time to Max. Force, t_{s0} (sec)		0.040	0.038	0.040	0.019
Snatch Force, F_s (lbs)		9,450	6,711	18,985	10,200
Opening Shock Force, F_o (lbs)		15,750	21,119	31,118	14,340
Avg. Drag Coefficient, C_D		-	0.80	-	-
Opening Shock Factor, X		1.34*	1.82	-	-
Area Ratio, A_R (%)		-	83.7	-	-
Stability, ϕ (deg.)		-	2.0 \pm 2.0	-	-
Parachute Damage	Canopy	NONE	NONE	Five panels blown out.	All panels ruptured.
	Lines	NONE	NONE	3 suspension lines severed at keeper. 8 torn from canopy.	1 suspension line severed at skirt attachment point.

*Based on 0.80 drag coefficient

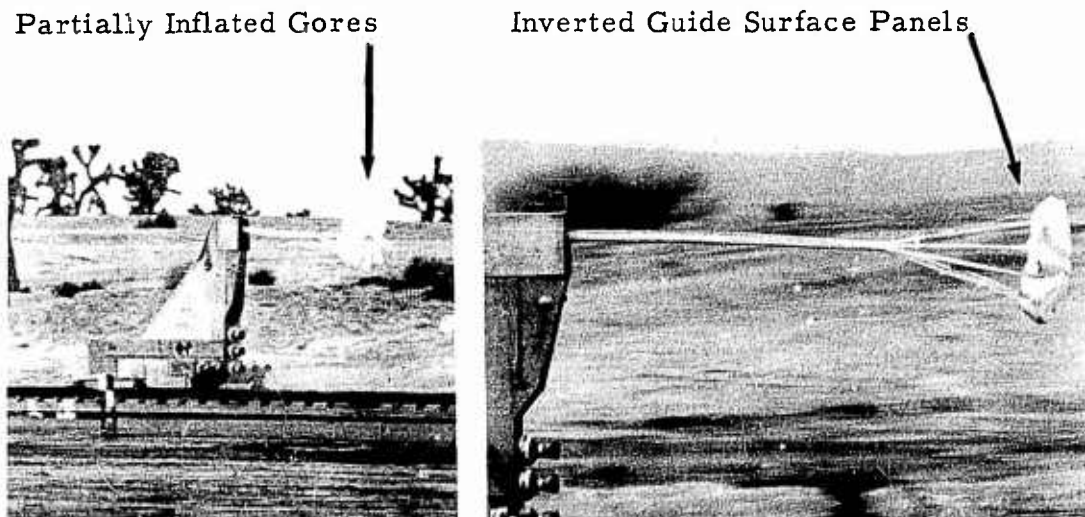


Figure 12. Abnormal Inflation Characteristics, Guide Surface Ribless Parachute - Test No. 2

were inflated to the proper convex shapes, several gores remained bunched together rather than expanding to the full gore widths exhibited by the other gores of the parachute. This did not seem to have significant effect on either the drag characteristics or the stability of the parachute. The steady state area ratio averaged 84 percent through the test period with a corresponding drag coefficient of 0.80. An opening shock factor of 1.82 resulted on this test. Although this value is high, it is not higher than might be expected for this type of parachute when the rapidity of inflation (0.038 second) is considered. Performance curves giving the inflated area ratios, drag and stability data from this test are shown in Figure 13.

Test No. 9, the third test which was made with the 4 foot diameter, 12 gore modified Guide Surface Ribless parachute reached a deployment velocity of 1,588 feet second ($M = 1.41$). Immediately after the opening shock force the parachute commenced to fail. Three (3) suspension lines were severed at the keeper and eight (8) other lines were torn completely from the canopy, skirt to vent. The canopy cloth in five (5) gores was partially or totally blown out. Complete destruction of the parachute resulted.

Curves of the instantaneous area ratios and force ratios during parachute inflation and through the period when the parachute failed, are shown in Figure 14.

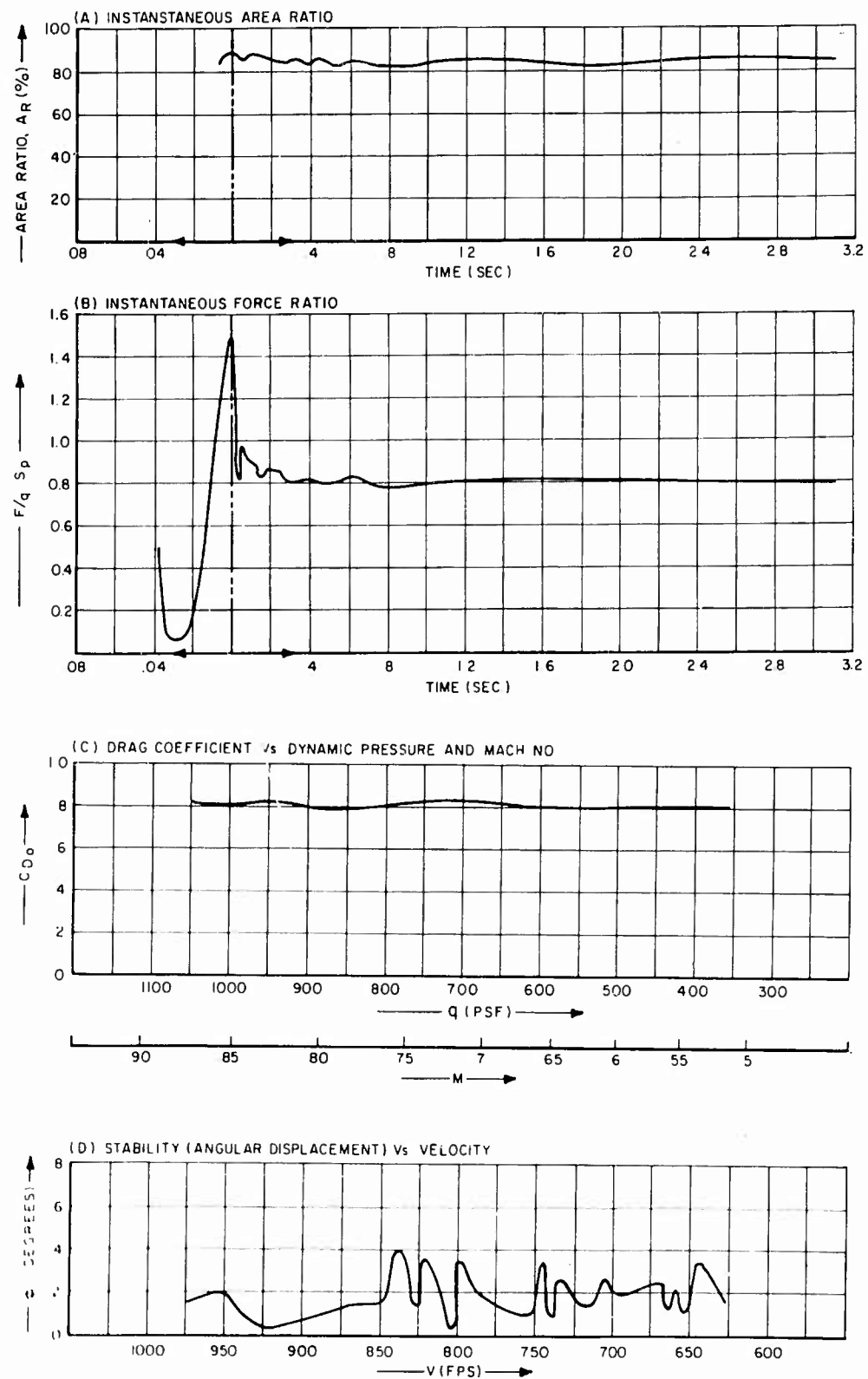


Figure 11. Performance Curves, Guide Surface Ribless Parachute - Test No. 3

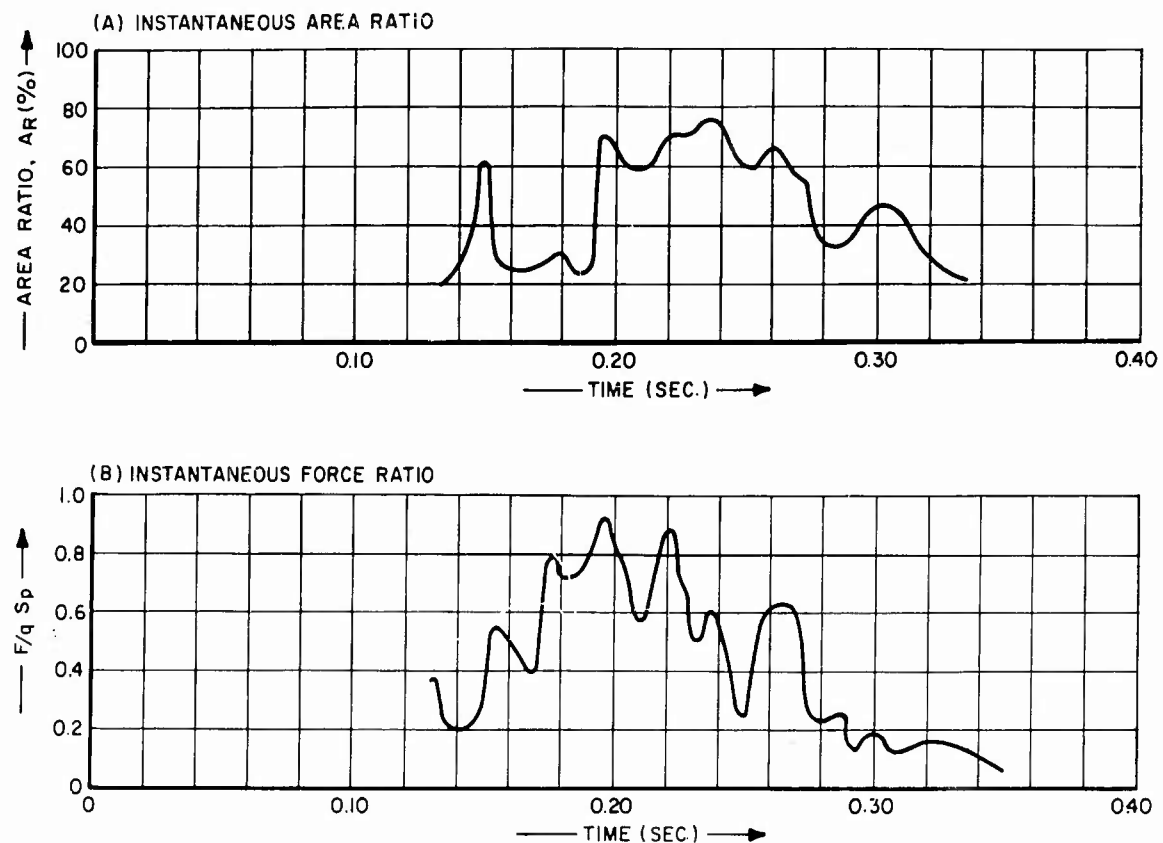


Figure 14. Performance Curves, Guide Surface Ribless Parachute - Test No. 9

b. Guide Surface Ribless, Type GS-202 (2 foot diameter, 6 gore)

Only one test, No. 14, was conducted with the 2 foot diameter, 6 gore configuration. This test resulted in total destruction of the parachute in approximately one half second of operation. The performance curve shown in Figure 15 indicates that the parachute probably remained structurally intact through this short period of operation. Although there were violent load fluctuations throughout the test until failure occurred, the parachute maintained an average drag coefficient of approximately 0.80. It is probable that these severe fluctuations, which occurred at a frequency of approximately 70 cycles per second and varied in amplitude between approximately half and full scale of the initial opening shock force, materially weakened the parachute to the point where final destruction occurred almost simultaneously throughout the parachute.

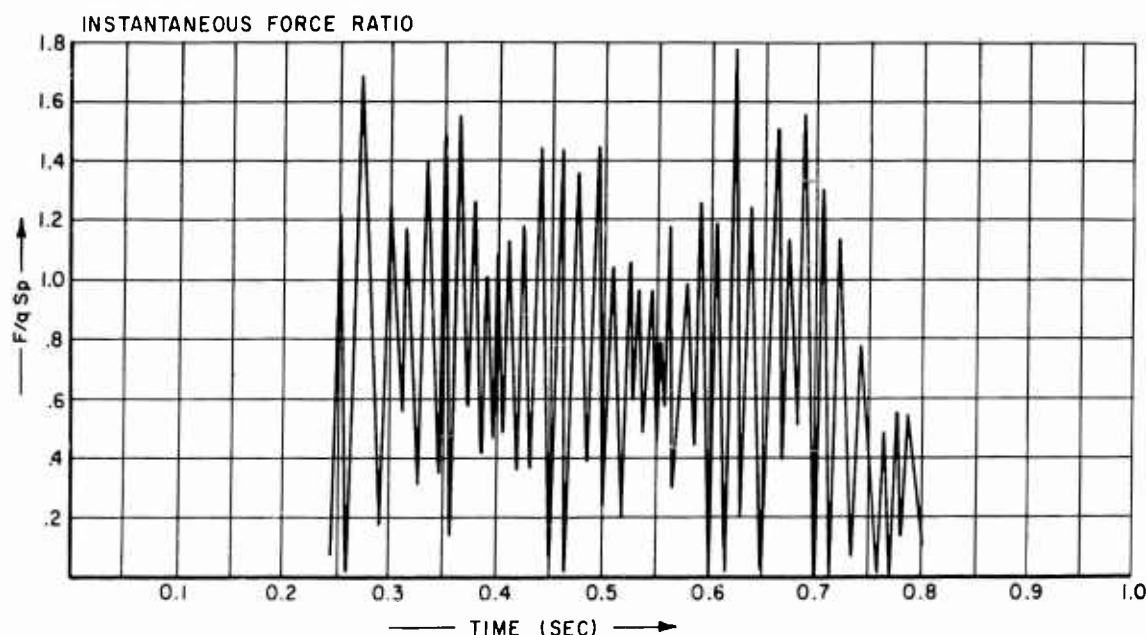


Figure 15. Performance Curves - Guide Surface Ribless Parachute

An explanation of the results of this test may be found in the operating conditions under which the parachute was deployed. For reasons undetermined, a premature deployment occurred during the latter part of the final powered stage. This caused the parachute to inflate and operate under acceleration and increasing dynamic pressure. Between the time of deployment and parachute failure, the Mach number had increased from 1.39 to 1.52, and the dynamic pressure from 2,660 pounds per square foot to 3,180 pounds per square foot. Although the time to maximum force was extremely short (0.019 second), the rapid inflation and the corresponding high opening shock factor apparently were not as major contributing factors to the ultimate failure of the parachute as was the succeeding operation under increasing high amplitude, high frequency load and inflation fluctuations.

B. FIST Ribbon Parachute

1. General

The FIST Ribbon parachute is basically a flat circular design, consisting of triangular gores which are assembled to form the regular polygon configuration of the parachute. Each gore is a grid of horizontal ribbons spaced and retained at close intervals by one or more

vertical ribbons. Radial bands extend from the vent to the skirt at the sides of each gore. These bands join adjacent gores together and transfer the forces developed in the canopy to the suspension lines. Figure 16 illustrates a typical FIST Ribbon gore assembly. The photograph in Figure 17 shows a parachute of the FIST Ribbon type in operation during a supersonic test.

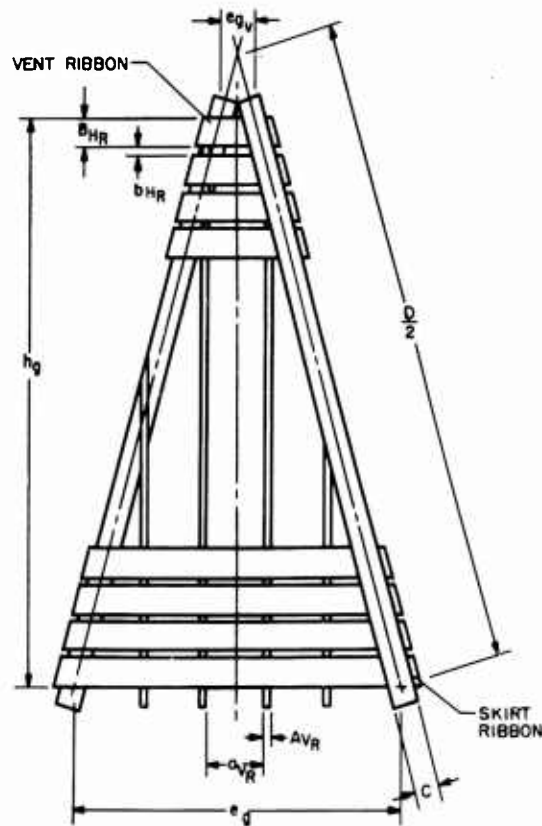


Figure 16. Typical FIST Ribbon Parachute Gore Assembly

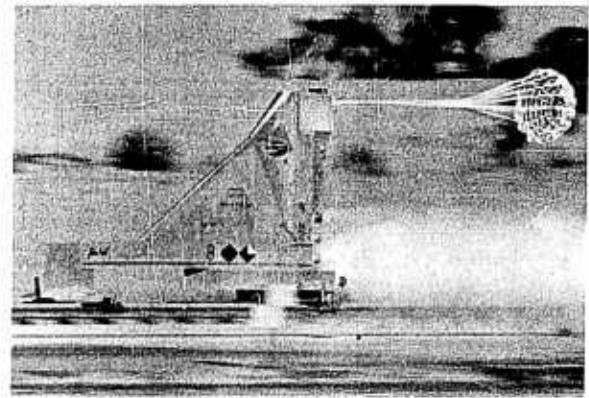


Figure 17. FIST Ribbon Parachute in Operation

2. Test Program

Eight (8) tests were conducted with FIST Ribbon type parachutes during the program. One of the tests was performed with a 6.17 foot diameter, 16 gore, Type FR-127 parachute having a geometric porosity of 26.2 percent. Two tests were conducted with 4.78 foot diameter, 16 gore, Type FR-130 parachutes with geometric porosities of 19.3 percent. Five (5) tests were made with the Type FR-130 parachute in triple clustered configuration. Test velocities with the clustered parachutes ranged from Mach number 0.81 to Mach number 1.53. On the two tests conducted with the single Type FR-130 parachutes, nearly identical Mach numbers of 1.01 and 1.05 resulted. The Type FR-127 parachute was tested at a deployment Mach number of 1.37.

All FIST Ribbon parachutes which were tested during the program were fabricated in accordance with military specification MIL-P-6635 (Reference 4) with design and revision information being furnished by the contracting agency.

Major dimensional details, materials and material specifications of the various FIST Ribbon parachutes tested in the program are listed in Tables XI and XII.

3. Parachute Performance

FIST Ribbon parachute performance data for the three parachute configurations considered in eight test runs are tabulated in table XIII. Summary curves showing important performance characteristics are graphically presented for each test and parachute type in the graphs in Figures 19, 21, 22, and 24. Where applicable, multiple sets of performance curves have been placed on graphs common to any one configuration group. This provides for rapid and accurate comparison and indicates the average characteristics of the type being presented. It also serves to highlight unusual or erratic operation during any particular test or portion thereof.

In the eight tests conducted with FIST Ribbon parachutes, two parachute designs, the Type FR-127 and the Type FR-130, were used. The Type FR-130 parachute was, however, tested in both single and triple cluster configurations. Performance of the parachutes in the tests of each configuration are discussed in the following paragraphs.

a. FIST Ribbon Type FR-127

The FIST Ribbon Type FR-127 parachute was a 6.17 foot diameter, 16 gore design having a geometric porosity of 26.2 percent.

Only one test, No. 1, was conducted with this configuration.

Although an early deployment occurred on this test, there were no adverse effects on the deployment system, inflation or subsequent operation of the parachute. Deployment was orderly and inflation appeared normal. Photographic data show that the time to full inflation was 0.071 second, essentially the same as the time required to reach the primary opening shock force. Deployment velocity, referred to snatch force, was 1,532 feet per second, or Mach 1.37. The photographic sequence in Figure 18 shows the deployment and inflation process of this parachute on Test No. 1.

Some ribbon flutter was evident in the first few ribbons at the skirt in several adjacent gores on opposite sides of the parachute. This flutter was particularly predominant in the early,

TABLE XI

PHYSICAL DETAILS AND DIMENSIONS OF FIST RIBBON PARACHUTES

FIST Ribbon Type	FR-127	FR-130
Nominal Diameter, D_o (ft)	6.17	4.78
Canopy Area, S_o (ft ²)	29.90	17.95
Geometric Porosity, λ_g (%)	26.2	19.3
No. of Gores and Suspension Lines, (n)	16	16
No. of Horizontal Ribbons	9	14
No. of Vertical Ribbons	3	2
Suspension Line Length, l_s (ft)	6.17	4.125
Length of Gore, h_g (in.)	29.65	24.9
Width of Gore at Skirt, e_g (in.)	14.45	11.34
Width of Gore at Vent, e_{gv} (in.)	2.90	1.62
Vent Line Length, (in.)	11.85	6.94
Spacing between Vertical Ribbons, a_{VR} (in.)	3	6
Spacing between Horizontal Ribbons, b_{HR} (in.)	1.456	0.57
Suspension Line Material	1 x 6000	1 x 3000
Horizontal Ribbon Material	2 x 1500	1-1/4 x 800
Vertical Ribbon Material	9/16 x 500	5/16 x 350
Radial Band Material	1-1/2 x 1500	1 x 1000
Horizontal Reinforcing Band Material	1-3/4 x 3600	-
Reinforcing Band on Ribbon Nos.	4-7	-
Weight, Parachute and Lines (lbs)	20.5	10.1
Bulk, Parachute and Lines (ft ³)	1.02	0.50
Used on Test Number	1	7, 10, 11, 15, 19, 23, 24
CRL Specification Number	597-7801	597-9280

TABLE XII

MATERIALS USED IN FIST RIBBON PARACHUTES

Part	Material	Size-Tensile Strength	Specification
Horizontal Ribbons	Webbing, Nylon Tape, Nylon	1-1/4 in. - 800 lb 2 in. - 1500 lb	MIL-W-4088B-III MIL-T-5038-IV
Vertical Ribbons	Tape, Nylon Webbing, Nylon	7/16 in. - 290 lb 9/16 in. - 500 lb	MIL-T-8363-II MIL-W-4088-I
Radial Ribbons	Tape, Nylon Tape, Nylon	1 in. - 1000 lb 1-1/2 in. - 1500 lb	MIL-T-5038-IV MIL-T-5038-IV
Horizontal Reinforcing	Webbing, Nylon	1-3/4 in. - 3600 lb	MIL-W-4088-VIII
Skirt Reinforcing	Tape, Nylon Webbing, Nylon	1 in. - 1000 lb 1-3/4 in. - 3600 lb	MIL-T-5038-IV MIL-W-4088-VIII
Vent Reinforcing	Webbing, Nylon	1 in. - 6000 lb	MIL-W-4088-XVIII
Suspension Lines	Webbing, Nylon Webbing, Nylon	1 in. - 3000 lb 1 in. - 6000 lb	MIL-W-5625 MIL-W-4088-XVIII
Pocket Bands	Tape, Nylon Webbing, Nylon	1 in. - 1000 lb 1-3/4 in. - 3600 lb	MIL-T-5038-IV MIL-W-4088-VIII
Thread	Nylon	FF - 14 lb 3 Cord - 24 lb 5 Cord - 40 lb	MIL-T-7807

TABLE XIII
PERFORMANCE SUMMARY DATA - FIST RIBBON PARACHUTES

Parachute Type Number		FR-127	FR-130 (Single)			FR-130 (Cluster)			
Geometric Porosity, λ_g (%)		26.2	19.3			19.3			
Test No.		1	23	24	7	10	11	15	19
Velocity, V_g (ft/sec)		1,532	1,220	1,158	916	1,165	1,734	1,680	1,002
Mach Number (M) at V_g		1.368	1.054	1.012	0.812	1.042	1.528	1.503	0.873
Dynamic Pressure, q_g (lbs/ft ²)		2,550	1,511	1,397	902	1,492	3,211	3,071	1,045
Deployment Time, t_d (sec)		-	0.222	0.372	0.285	0.235	0.143	0.159	0.324
Inflation Time, t_f (sec)		0.07	0.10	0.11	-	0.165	-	-	0.186
Time to Max. Force, t_{S_0} (sec)		0.205	0.038	0.665	0.195	0.155	0.337	0.146	0.156
Snatch Force, F_s (lbs)		12,272	7,590	11,749	12,360	11,082	34,181	26,186	11,047
Opening Shock Force, F_o (lbs)		31,600	14,368	12,048	24,422	36,032	39,136	32,221	31,720
Avg. Drag Coefficient, C_{D_0}		0.47/0.30	0.51	0.52	0.53	0.52	0.50/0.28-0.37	0.52/0.20-0.25	0.52
Opening Shock Factor, X		-/1.31	1.03	0.92	0.935	0.86	-/0.70	-/0.87	1.085
Area Ratio, A_R (%)		36.9	43.8	41.4	-	47.0	41.0/23-35	40.3/25-32	44.8
Stability, ϕ (deg.)		3.0 \pm 1.0	1.5 \pm 1.0	2.5 \pm 1.0	-	2.75 \pm 1.25	2.0 \pm 1.0/7.0 \pm 5.0	2.0 \pm 1.0/7.5 \pm 2.5	3.0 \pm 0.5
Parachute Damage	Canopy	*	NONE	NONE	NONE	NONE	NONE	NONE	NONE
	Lines		NONE	NONE	NONE	NONE	NONE	NONE	NONE

(Subsonic/Supersonic)

*Several horizontal ribbons torn. Considerable stitching damage.

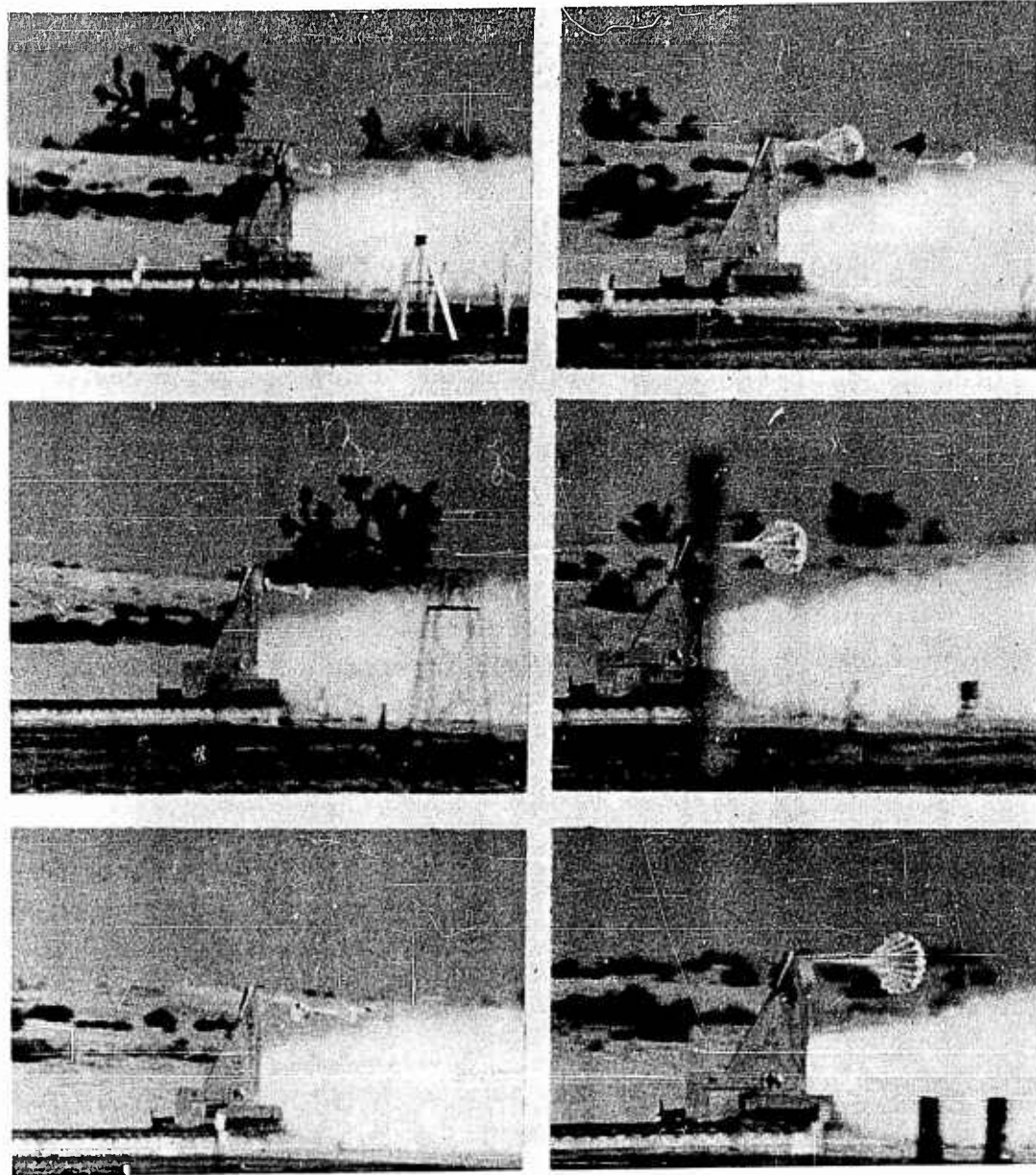


Figure 18. Deployment and Inflation Sequence, FIST Ribbon Type FR-127 Parachute - Test No. 1

high velocity portion of the test.

Significant amounts of minor damage resulted from the flutter. Several ribbons were severed and stitching was torn loose all around the parachute. The damage, however, was limited to the first unreinforced ribbon near the skirt, and occurred almost entirely at the junction of horizontal and vertical ribbons.

The parachute exhibited very good stability characteristics throughout the test. Angles of oscillation averaged 3.0 plus or minus 1.0 degree. Oscillatory changes were gradual and no significant canopy rotation was present.

This test showed a definite difference in the drag characteristics of the parachute in supersonic and subsonic operation. The steady state drag coefficient ranged from approximately 0.30 at the high velocity end of the test to approximately 0.47 at the low velocity end. Opening shock factor, based on supersonic drag coefficient was 1.31. Based on the subsonic coefficient, the factor was 0.91. There were no significant changes in the inflated area ratios during the test period. Through both the supersonic and subsonic phases of the test, the area ratio averaged approximately 37 percent of the design nominal area. Performance summary data for this parachute are presented in the curves in Figure 19.

b. FIST Ribbon Type FR-130

The FIST Ribbon Type FR-130 parachute was a 4.78 foot diameter, 16 gore design having a geometric porosity of 19.3 percent.

Although this parachute was designed for testing in a clustered configuration, two tests - Nos. 23 and 24 - were conducted with the parachute as a single test item.

Similar over-all operational characteristics were noted on both of the tests. After initial opening shock factor, high amplitude force oscillations were initiated in the parachute and line system. These pulsations occurred at a frequency of approximately 50 cycles per second, and were concurrent with similar fluctuations in the area ratios. The pulsation and pulsation rate continued throughout the tests with little indication that the combined oscillatory motion was being damped as the velocity was decreasing.

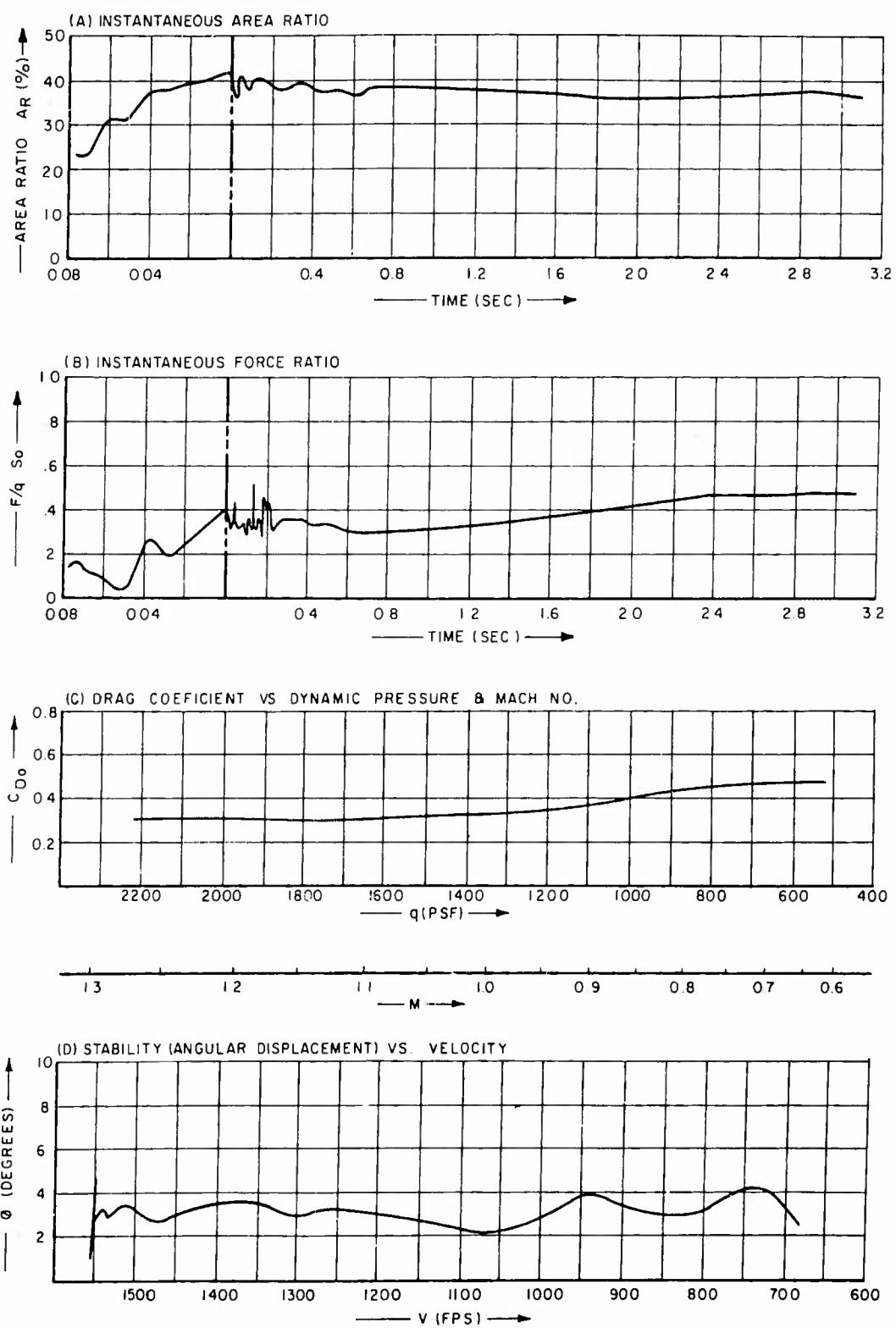


Figure 19. Performance Curves - FIST Ribbon Type FR-127 Parachute

It is significant that neither parachute in the two tests was damaged by this violent action. Similar phenomena were noted in several tests in an earlier program (Reference 2), but these resulted in rapid destruction of the parachute or damping of the high frequency fluctuations. It was suspected at that time, as it is now with the parachute on tests 23 and 24, that the combination of physical properties of the parachute system with the operational conditions applied to the parachutes allowed the system to attain its natural frequencies and interact in the inflation and force modes.

Deployment velocities on the two tests were approximately the same. On test No. 23, the deployment Mach number was 1.05. On test No. 24, it was 1.01. The inflation times or time to primary opening shock appears to vary significantly between the two. On test No. 23, the time is recorded as 0.038 second, while the corresponding time on test No. 24 is 0.106 second. The longer time on test No. 24 occurred because of an erratic inflation, that is, several gores in the parachute hesitated in filling out, causing the parachute to whip several times before finally inflating. If the parachute had remained inflated as the first peak was reached, identical inflation times would have been recorded in the two tests. Figure 20 shows the deployment and inflation of the parachute on test No. 24.

Opening shock factors of 1.03 on test No. 23 and 0.92 on test No. 24 were generally on the same order of magnitude and within the expected limits for the FIST Ribbon type of parachute.

Although the rapid pulsations of the parachutes throughout both tests caused corresponding fluctuations in the drag coefficient, nearly identical average drag coefficients of 0.51 and 0.52 were attained.

Generally good stability resulted in both tests despite the pulsations present in the system.

Inflated area ratios on both tests had wide variations in the maximum and minimum values due to the pulsations of the parachutes. Averages of these pulsations varied approximately 15 percent during the steady state portion of the tests.

Performance summary data showing the average characteristics of these parachutes on test Nos. 23 and 24 are shown in the curves in Figure 21. Figure 22 shows a small segment of the

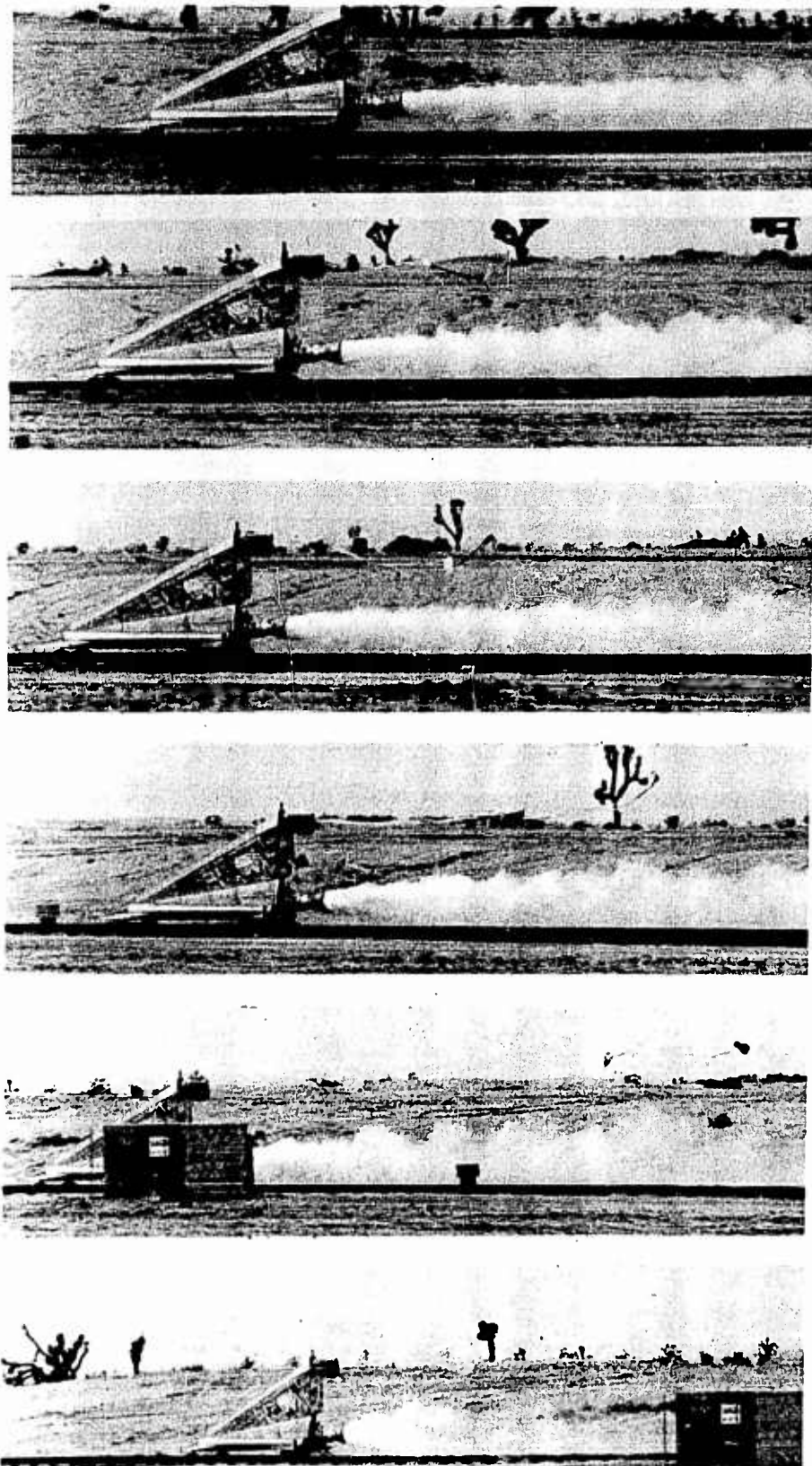


Figure 20. Deployment and Inflation Sequence, FIST Ribbon Type FR-130 Parachute - Test No. 24

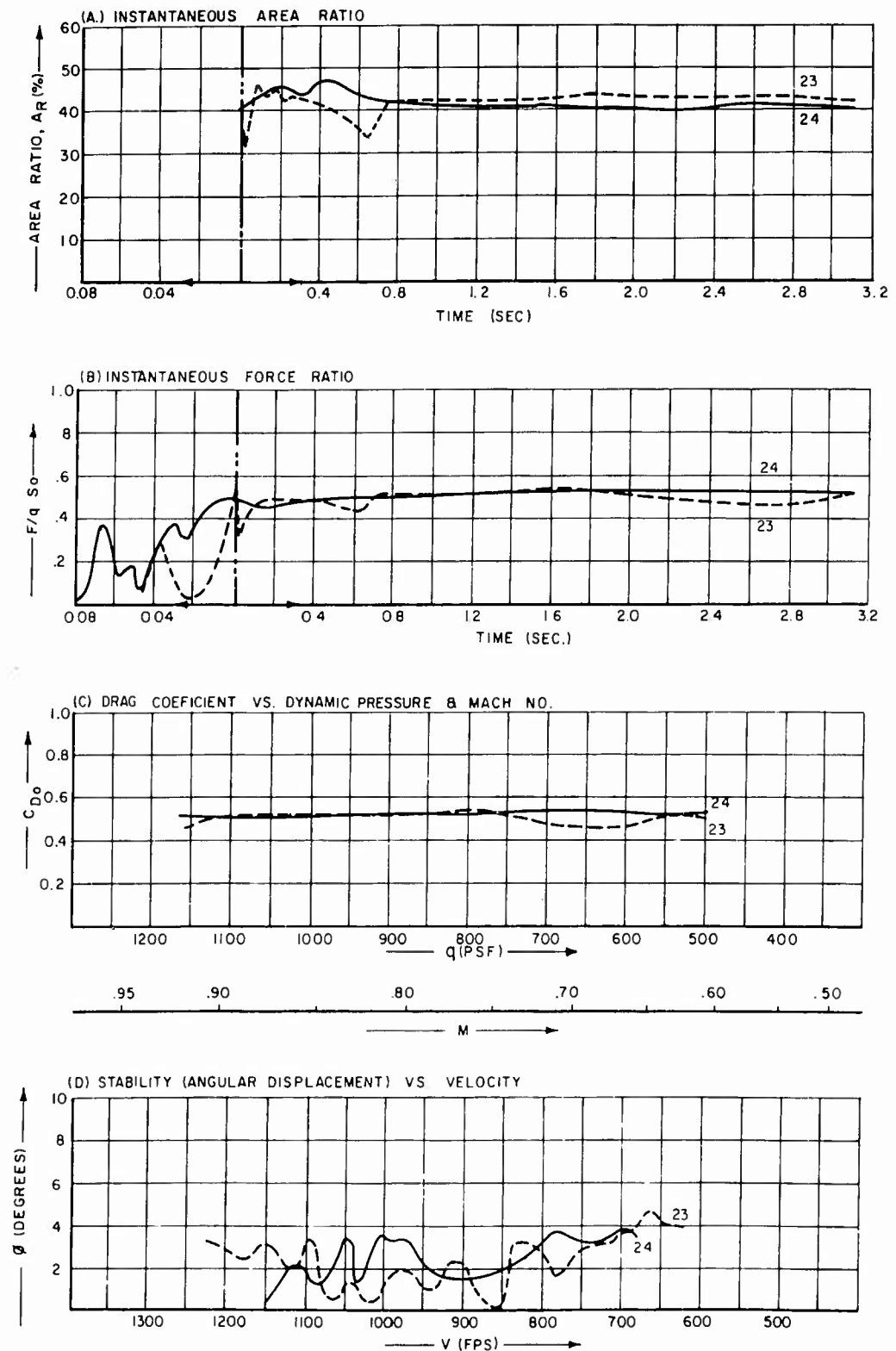


Figure 21. Performance Curves - FIST Ribbon Type FR-130 Parachute

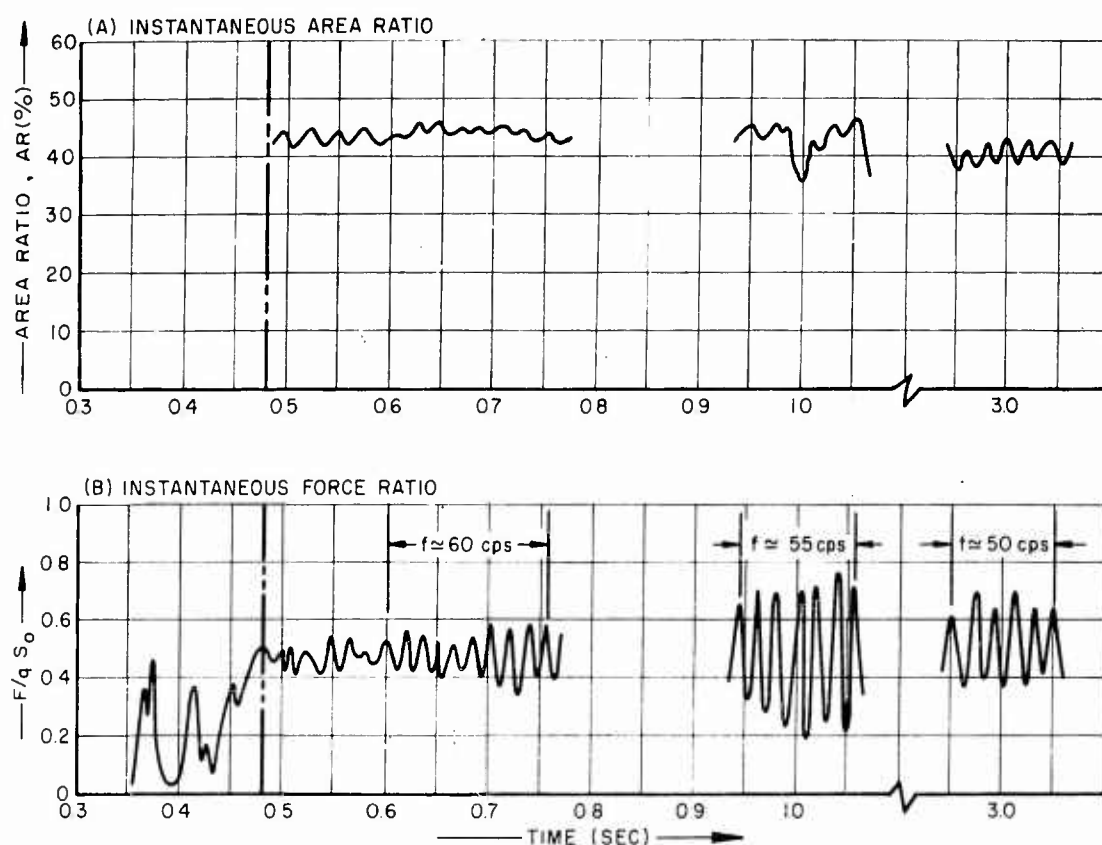


Figure 22. Performance Curves (Expanded) - FIST Ribbon Type FR-130 Parachutes

performance curves at a scale sufficiently expanded to illustrate actual oscillatory variations in parachute force and inflation characteristics.

c. FIST Ribbon Type FR-130 Triple Cluster

The FIST Ribbon Type FR-130 Triple Cluster configuration consisted of three single Type FR-130 parachutes and line systems assembled to a common confluence point on the riser. Figure 23 shows the geometry of the triple cluster configuration as used on the test vehicle in this program.

Five tests, Nos. 7, 10, 11, 15 and 19, were conducted with identical triple cluster configurations at Mach numbers ranging from 0.81 to 1.53. Generally satisfactory operation resulted on all tests.

A summary of the performance characteristics of the five

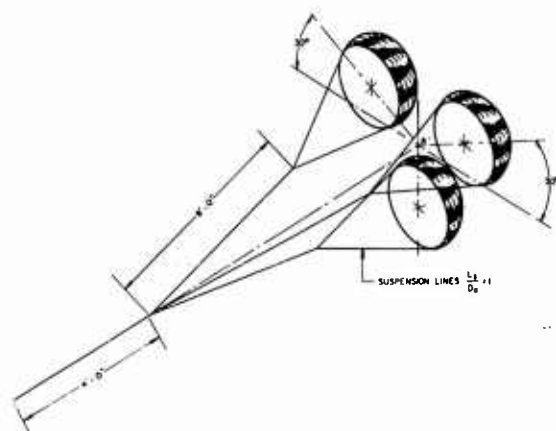


Figure 23. Geometry of Triple Cluster Configuration

cluster tests is graphically illustrated in the performance curves in Figure 24. Individual and average values of the major performance characteristics of this configuration group are recorded in Table XIV.

Supersonic deployments were attained on two of the tests with the triple cluster configuration. These tests, Nos. 11 and 15, yielded supersonic performance information as well as subsonic data. In tests 7, 10 and 19, only subsonic data were obtained.

As shown in the performance curves in Figure 24 and in Table XIV, the average subsonic drag coefficient was essentially the same in all of the cluster tests conducted. For the supersonic portions of the two tests, where this information is available, the average drag coefficients differed somewhat between the two tests. There was also some variation in the drag coefficient during each of the supersonic tests. This variation, however, appears to be a function of the inflation characteristics of the parachutes and would be expected under conditions of changing drag area.

The opening shock factor (X) was within expected limits for the subsonic deployments. The average of 0.93 shown in Table XIV does not include the subsonic figures shown for tests 11 and 15, since a subsonic value which is obtained for a supersonic deployment is characteristically lower than that for a normal subsonic deployment. This is because of the comparatively lower opening shock force which is caused by the underinflation characteristics of a parachute under supersonic deployment conditions, and because the factor is referenced to steady state subsonic conditions. Except for comparison of several tests in a series of the same configuration, the subsonic factor derived from a supersonic test is of little value.

The supersonic opening shock factor of 0.78 was the average of the factors obtained on the two tests in which supersonic operation was obtained. Like the drag coefficient, the opening shock factor is affected by the inflation characteristics of the parachute, and is generally of lower magnitude than the subsonic factor for the same parachute.

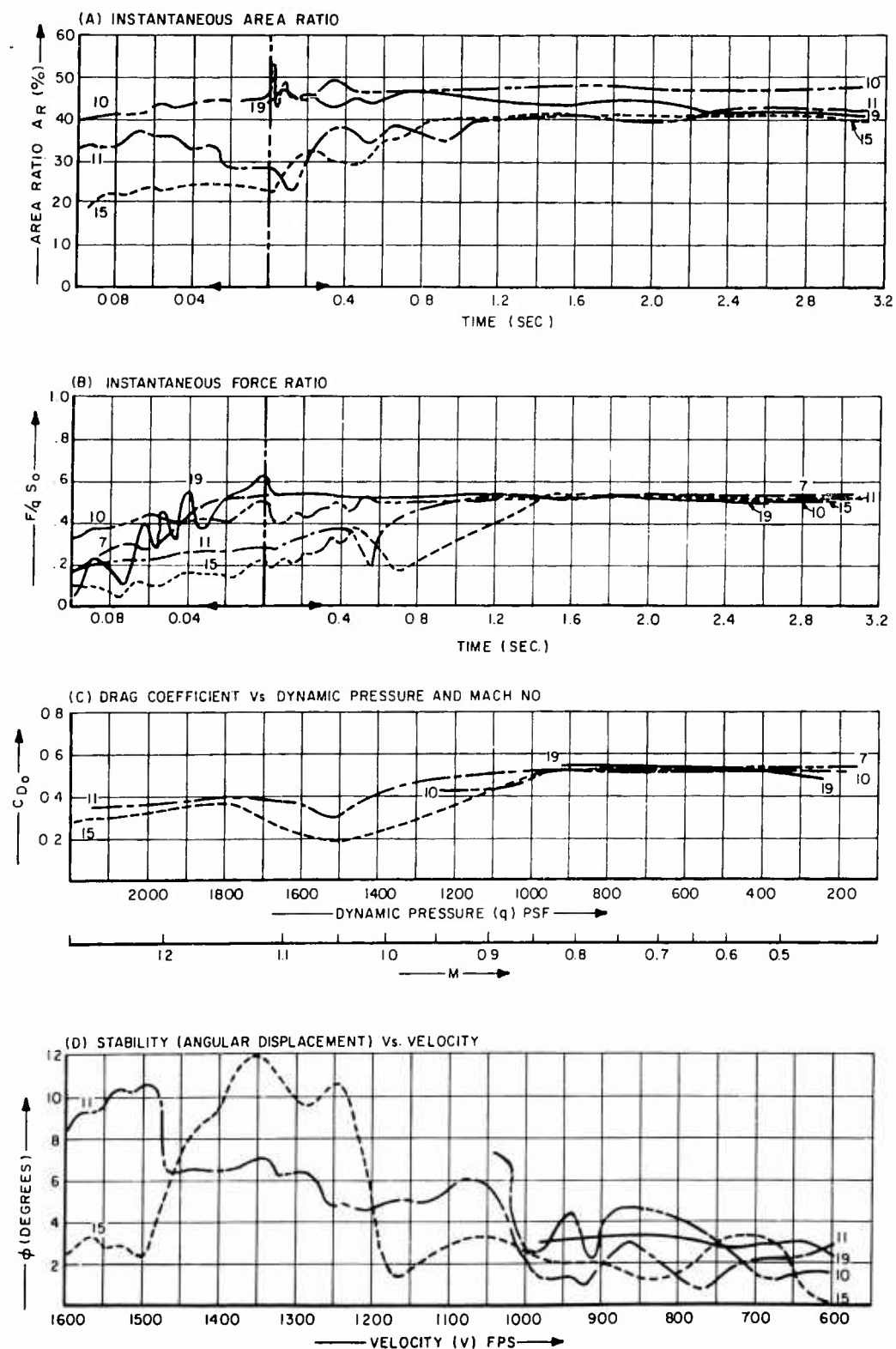


Figure 24. Performance Curves - Triple Cluster, FIST Ribbon Type FR-130 Parachutes

TABLE XIV

AVERAGE PERFORMANCE CHARACTERISTICS -
TRIPLE CLUSTER-FIST RIBBON TYPE FR-130 PARACHUTES

Test No.	Deployment Mach No.	t_f	C_{D_0}	X	A_R	\emptyset
7	0.81	~0.195	0.53	0.94	-	-
10	1.04	0.165	0.52	0.86	47	2.75 \pm 1.25
11	1.53	See Text	0.32* 0.50	0.70* -	23-35* 41	7.0 \pm 5.0 * 2.0 \pm 1.0
15	1.50	See Text	0.23* 0.52	0.87* -	25-32* 40	7.5 \pm 2.5 * 2.0 \pm 1.0
19	0.87	0.186	0.52	1.08	45	3.0 \pm 0.5
Average	-	-	0.28* 0.52	0.78* 0.93	24-34* 43.5	7.0 \pm 3.5 * 2.0 \pm 1.0

*Supersonic

As mentioned above, the drag coefficients and the opening shock factors were affected by the inflation characteristics of the parachutes under supersonic operating conditions. Although all of the tests in which inflation information was obtained yielded quite consistent data in subsonic steady state region, quite significant differences were observed between this information and the supersonic inflation data. Whereas an average subsonic steady state area ratio of 43.5 was recorded, the average for the supersonic tests was 28 percent. The supersonic average was based on rapidly changing conditions during the supersonic portion of each test. Actual area ratios varied from 23 to 35 percent on test No. 11 and from 25 to 32 percent on test No. 15. The average area ratios, like the average drag coefficients which showed similar variations are, however, representative of the typical supersonic characteristics of this parachute configuration.

Inflation time (t_f) is shown in the table for the three subsonic tests. Similar data are not shown for the supersonic tests because no definite point can be chosen in the inflation sequence, during supersonic operation, at which it can be said that maximum inflation had occurred. It is also noteworthy that in both of the supersonic tests, one or more of the parachutes in the cluster partially deflated or collapsed during the transition from supersonic to subsonic operation. The photographs in Figures 25 and 26 show the triple cluster in operation in test No. 15. In Figure 25 a standing shock wave is evident in front of the parachute cluster. There is also a second shock wave present in the photo which originates at the motor section of the test vehicle and passes over the parachute cluster. Figure 26 shows the bottom parachute of the cluster collapsing during the transition period in transonic operation. This deflation tendency is also evident in the performance curves in Figure 24.

Two deployment and inflation sequences are included for illustration. Figure 27 shows the cluster configuration being deployed at subsonic



Figure 25. Shock Waves on Clustered Parachutes - Test No. 15

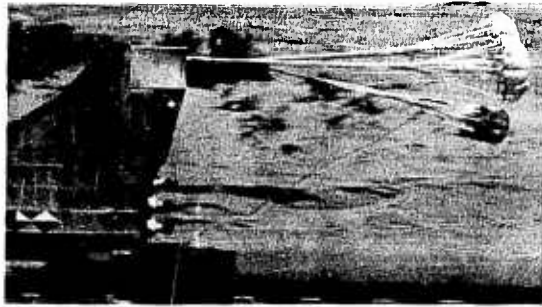


Figure 26. Collapsed Parachute Cluster on Test No. 15

velocity on test No. 7. The supersonic deployment and inflation sequence of test No. 11 is shown in Figure 28.

Four of the tests yielded information from which stability analysis could be made.

For the cluster, these analyses were made on the basis of the location of the theoretical center (Point A, Figure 23) of the cluster of three parachutes. Figure 24(d) shows the cluster stability plotted as a function of velocity. Average values of stability, in degrees, are also shown in Table XIV.

Good stability was exhibited in all tests during subsonic portions of the operations. Average stability in this regime varied from approximately 1.0 to 3.5 degrees. Much more instability was present during the supersonic portions of the two representative tests. In test No. 11, stability characteristics of the parachute improved through the test from a maximum of approximately 10 degrees to approximately five degrees at transonic. On test No. 15, the parachutes were quite stable initially but gyrated to a maximum value of approximately 12 degrees. After this gyration, the parachutes again stabilized at average angles of oscillation from two to three degrees.

Individual parachute stability within the cluster grouping was also investigated.

The most significant data that resulted from these analyses showed that the steady state position of the parachutes in the clustered configuration was between eight and 10 degrees when measured from the attachment point on the test vehicle. In terms of parachute separation, this corresponds to a center to center dimension equaling between 0.85 and 1.0 nominal diameter. In general, the cluster stability was good when single parachute stability was good. The cluster, however, was not necessarily unstable when large angles of oscillation were present in the individual parachutes, but only when these angles presented an unsymmetrical pattern.

C. Conical Ribbon Parachute

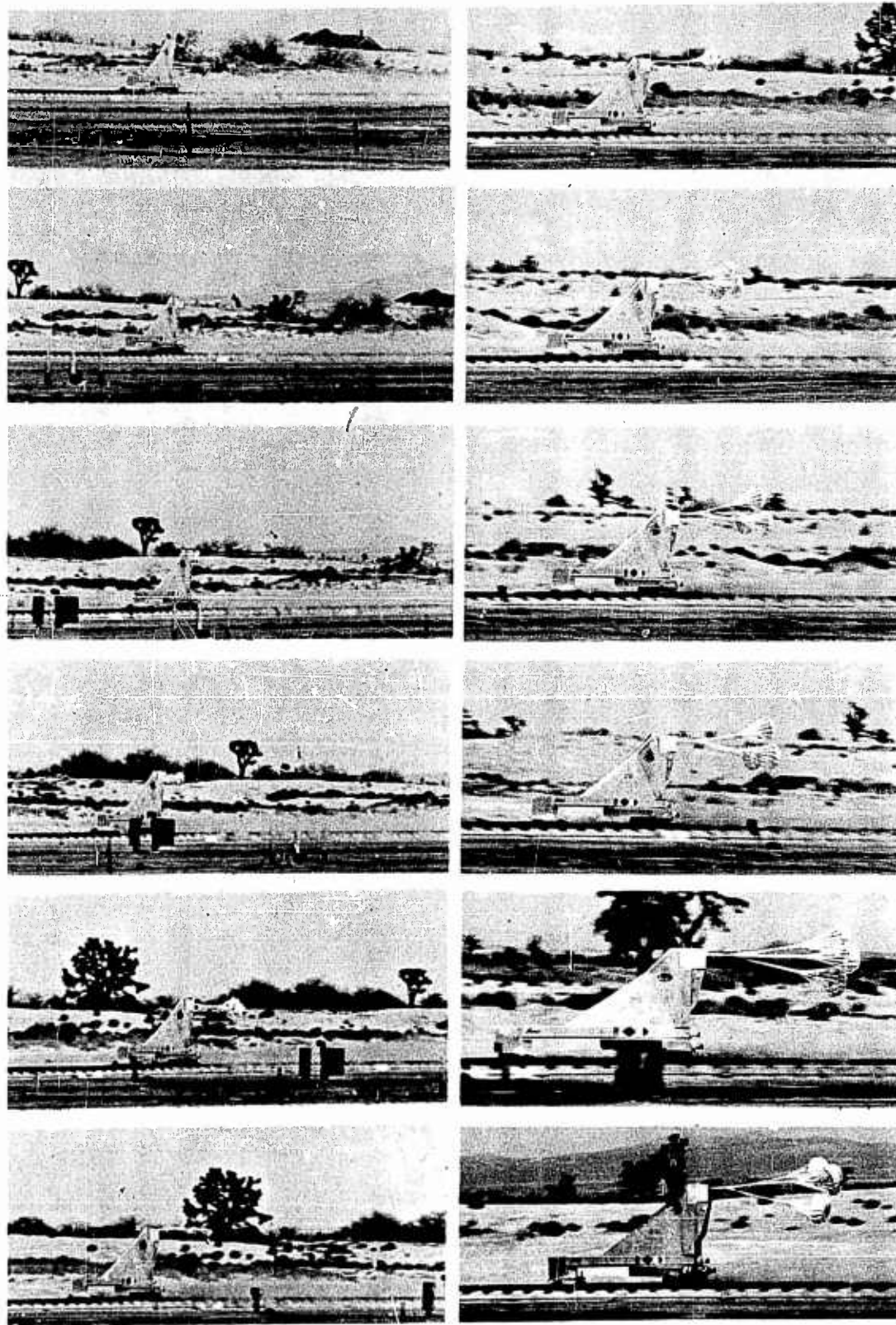


Figure 27. Subsonic Deployment and Inflation Sequence on Cluster Test No. 7



Figure 28. Supersonic Deployment and Inflation Sequence on Cluster Test No. 11

1. General

The Conical Ribbon parachute, unlike the FIST Ribbon parachute, is a shaped parachute with a design geometric shape like a right regular pyramid. The gores of the parachute, represented by the sides of the pyramid are, like the FIST design, composed of a grid of horizontal ribbons spaced and retained at close intervals by one or more vertical ribbons. Radial bands extend from the vent, or apex of the pyramid to the skirt, or base, at the sides of each gore along the edges formed by the faces of the pyramid shape. These bands join adjacent gores together and transfer the forces developed in the canopy to the attached suspension lines.

Figure 29 illustrates the geometry of a typical Conical Ribbon parachute and shows a typical gore assembly.

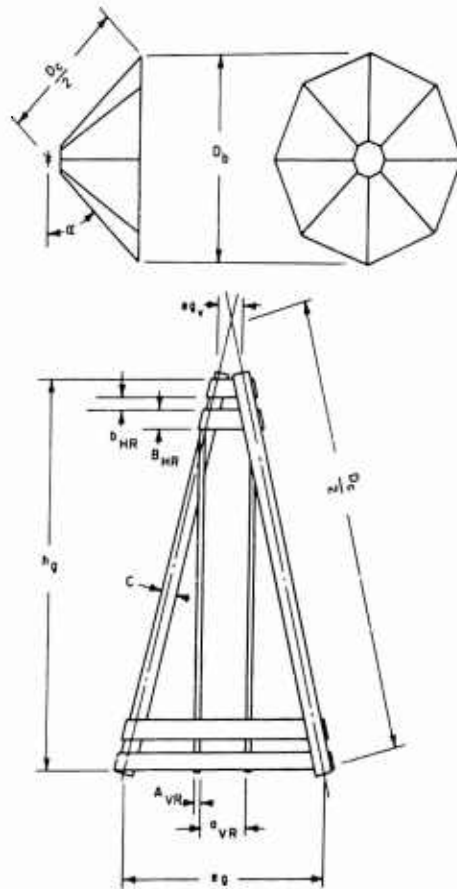


Figure 29. Typical Geometry and Gore Layout - Conical Ribbon Parachute

Construction of the Conical Ribbon parachute is based on standard FIST Ribbon procedure. Therefore, the general specification, as presented in Reference 4, is applicable.

2. Test Program

Eleven tests were conducted with the four configurations of Conical Ribbon parachutes during the program. Two of the tests were made with the 15 degree Conical Type 15CR134 parachute, and three tests each were made with the 20 degree Type 20CR128, 30 degree Type 30CR129 and 45 degree Type 45CR131 parachutes. Deployment velocities ranged from Mach number 0.76 to Mach number 1.48. All of the Conical Ribbon parachutes tested were 16 gore parachutes designed to have a subsonic drag area of approximately 16 square feet and all had geometric porosities between 25 and 26 percent.

Major dimensional details and materials used in fabrication of the

parachutes are listed in Table XV. A general list of materials and related material specifications are tabulated in Table XVI.

3. Parachute Performance

Conical Ribbon parachute performance summary data for the four parachute types used in 11 test runs are presented in Table XVII. Summary curves showing performance characteristics for each test and parachute type are graphically presented in Figures 33, 36, 41 and 44. For rapid and accurate comparison of the average characteristics of the parachute type being discussed, multiple sets of performance curves have been placed on graphs common to that configuration. This also helps to emphasize unusual behavior which should be considered in the determination of typical operational characteristics of a particular parachute configuration.

Performance details of the parachutes in the tests of each Conical Ribbon configuration group are presented in the following paragraphs.

a. 15 Degree Conical Ribbon Type 15CR134

The Conical Ribbon Type 15CR134 parachute was a 6.24 foot diameter, 16 gore conical ribbon parachute having a design apex angle of 150 degrees. The geometric porosity of this parachute was 25.2 percent. Figure 30 shows a Type 15CR134 parachute in operation.

Two tests, Nos. 25 and 26, were conducted with this configuration. In both of these tests, good deployments and inflations were obtained. Although neither test was conducted at supersonic velocity, the deployment conditions were separated sufficiently to provide information in two distinct performance ranges. The parachute in test No. 25

was deployed at Mach number 1.09 and operated through the dynamic pressure range from an initial value of 1,600 pounds per square foot. Figure 31 shows the deployment and inflation sequence of this test. The deployment in test No. 26 was at Mach number 0.76 with an initial dynamic pressure of approximately 800 pounds per

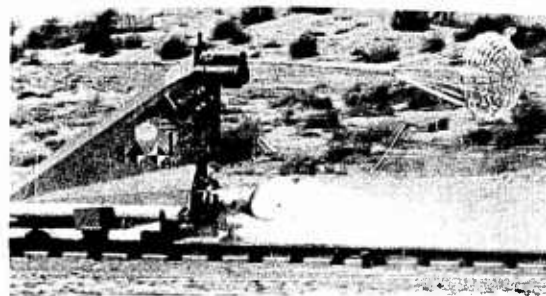


Figure 30. 15 Degree Conical Ribbon
Type 15CR128 Parachute
in Operation

TABLE XV

PHYSICAL DETAILS AND DIMENSIONS
OF CONICAL RIBBON PARACHUTES

Conical Ribbon Type	15CR134	20CR128	30CR129	45CR131
Nominal Diameter, D_o (ft)	6.24	6.24	6.07	6.18
Canopy Area, S_o (ft ²)	30.58	30.58	28.94	30.00
Geometric Porosity, λ_g (%)	25.2	25.8	25.7	25.6
No. of Gores and Suspension Lines	16	16	16	16
No. of Horizontal Ribbons	10	10	10	11
No. of Vertical Ribbons	3	3	3	3
Suspension Line Length (ft)	6.42	6.24	6.24	7.40
Length of Gore, h_g (in.)	31.53	31.78	32.10	36.0
Width of Gore at Skirt, e_g (in.)	14.5	14.3	13.4	12.26
Width of Gore at Vent, e_{gv} (in.)	2.75	2.76	2.64	2.52
Vent Line Length (in.)	11.09	11.2	10.7	11.2
Spacing between Vertical Ribbons, a_{VR} (in.)	3	3	3	3
Spacing between Horizontal Ribbons, b_{HR} (in.)	1.28	1.31	1.34	1.40
Suspension Line Material	1 x 6000	1 x 6000	1 x 6000	1 x 6000
Horizontal Ribbon Material	2 x 1500	2 x 1500	2 x 1500	2 x 1500
Vertical Ribbon Material	9/16 x 500	9/16 x 500	9/16 x 500	9/16 x 500
Radial Band Material	1-1/2 x 1500	1-1/2 x 1500	1-1/2 x 1500	1-1/2 x 1500
Horizontal Reinforcing Band Material	1-3/4 x 3600	1-3/4 x 3600	1-3/4 x 3600	1-3/4 x 3600
Reinforcing Band on Ribbon Nos.	4-7	4-7	4-7	4-7
Weight, Parachute and Lines (lbs)	20.4	21.3	20.4	20.1
Bulk, Parachute and Lines (ft ³)	1.02	1.06	1.02	1.00
CRL Specification Number	597-8414	597-8724	597-8725	597-9717
Used on Test Number	25, 26	4, 6, 21	5, 8, 22	12, 13, 18

TABLE XVI

MATERIALS USED IN CONICAL RIBBON PARACHUTES

Part	Material	Size-Strength	Specification
Horizontal Ribbons	Ribbon, Nylon	2 in. - 1500 lb	MIL-R-5608B-EIII
Vertical Ribbons	Webbing, Nylon	9/16 in. - 500 lb	MIL-W-4088-I
Radial Ribbons	Tape, Nylon	1-1/2 in. - 1500 lb	MIL-T-5038-IV
Horizontal Reinforcing	Webbing, Nylon	1-3/4 in. - 3600 lb	MIL-W-4088-VIII
Skirt Reinforcing	Webbing, Nylon	1-3/4 in. - 3600 lb	MIL-W-4088-VIII
Vent Reinforcing	Webbing, Nylon	1 in. - 6000 lb	MIL-W-4088-XVIII
Suspension Lines	Webbing, Nylon	1 in. - 6000 lb	MIL-W-4088-XVIII
Pocket Bands	Webbing, Nylon	1-3/4 in. - 3600 lb	MIL-W-4088-VIII
Thread	Nylon	FF - 16 lb	MIL-T-7807
		3 Cord - 24 lb	
		5 Cord - 40 lb	

TABLE XVII
PERFORMANCE SUMMARY DATA - CONICAL RIBBON PARACHUTES

Parachute Type Number Conical Angle, α (deg.) Geometric Porosity, λ_g (%)	15CR134		20CR128			30CR129			45CR131		
	15		20			30			45		
	25.2		25.8			25.7			25.6		
Test No.	25	26	4	6	21	5	8	22	12	13	18
Velocity, V_s (ft/sec)	1,250	886	1,174	1,464	1,239	1,161	1,657	1,195	1,165	1,211	1,126
Mach Number, M at V_s	1.087	0.756	1.045	1.300	1.081	1.044	1.480	1.043	1.026	1.081	0.979
Dynamic Pressure, q_s (lbs/ft ²)	1,600	796	1,490	2,420	1,598	1,490	2,990	1,488	1,438	1,586	1,306
Deployment Time, t_d (sec)	0.220	0.262	-	0.237	0.215	0.210	0.190	0.225	0.207	-	0.247
Inflation Time, t_f (sec)	0.110	0.080	-	0.050	0.060	0.16	0.076	0.075	0.110	0.080	0.080
Time to Opening Shock Force, t_{so} (sec)	0.109	0.083	0.154	0.048	0.060	0.194	0.076	0.071	0.096	0.085	0.081
Snatch Force, F_s (lbs)	14,531	11,161	6,490	22,900	19,139	19,846	8,375	22,651	6,828	10,150	8,100
Opening Shock Force, F_o (lbs)	24,315	18,310	22,900	36,450	24,357	21,450	38,545	26,341	19,842	28,100	18,000
Avg. Drag Coefficient, C_{Do}	0.52	0.52	0.52	0.52/0.46	0.50	0.48	0.48/0.36	0.49	0.48	0.46	0.45
Opening Shock Factor, X	0.945	1.49	0.96	-----/1.06	1.01	0.95	-----/1.20	1.24	0.96	1.28	1.00
Area Ratio, A_R (%)	45.7	46.5	45.6	45.9	44.8	49.3	45.5	44.2	38.9	38.1	39.5
Stability, θ (deg.)	2.5 \pm 1.5	4.5 \pm 1.0	2.0 \pm 1.0	2.0 \pm 1.0	3.0 \pm 2.0	2.5 \pm 2.5	2.0 \pm 2.0	4.0 \pm 3.0	4.0 \pm 1.0	4.0 \pm 3.0	5.0 \pm 2.0
Parachute Damage	Canopy		NONE	NONE	NONE	NONE	NONE	NONE	NONE	NONE	NONE
	Lines		NONE	NONE	NONE	NONE	NONE	NONE	NONE	NONE	NONE

(Subsonic/Supersonic)

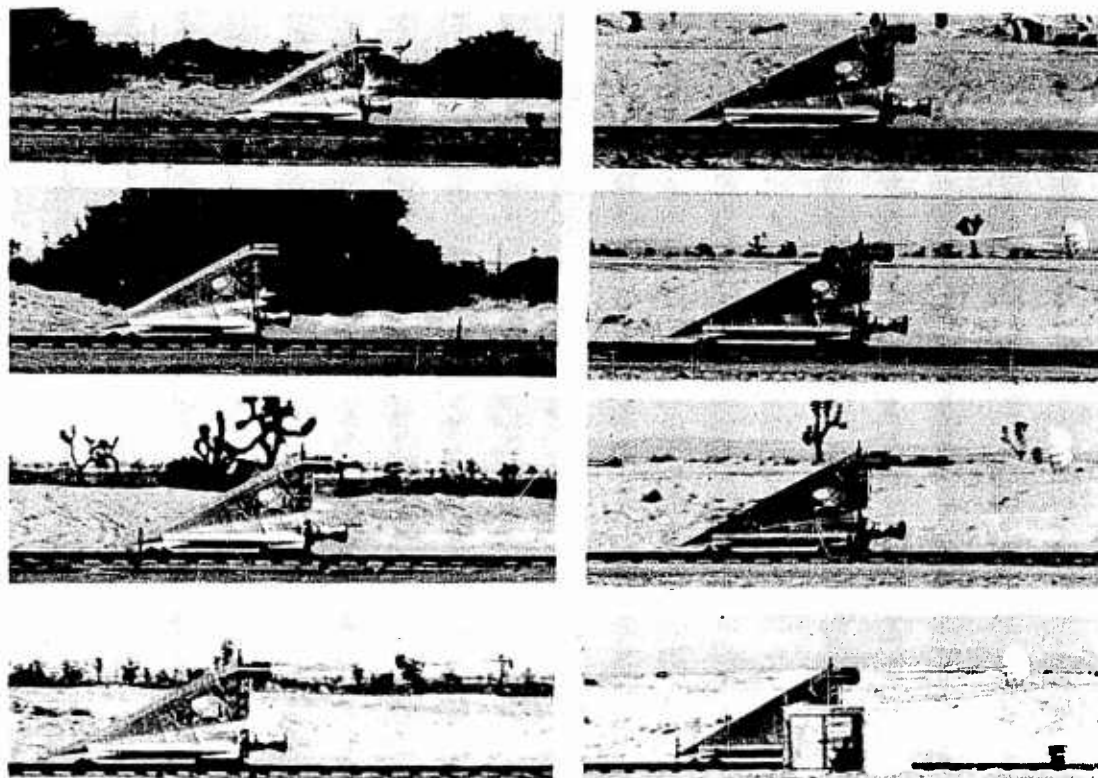


Figure 31. Deployment and Inflation Sequence, 15 Degree Conical Ribbon Type 15CR134 Parachute - Test No. 25

square foot, or half of that of test No. 25. This deployment and inflation sequence is shown in the photograph in Figure 32.

Performance curves for these two tests are shown in the graphs of Figure 33. The average performance characteristics of the 15 degree Conical Ribbon Type 15CR134 parachute as tested in this program, are given in Table XVIII.

TABLE XVIII

AVERAGE PERFORMANCE CHARACTERISTICS -
15 DEGREE CONICAL RIBBON TYPE 15CR134 PARACHUTES

Test No.	Deployment Mach No.	t_f (sec)	C_{D0}	X	AR (%)	ϕ (deg.)
25	1.087	0.11	0.52	0.94	45.7	2.5 \pm 1.5
26	0.765	0.08	0.52	1.49	46.5	4.5 \pm 1.0
Average	-	-	0.52	-	46.0	3.5 \pm 1.0

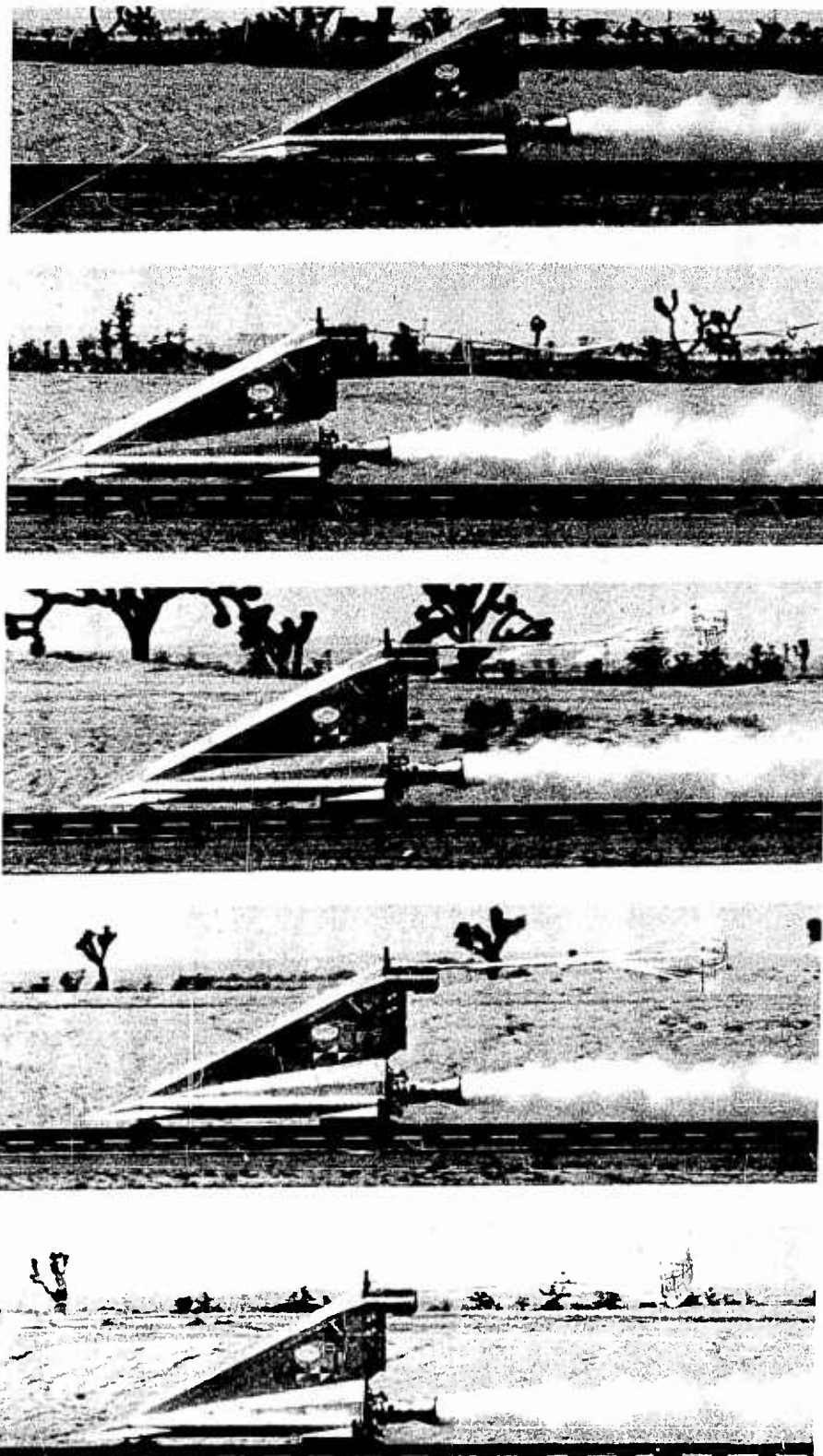


Figure 32. Deployment and Inflation Sequence, 15 Degree Conical Ribbon
Type 15CR134 Parachute - Test No. 26

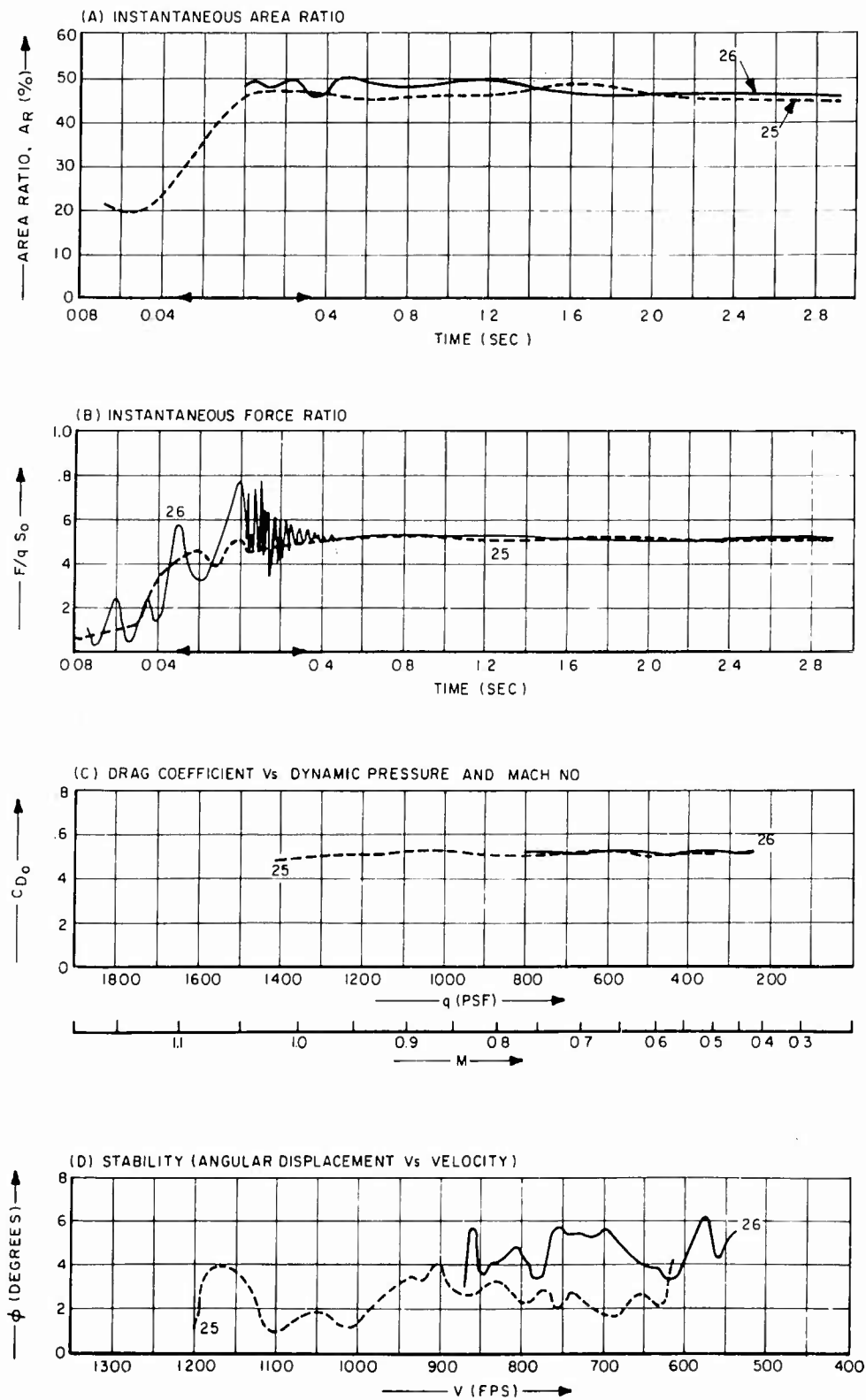


Figure 33. Performance Curves - 15 Degree Conical Ribbon Type 15CR134 Parachutes

An average drag coefficient of 0.52 was recorded on both tests with the 15 degree Conical Ribbon parachute. This average was consistent throughout the steady state portion of each test, and is consistent with the value which would be expected from this type of parachute under optimum conditions. The opening shock factor was higher than normal on test No. 26. The reason for this was not apparent in the inflation information but the instantaneous force curves show that there were considerable force variations during the inflation sequence with a peak at maximum force. Because this is not considered normal for this type of parachute, an average value for this parameter is not shown in the performance characteristics in Table XVIII. Steady state inflation characteristics were nearly identical in both tests. The average ratio was 46 percent of the nominal design area, generally as expected for a fully inflated parachute. Good stability was apparent in both tests with average oscillations of approximately one degree about a mean displacement of 3.5 degrees.

No structural damage was incurred during either test.

Generally, the 15 degree Conical Ribbon Type 15CR134 parachute exhibited good performance characteristics.

b. 20 Degree Conical Ribbon Type 20CR128

The Type 20CR128 Conical Ribbon parachute, shown in Figure 34 in operation behind the test vehicle, was a 6.24 foot diameter, 16 gore configuration having a design apex angle of 140 degrees. The geometric porosity of this parachute was 25.8 percent.



Figure 34. 20 Degree Conical Ribbon Type 20CR128 Parachute in Operation

Three tests, Nos. 4, 6, and 21 were conducted with the 20 degree conical design. Because of a premature deployment on test No. 4, deployment and inflation times were not available for this test. Based on the time to opening shock force, the inflation took somewhat longer than expected. There was, however, no evidence of abnormal operation during this process. Shortly after deployment, the parachute dipped momentarily and evidenced near collapse of three or four gores. At the same time there was significant ribbon

flutter in the skirt region. Recovery to a normal position followed immediately, and the parachute remained very stable throughout the remainder of the test.

A normal deployment and inflation was obtained on test No. 6 at a deployment velocity of Mach 1.30. Considerable pulsation, accompanied by ribbon flutter in the skirt portion of the parachute canopy, was present immediately after the parachute inflated. Both of these conditions continued, with diminishing magnitude throughout the major portion of the test.

On test No. 21 good deployment and inflation were also obtained. An operational sequence of this is shown in Figure 35.

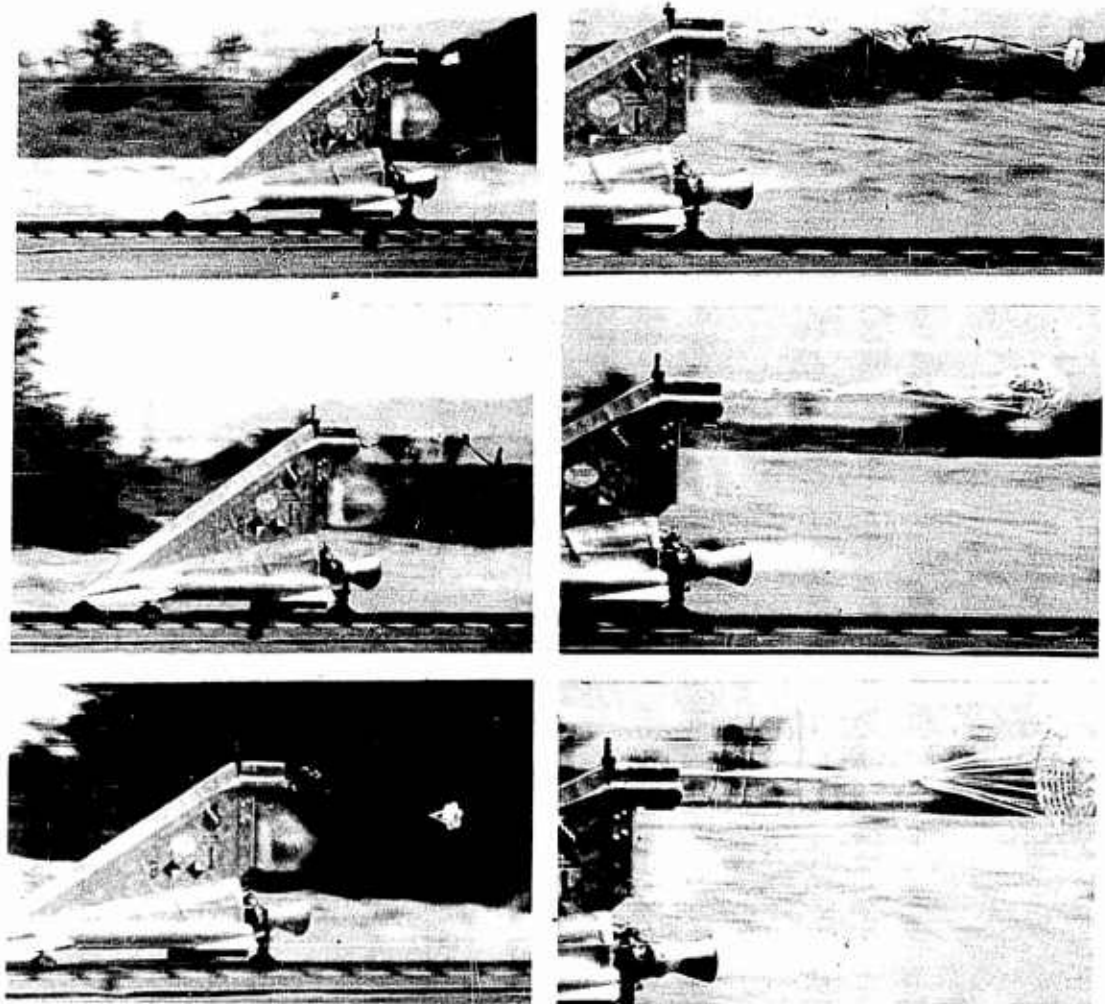


Figure 35. Deployment and Inflation Sequence, 20 Degree Conical Ribbon Type 20CR128 Parachute - Test No. 21

Test No. 6, the one test with the 20 degree conical configuration which attained supersonic deployment velocity, yielded performance information in both the transonic and subsonic ranges. The other two tests, Nos. 4 and 21 produced good subsonic data.

Summary performance data for the three tests conducted with 20 degree Conical Ribbon Type 20CR128 parachutes are shown in Figure 36. Average performance characteristics for the parachutes of this configuration, as tested in this program, are given in Table XIX. The subsonic drag coefficient of 0.51

TABLE XIX

AVERAGE PERFORMANCE CHARACTERISTICS -
20 DEGREE CONICAL RIBBON TYPE 20CR128 PARACHUTES

Test No.	Deployment Mach No.	(sec)	C_{D_0}	X	A_R (%)	ϕ (deg.)
4	1.045	-	0.52	0.96	45.6	2.0 \pm 1.0
6	1.300	0.05	0.52	0.95	45.9	2.0 \pm 1.0
21	1.081	0.06	0.50	1.01	44.8	3.0 \pm 2.0
Average	-	-	0.51	0.97	45.4	2.3 \pm 1.3

was quite consistent on the three tests and represents the average of 0.52 on two tests and 0.50 on one test. On test No. 6, the drag coefficient was about 0.46 in the high transonic portion of the test. This rose to a value of approximately 0.55 through sonic and then steadied out to the subsonic value of 0.52. The opening shock factor was essentially constant for this parachute. The average for the three tests was 0.97. Very consistent steady state area ratios were also recorded on these three tests. The average area ratio of 45.4 percent was the result of less than one percent average area ratio variation of the individual tests from that of the over-all average.

Although the canopy and line systems of these parachutes were subject to cyclic pulsation and skirt flutter at the more severe test conditions, general stability of the parachutes was very good. With the exception of the initial drop of the parachutes on test Nos. 4 and 21, the average oscillatory amplitudes about

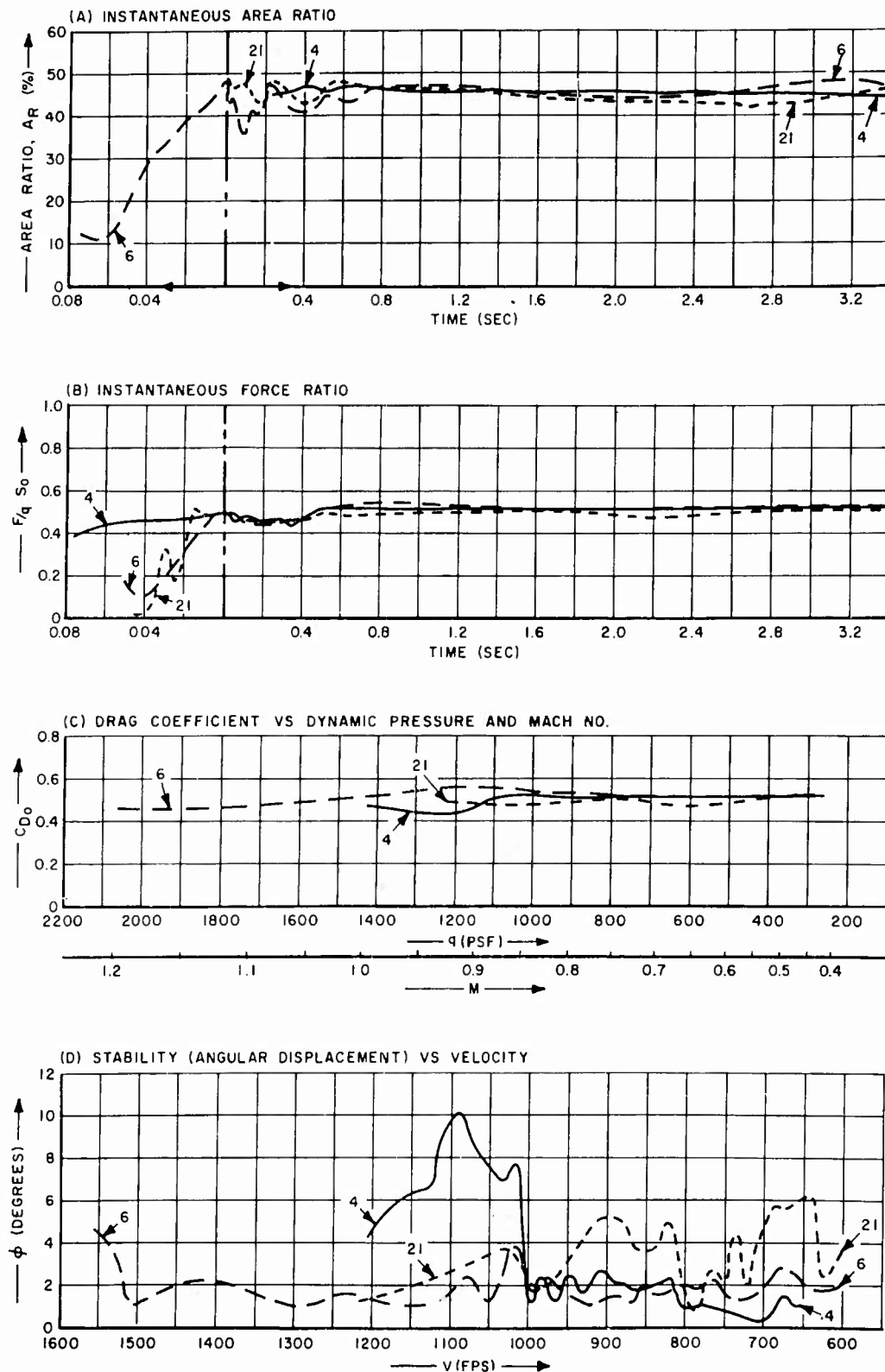


Figure 36. Performance Curves - 20 Degree Conical Ribbon Type 20CR128 Parachutes

about the mean displacement of 2.3 degrees was plus or minus 1.3 degrees.

There was no structural damage to any of the three parachutes of this configuration during the tests on this program.

Generally good performance characteristics were exhibited by the 20 degree Conical Ribbon Type 20CR128 parachutes.

c. 30 Degree Conical Ribbon Type 30CR129

The Type 30CR129 Conical Ribbon parachute, shown in Figure 37 in operation during a supersonic test, was a 6.07 foot diameter, 16 gore configuration having a design apex angle of 120 degrees and a geometric porosity of 25.7 percent.

Three tests, Nos. 5, 8 and 22 were conducted with the 30 degree conical design. On test No. 8, the parachute was deployed at Mach 1.48. Good supersonic, as well as subsonic, data were obtained on this test. On the other two tests, Nos. 5 and 22, almost identical deployment velocities, Mach 1.044 and Mach 1.043, respectively, were attained. Good, though somewhat varying data, resulted from these tests.

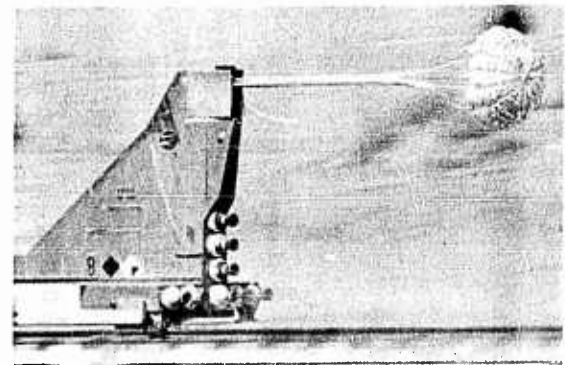


Figure 37. 30 Degree Conical Ribbon Type 30CR128 Parachute in Operation

Satisfactory deployment and inflation were obtained on all three tests. Some parachute pulsation and canopy skirt ribbon flutter was present on all tests. This was particularly in evidence at the higher test velocities and diminished as the test progressed in all cases. Sequence photographs, showing the deployment and inflation process of the 30 degree conical parachutes tested in the program, are presented in Figures 38, 39 and 40.

Summary performance data for the three tests conducted with the 30 degree Conical Ribbon Type 30CR129 parachutes are graphically illustrated in the performance curves in Figure 41. Average

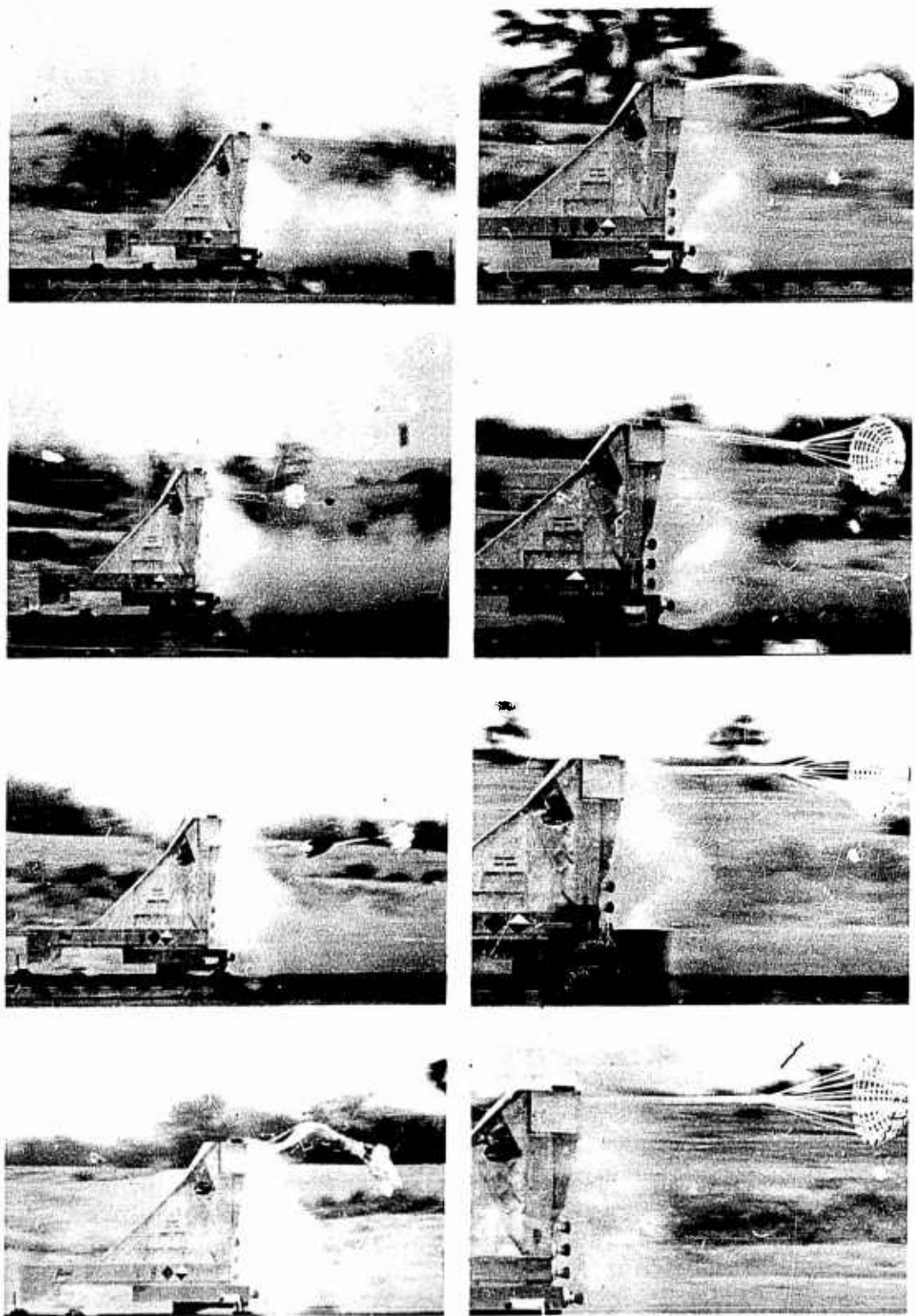


Figure 38. Deployment and Inflation Sequence, 30 Degree Conical Ribbon
Type 30CR129 Parachute - Test No. 5

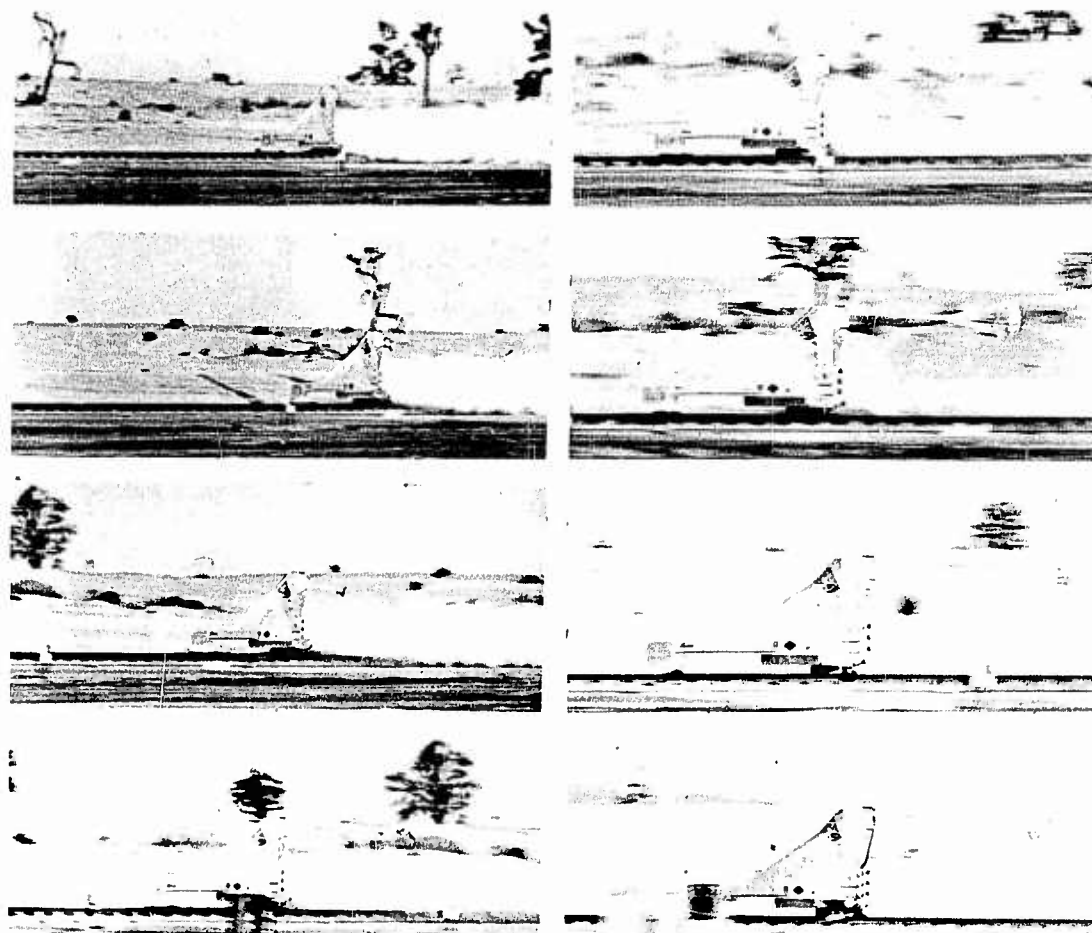


Figure 39. Deployment and Inflation Sequence, 30 Degree Conical Ribbon Type 30CR129 Parachute - Test No. 8

performance characteristics for the tests are summarized in Table XX.

TABLE XX

AVERAGE PERFORMANCE CHARACTERISTICS -
30 DEGREE CONICAL RIBBON TYPE 30CR129 PARACHUTES

Test No.	Deployment Mach No.	t_f (sec)	C_{D0}	X	A_R (%)	ϕ (deg.)
5	1.044	0.16	0.48	0.946	49.3 ¹	2.5 ± 2.5
8	1.480	0.076	0.36* 0.48	1.20* -	45.5	2.0 ± 2.0
22	1.043	0.075	0.49	1.24	44.2	4.0 ± 3.0
Average	-	-	0.36* 0.48	1.20* 1.09	44.8	2.8 ± 2.5

*Supersonic; 1 - Not used in average

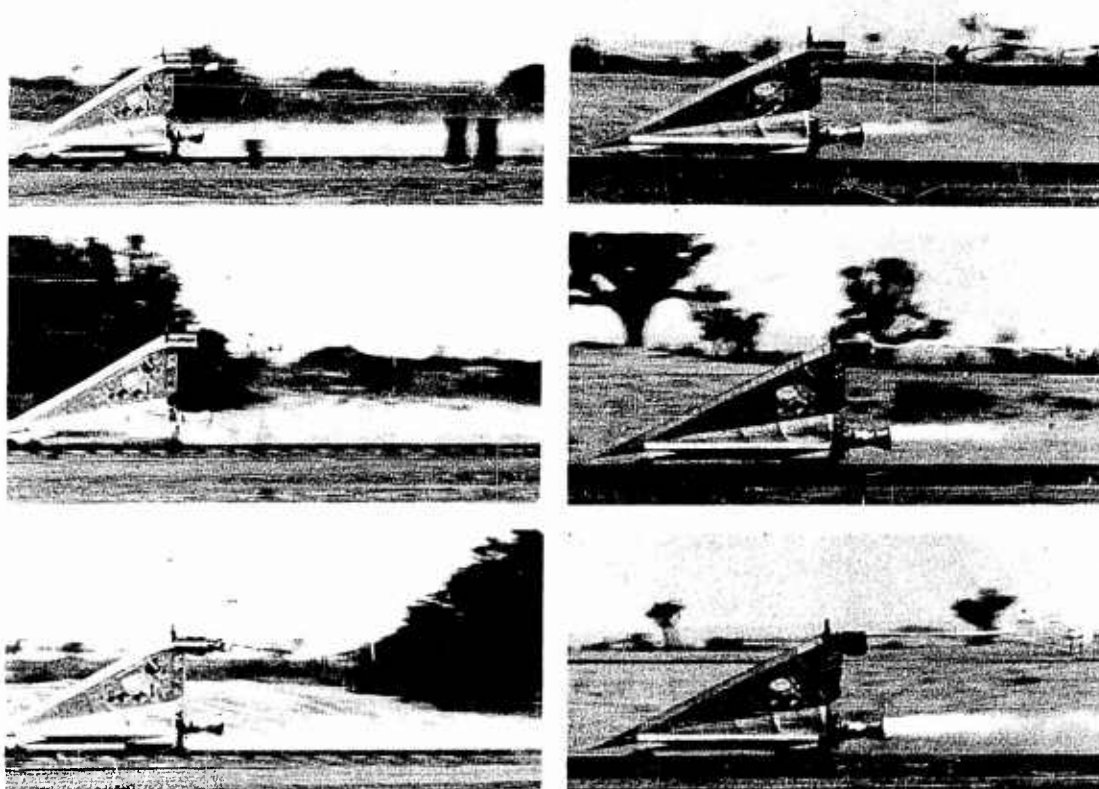


Figure 40. Deployment and Inflation Sequence, 30 Degree Conical Ribbon Type 30CR129 Parachute - Test No. 22

As shown in the curves and table, the subsonic drag coefficient was essentially the same on the three tests. In test No. 8, which also yielded supersonic results, a supersonic drag coefficient of 0.36 was recorded. The opening shock factor (X) for the supersonic inflation was 1.20. In test Nos. 5 and 22, which had essentially the same deployment Mach numbers, the opening shock factors differed considerably. There was, however, also considerable difference in the inflation times on these two tests. This difference does not necessarily reflect a true relationship because test No. 22, which had the high opening shock factor and shorter inflation time, had the more normal inflation time while test No. 5 had an excessively long inflation time, but quite normal opening shock factor. The opening shock factor shown in the table is, therefore, an average of these two scattered values and, although it is within acceptable limits should be considered with this in mind.

Steady state area ratios were reasonably consistent on the

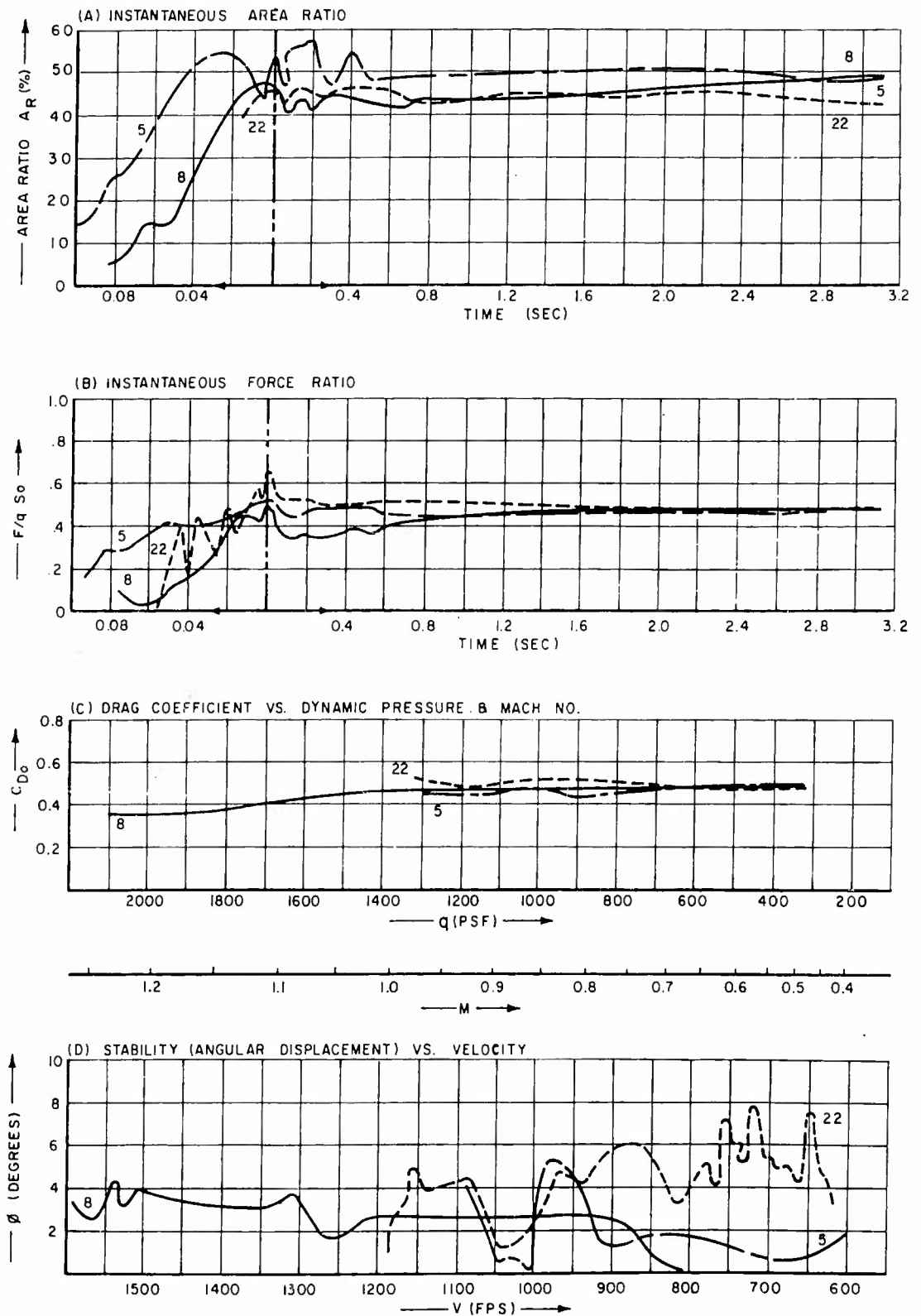


Figure 41. Performance Curves - 30 Degree Conical Ribbon Type 30CR129 Parachutes

three tests. One of the tests, No. 5, had area ratios approximately 10 percent over that of the others. Because of this, the average of 46.3 percent may be slightly higher than is indicative on the other two tests.

All three tests yielded information from which stability analysis could be made. The average mean deviation was 2.8 degrees with oscillatory amplitudes of plus or minus 2.5 degrees. With the exception of a portion of test No. 22, in which the parachute tended to drift to a mean displacement of approximately five degrees at the lower velocity end of the test, the parachutes remained within two to three degrees of neutral stability and exhibited very little tendency to oscillate.

None of the 30 degree Conical Ribbon Type 30CR129 parachutes, which were tested in the program, suffered operational structural damage.

d. 45 Degree Conical Ribbon Type 45CR131

The Type 45CR131 Conical Ribbon parachute was a 6.18 foot diameter, 16 gore configuration having a design apex angle of 90 degrees. The geometric porosity of this parachute was 25.6 percent. Figure 42 shows a parachute of this type in operation on the test vehicle.

Three tests, Nos. 12, 13 and 18 were conducted with the 45 degree conical design. On all of these tests, the parachutes were deployed at approximately the same test conditions.

On test No. 13, which should have been a supersonic deployment, the parachute deployed prematurely. Be-

cause of this, the parachute operated first under increasing dynamic pressure and then under decreasing dynamic conditions. Although the deployment was at Mach 1.08, the test vehicle and inflated parachute accelerated to Mach 1.36 test conditions.



Figure 42. 45 Degree Conical Ribbon Type 45CR131 Parachute in Operation

Satisfactory deployment and inflation were obtained on all three of the tests. Sequence photos, showing the deployment and inflation of the test parachute on test No. 12, are shown in Figure 43.

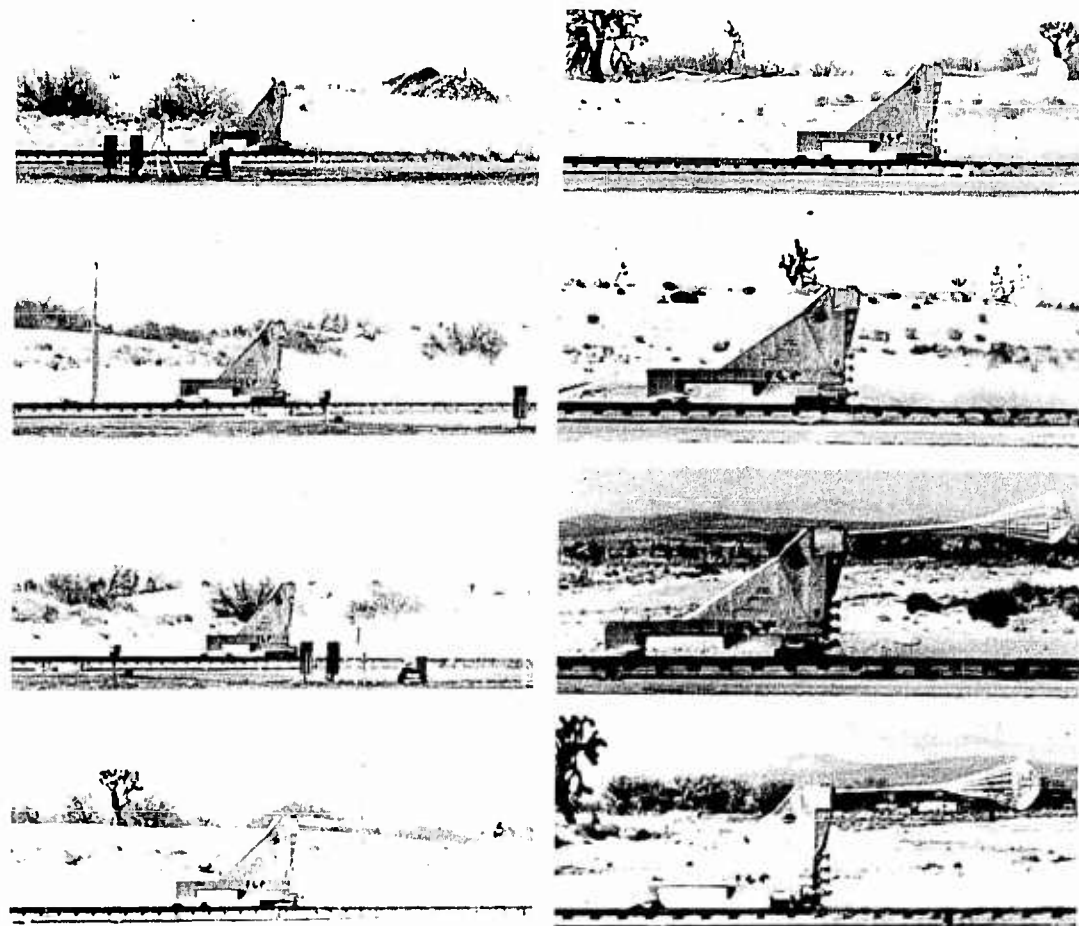


Figure 43. Deployment and Inflation Sequence, 45 Degree Conical Ribbon Type 45CR131 Parachute in Operation

Summary performance data for the three tests conducted with the 45 degree Conical Ribbon Type 45CR131 parachutes are graphically presented in Figure 44. Average performance characteristics for the tests are summarized in Table XXI.

TABLE XXI

AVERAGE PERFORMANCE CHARACTERISTICS -
45 DEGREE CONICAL RIBBON TYPE 45CR131 PARACHUTES

Test No.	Deployment Mach No.	t_f (sec)	C_{Do}	X	AR (%)	ϕ (deg.)
12	1.026	0.11	0.48	0.965	38.9	4.0 \pm 1.0
13	1.081	0.08	0.46	1.28	38.1	4.0 \pm 3.0
18	0.979	0.08	0.46	0.997	39.5	5.0 \pm 2.0
Average	-	-	0.47	0.98	38.8	4.0 \pm 2.0

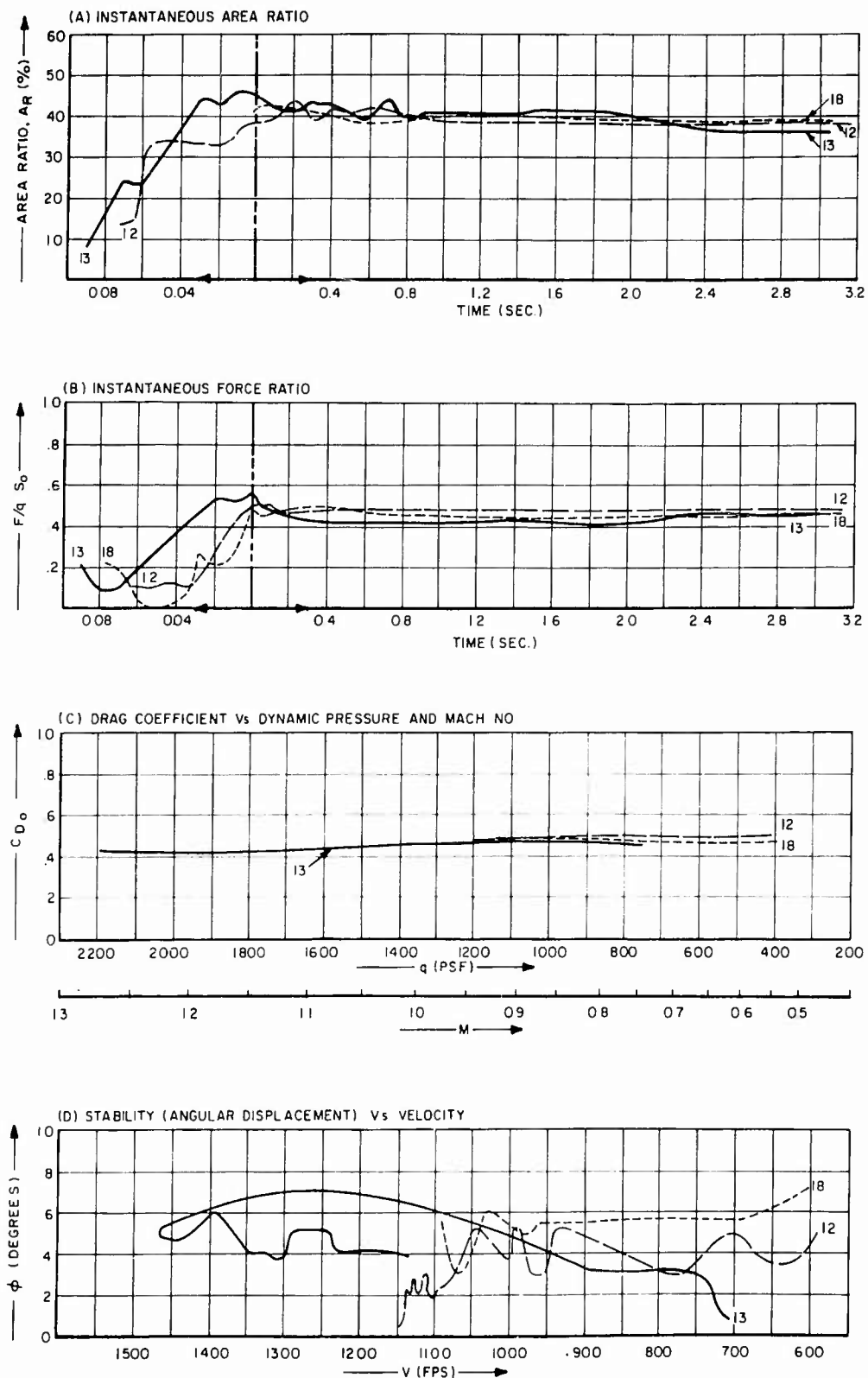


Figure 44. Performance Curves - 45 Degree Conical Ribbon Type 45CR131 Parachutes

The subsonic drag coefficients were essentially the same on the three tests. Test No. 13, in which the parachute deployed prematurely and operated under conditions of acceleration, showed a somewhat lower drag coefficient during this operation. The opening shock factor (X) for this test was also higher than expected under normal deployment conditions. Because this was a special case, this value is not included in the average shown for the 45 degree conical configuration. Good agreement was obtained on the other two tests, so these results were used as the basis of the average shown in Table XXI.

Steady state area ratios were consistent on the tests. All were within one percent of the average area ratio of 38.8 percent.

No significant pulsation or skirt flutter was in evidence on any of the tests conducted with the 45 degree conical configuration. Stability measurements from the three tests showed an average displacement of approximately four degrees with deviations from this mean value of plus or minus two degrees. For test No. 13, the stability curve shows the angular displacement of the parachute during both the acceleration and deceleration portion of the test. Except for a slow three degree drift during the deceleration period, the parachute on this test remained within plus or minus one degree of its mean position.

All of the 45 degree Conical Ribbon Type 45CR131 parachutes, which were tested in the three tests conducted during the program, remained structurally intact. There was no operational damage to canopy or lines on any of the tests.

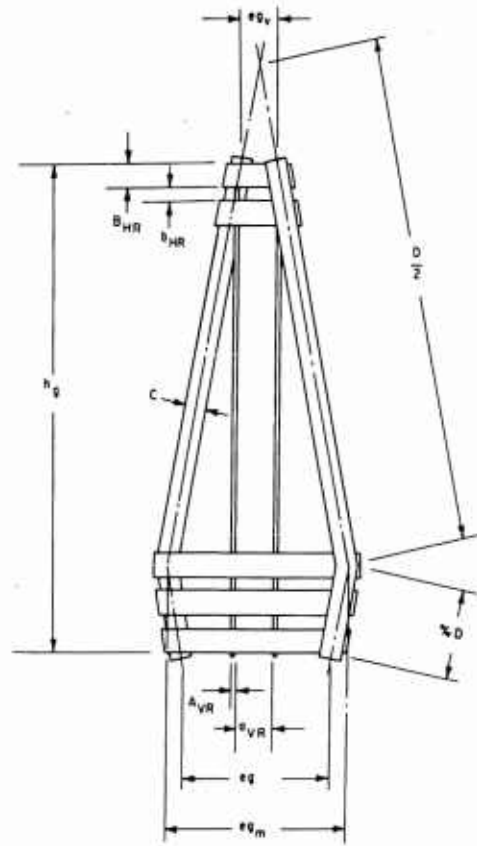
D. Equiflo Parachute

1. General

The Equiflo design is a FIST Ribbon type full extended skirt parachute. It is basically a flat circular design with a skirt extension added to the areas between adjacent suspension lines. The extension is expressed in percent of constructed diameter and establishes the percent extension as a part of the nomenclature of this particular parachute design. When the parachute is assembled the extensions form a truncated cone below the basic flat circular roof portion of the canopy.

The individual gore is constructed as a continuous flat assembly, and consists of a triangular portion, which represents the roof of the canopy, and a trapezoidal portion which represents the skirt extension.

Based on standard FIST Ribbon construction, each gore is a grid of horizontal ribbons spaced and retained at regular intervals by one or more vertical ribbons. Radial bands extend from the vent to the skirt at the sides of each gore to join the gores together in the canopy assembly. These bands transfer the forces developed in the gore assemblies to the suspension lines. Figure 45 illustrates a typical Equiflo parachute gore assembly.



2. Test Program

Three tests were conducted with Equiflo parachutes during the program. Two of these tests were performed with 6.20 foot diameter, 16 gore Type ESR-132 design having a 10 percent fully extended skirt and a geometric porosity of 25.8 percent. The third test was conducted with a Type ESR-133 design, which was identical to the original parachute, except for the addition of butterfly reinforcements at the suspension line canopy connections. Both of the Equiflo configurations which were tested were designed with two diameter suspension line lengths, ($L_s/D = 2$). The Equiflo Type ESR-132 parachutes were tested at deployment velocities of Mach 1.05 and 1.57. The ESR-133 design was deployed at a test Mach number of 1.07.

Figure 45. Typical Gore Assembly, Equiflo Parachute

All Equiflo parachutes which were fabricated for the test program were constructed in accordance with the specification of MIL-P-6635 (Reference 4). Major dimensional details of the parachutes and materials used in this construction are shown in Table XXII.

A general listing of materials and the corresponding specifications are tabulated in Table XXIII.

3. Parachute Performance

Equiflo parachute performance summary data for the three tests

TABLE XXII

PHYSICAL DETAILS AND DIMENSIONS OF EQUIFLO PARACHUTES

Equiflo Type	ESR-132	ESR-133
Nominal Diameter, D_0 (ft)	6.20	6.20
Canopy Area, S_0 (ft ²)	30.19	30.19
Geometric Porosity, λ_g (%)	25.8	25.8
No. of Gores and Suspension Lines	16	16
No. of Horizontal Ribbons	10	10
No. of Vertical Ribbons	3	3
Suspension Line Length (ft)	10.7	10.7
Length of Gore, h_g (in.)	31.54	31.54
Width of Gore at Skirt, e_g (in.)	11.32	11.32
Width of Gore at Vent, e_{gv} (in.)	2.8	2.8
Max. Width of Gore, e_{gm} (in.)	12.50	12.50
Vent Line Length (in.)	11.40	11.40
Spacing between Vertical Ribbons, a_{VR} (in.)	3.0	3.0
Spacing between Horizontal Ribbons, b_{HR} (in.)	1.28	1.28
Suspension Line Material	1 x 6000	1 x 6000
Horizontal Ribbon Material	2 x 1500	2 x 1500
Vertical Ribbon Material	9/16 x 500	9/16 x 500
Radial Band Material	1-1/2 x 1500	1-1/2 x 1500
Horizontal Reinforcing Band Material	1-3/4 x 3600	1-3/4 x 3600
Reinforcing Band on Ribbon Nos.	4-7	4-7
Weight, Parachute and Lines (lbs)	20.7	20.7
Bulk, Parachute and Lines (ft ³)	1.03	1.03
CRL Specification Number	597-9774	596-0049
Used on Test Number	16, 17	20

TABLE XXIII
MATERIALS USED IN EQUIFLO PARACHUTES

Part	Material	Size-Tensile Strength	Specification
Horizontal Ribbon	Ribbon, Nylon	2 in. - 1500 lb	MIL-R-5608D-EIII
Vertical Ribbon	Webbing, Nylon	9/16 in. - 500 lb	MIL-W-4088
Radial Ribbons	Tape, Nylon	1-1/2 in. - 1500 lb	MIL-T-5038-IV
Horizontal Reinforcing	Webbing, Nylon	1-3/4 in. - 3600 lb	MIL-W-4088-VIII
Skirt Reinforcing	Webbing, Nylon	1-3/4 in. - 3600 lb	MIL-W-4088-VIII
Vent Reinforcing	Webbing, Nylon	1 in. - 6000 lb	MIL-W-4088-XVIII
Suspension Lines	Webbing, Nylon	1 in. - 6000 lb	MIL-W-4088-XVIII
Thread	Nylon	FF - 16 lb 3 Cord - 24 lb 5 Cord - 40 lb	MIL-T-7807

conducted with these designs are presented in Table XXIV. Summary curves showing performance characteristics for each test are graphically presented in Figure 46.

A discussion of the performance of the parachutes in the tests of each configuration are discussed in the following paragraphs.

a. Equiflo Type ESR-132, ESR-133

Three tests, Nos. 16, 17 and 20, were conducted with these configurations. In all three of these tests, good deployments were obtained.

Immediately after initial inflation on test No. 16, three gores in the lower portion of the parachute appeared underinflated. There was also slight pulsation and pronounced skirt flutter during the initial portion of the test. The pulsations were damped rapidly and the skirt flutter diminished as the test progressed. Minor stitching damage was incurred to the test parachute at several junctures of the suspension line, skirt and vent reinforcements.

On test No. 17 severe damage to the canopy during inflation resulted in partial collapse of the parachute. Figure 47 shows the parachute in operation shortly after canopy failure occurred. Although this damage is considered to be operational, there is some question whether or not contributory factors were involved. Just prior to deployment, at a velocity of approximately Mach 1.6, a small bird impacted with the front fairing of the test vehicle. This caused the ruptured fairing to explode and separate from the vehicle. About the same time that the debris was leaving the sled, the parachute was deployed. Existing photo data alone are not sufficient to determine precise sequence of events. However, correlation of photo data and recorded data indicates that the time required to deploy the parachute would have been sufficient to allow the initial mass of debris to clear the vehicle and test parachute zone. If some parts of the disintegrated fairing were delayed in tearing loose from the fairing attachments, it is possible that some such piece could have entered the parachute. On the other hand, there was no evidence on the tested canopy that any sizeable piece of metal had been in contact with the material. The type of damage, mostly stitching failures and minor tears, also indicated that the damage was operational.

Because of the failure of the parachute on test No. 17, limited performance data were obtained.

TABLE XXIV

PERFORMANCE SUMMARY DATA - EQUIFLO PARACHUTES

Parachute Type Number		ESR-132		ESR-133
Geometric Porosity, λ_g (%)		25.8		25.8
Test Number		16	17	20
Velocity, V_s (ft/sec)		1,184	1,797	1,226
Mach Number (M) at V_s		1.052	1.567	1.071
Dynamic Pressure, q_s (lbs/ft ²)		1,509	3,339	1,571
Deployment Time, t_d (sec)		0.150	0.134	0.250
Inflation Time, t_f (sec)		0.120	0.090	0.080
Time to Opening Shock Force, t_{s_o}		0.120	0.084	0.080
Snatch Force, F_s (lbs)		13,748	13,669	10,056
Opening Shock Force, F_o (lbs)		20,315	29,340	26,009
Avg. Drag Coefficient, C_{D_o}		0.485	-	0.51
Opening Shock Factor, X		0.92	-	1.08
Area Ratio, A_R (%)		46.1	-	45.0
Stability, ϕ (deg.)		1.0 \pm 0.8	-	2.0 \pm 1.6
Parachute Damage	Canopy	Stitching loose at skirt-lines connection	Severe stitching damage - some-ribbon tears	NONE
	Lines	NONE	NONE	NONE

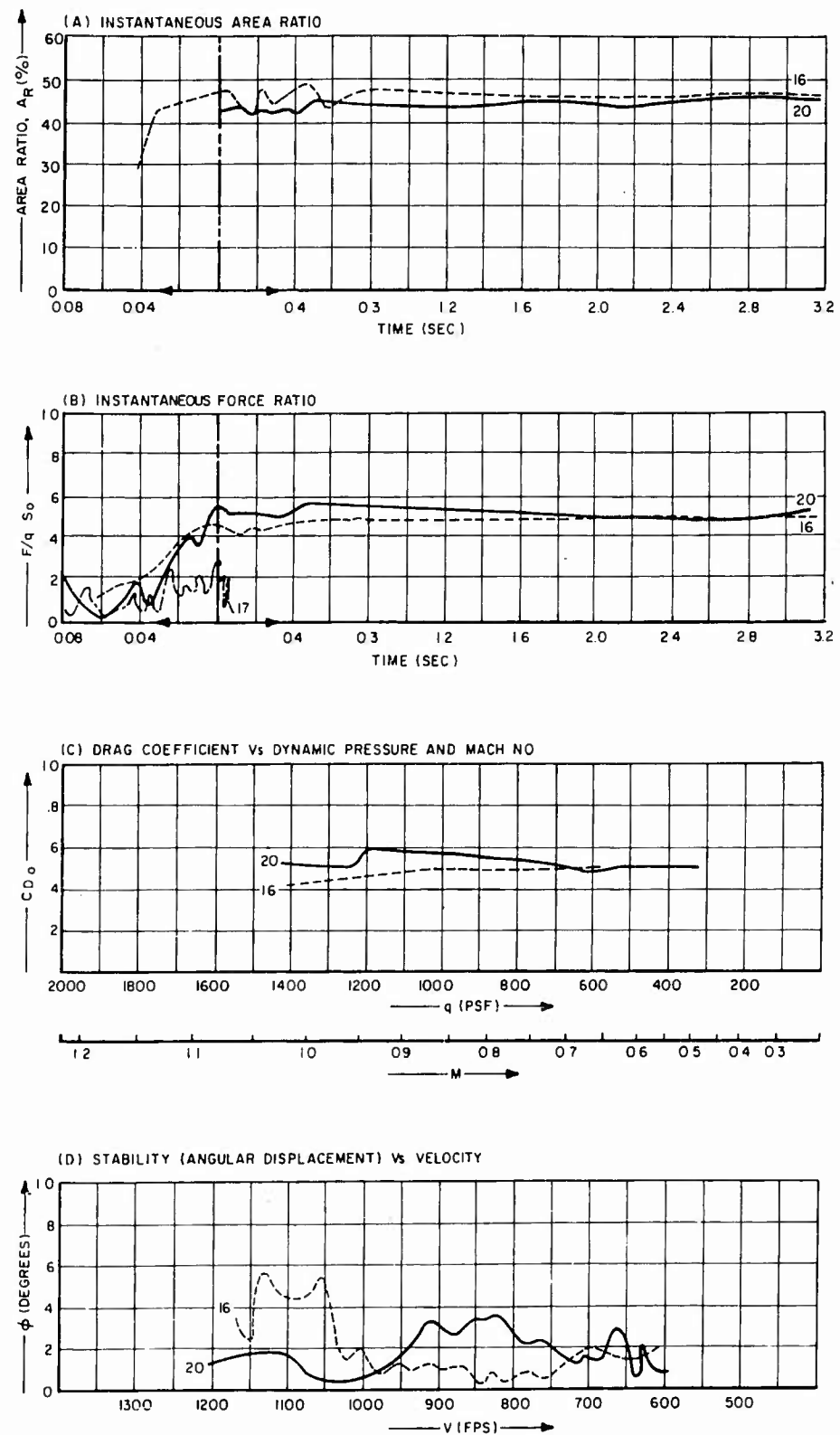


Figure 46. Performance Curves - Equiflo Type ESR-132, 133 Parachutes

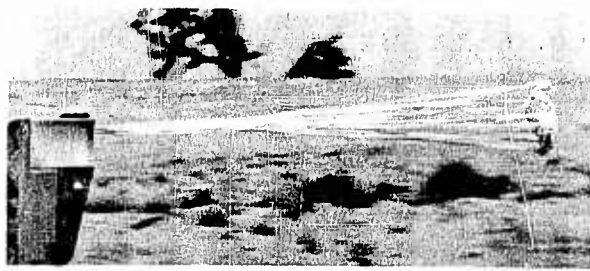


Figure 47. Equiflo Type ESR-132
Parachute in Operation -
Test No. 17

In test No. 20 there was slight evidence of skirt flutter immediately after deployment. This was predominant only in the lower portion of the parachute and did not last very long. A photographic sequence of the deployment and inflation of the parachute on this test is shown in Figure 48.

Performance curves for the tests with Equiflo parachutes are shown in the graphs in Figure 46. Average performance characteristics are summarized in Table XXV.

TABLE XXV

AVERAGE PERFORMANCE CHARACTERISTICS -
EQUIFLO TYPE ESR-132, 133 PARACHUTES

Test No.	Deployment Mach No.	t_f (sec)	C_{D0}	X	A_R (%)	ϕ (deg.)
816	1.052	0.12	0.49	0.92	46.1	1.0 ± 0.8
820	1.071	0.08	0.51	1.08	45.0	2.0 ± 1.6
Average	-	-	0.50	1.00	45.5	1.5 ± 1.2

An average drag coefficient of 0.50 is shown for this parachute configuration. Although the averages from the two tests were very close to this, there was considerable difference in the drag coefficient values in the higher velocity portions of the individual tests. The opening shock factors were within eight percent of the average value of 1.0 on the two tests. This is considered to be quite consistent for this parameter and is within the expected range for this type of parachute. Steady state area ratios were also consistent on these tests. The average of 45.5 percent represents a variation of only one percent total area ratio difference on the two tests from which such information was available. General stability of this parachute design was very good. With the exception of a momentary whip in the system on test No. 16, the mean displacement averaged approximately 1.5 degrees. Average oscillatory deviations about this displacement were plus or minus 1.2 degrees.

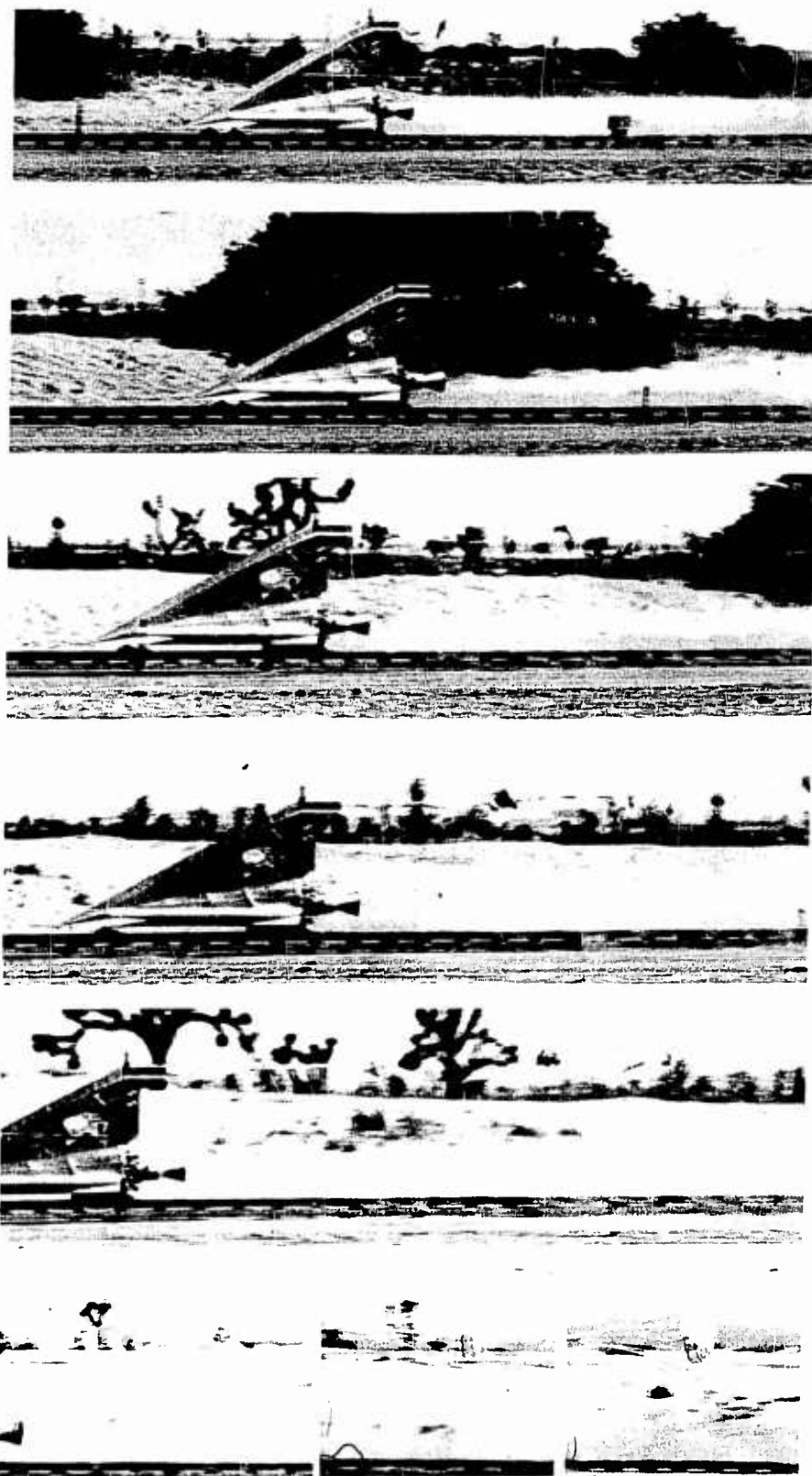


Figure 48. Deployment and Inflation Sequence, Equiflo Type ESR-133 Parachute - Test No. 20

E. Hemisflo Parachute

1. General

The Hemisflo design is a ribbon type full extended skirt hemispherical parachute. It is a hemispherical shape above the equator with a skirt extension added to the areas between adjacent suspension lines. The skirt extensions are expressed in percent of the basic constructed diameter and become part of the nomenclature of this parachute as percent extension. The constructed diameter is the circumferential distance of the hemispherical portion, measured from skirt to skirt over the apex of the parachute. Suspension line length is also related to this diameter.

The individual gore is constructed as a continuous flat assembly from dimensional characteristics of the shaped gore. Because of the flexibility of the nylon material, little error is introduced.

Based on standard FIST Ribbon construction, each gore is a grid of horizontal ribbons spaced and retained at regular intervals by one or more vertical ribbons. Radial bands extend from the vent to the skirt at the sides of each gore to join the gores together in the canopy assembly. These bands transfer the forces developed in the canopy to the suspension lines. Figure 49 shows a typical Hemisflo parachute gore assembly.

2. Test Program

Only one test, the last in the program, was conducted with the Hemisflo parachute. The EHR-134 design was a 6.24 foot diameter, 16 gore configuration having a 10 percent fully extended skirt and a geometric porosity of 25.4 percent. Suspension lines were two diameter length, ($L_S/D_0 = 2$).

The Hemisflo parachute which was fabricated for the test was constructed in accordance with the specifications of MIL-P-6635 (Reference 4). Major dimensional details of the parachute and materials used in its construction are shown in Table XXVI. Corresponding material specifications are

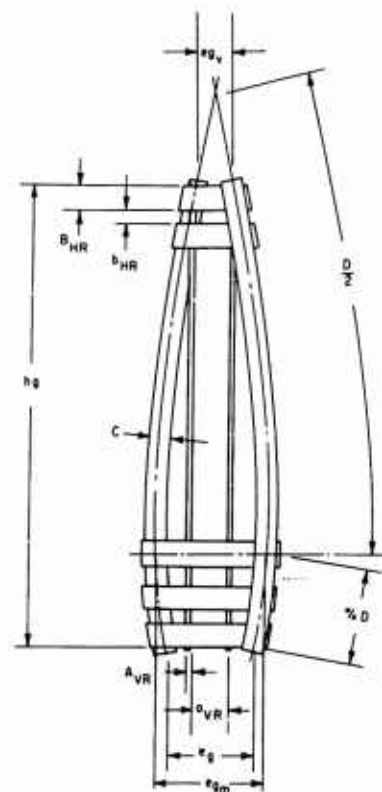


Figure 49. Typical Gore Assembly - Hemisflo Parachute

TABLE XXVI

PHYSICAL DETAILS AND DIMENSIONS OF HEMISFLO PARACHUTES

Hemisflo Type	EHR-135
Nominal Diameter, D_0 (ft)	6.24
Canopy Area, S_0 (ft ²)	30.58
Geometric Porosity, λ_g (%)	25.4
No. of Gores and Suspension Lines	16
No. of Horizontal Ribbons	12
No. of Vertical Ribbons	1
Suspension Line Length (ft)	12.25
Length of Gore (in.)	36.93
Width of Gore at Skirt, e_g (in.)	8.70
Width of Gore at Vent, e_{gv} (in.)	2.86
Max. Width of Gore, e_{gm} (in.)	9.12
Vent Line Length (in.)	11.25
Spacing between Vertical Ribbons, a_{VR} (in.)	-
Spacing between Horizontal Ribbons, b_{HR} (in.)	1.175
Suspension Line Material	1 x 6000
Horizontal Ribbon Material	2 x 1500
Vertical Ribbon Material	9/16 x 500
Radial Band Material	1-1/2 x 1500
Horizontal Reinforcing Band Material	1-3/4 x 3600
Reinforcing Band on Ribbon Nos.	4-7
Weight, Parachute and Lines (lbs)	19.4
Bulk, Parachute and Lines (ft ³)	0.97
CRL Specification Number	596-0325
Used on Test Number	27

TABLE XXVII

MATERIALS USED IN HEMISFLO PARACHUTES

Part	Material	Size-Strength	Specification
Horizontal Ribbons	Ribbon, Nylon	2 in. - 1500 lb	MIL-R-56080-EIII
Vertical Ribbons	Webbing, Nylon	9/16 in. - 500 lb	MIL-W-4088-I
Radial Ribbons	Tape, Nylon	1-1/2 in. - 1500 lb	MIL-T-5038-IV
Horizontal Reinforcing	Webbing, Nylon	1-3/4 in. - 3600 lb	MIL-W-4088-VIII
Skirt Reinforcing	Webbing, Nylon	1-3/4 in. - 3600 lb	MIL-W-4088-VIII
Vent Reinforcing	Webbing, Nylon	1 in. - 6000 lb	MIL-W-4088-XVIII
Suspension Lines	Webbing, Nylon	1 in. - 6000 lb	MIL-W-4088-XVIII
Thread	Nylon	FF - 16 lb	MIL-T-7807
		3 Cord - 24 lb	
		5 Cord - 40 lb	

tabulated in Table XXVII.

3. Parachute Performance

Parachute performance summary data for the one test (No. 27) conducted with the Hemisflo parachute are presented in Table XXVIII. Summary curves showing performance characteristics of the parachute on this test are graphically presented in Figure 50.

TABLE XXVIII
PERFORMANCE SUMMARY DATA
HEMISFLO PARACHUTES

Parachute Type Number		EHR-135
Geometric Porosity, λ_g (%)		25.4
Test Number		27
Velocity, V_s (ft/sec)		875
Mach Number (M) at V_s		0.765
Dynamic Pressure, q_s (lbs/ft ²)		794
Deployment Time, t_d (sec)		0.266
Inflation Time, t_f (sec)		-
Time to Opening Shock Force, t_{S_0} (sec)		0.081
Snatch Force, F_s (lbs)		7,504
Opening Shock Force, F_o (lbs)		15,204
Avg. Drag Coefficient, CD_o		0.51
Opening Shock Factor, X		1.23
Area Ratio, A_R (%)		37.5
Stability, ϕ (deg.)		3.0 \pm 2.0
Parachute Damage	Canopy	NONE
	Lines	NONE

Deployment and inflation were normal on this test. After the parachute inflated initially, it maintained an essentially constant inflated shape throughout the test. The average steady state area ratio was 37.5 percent.

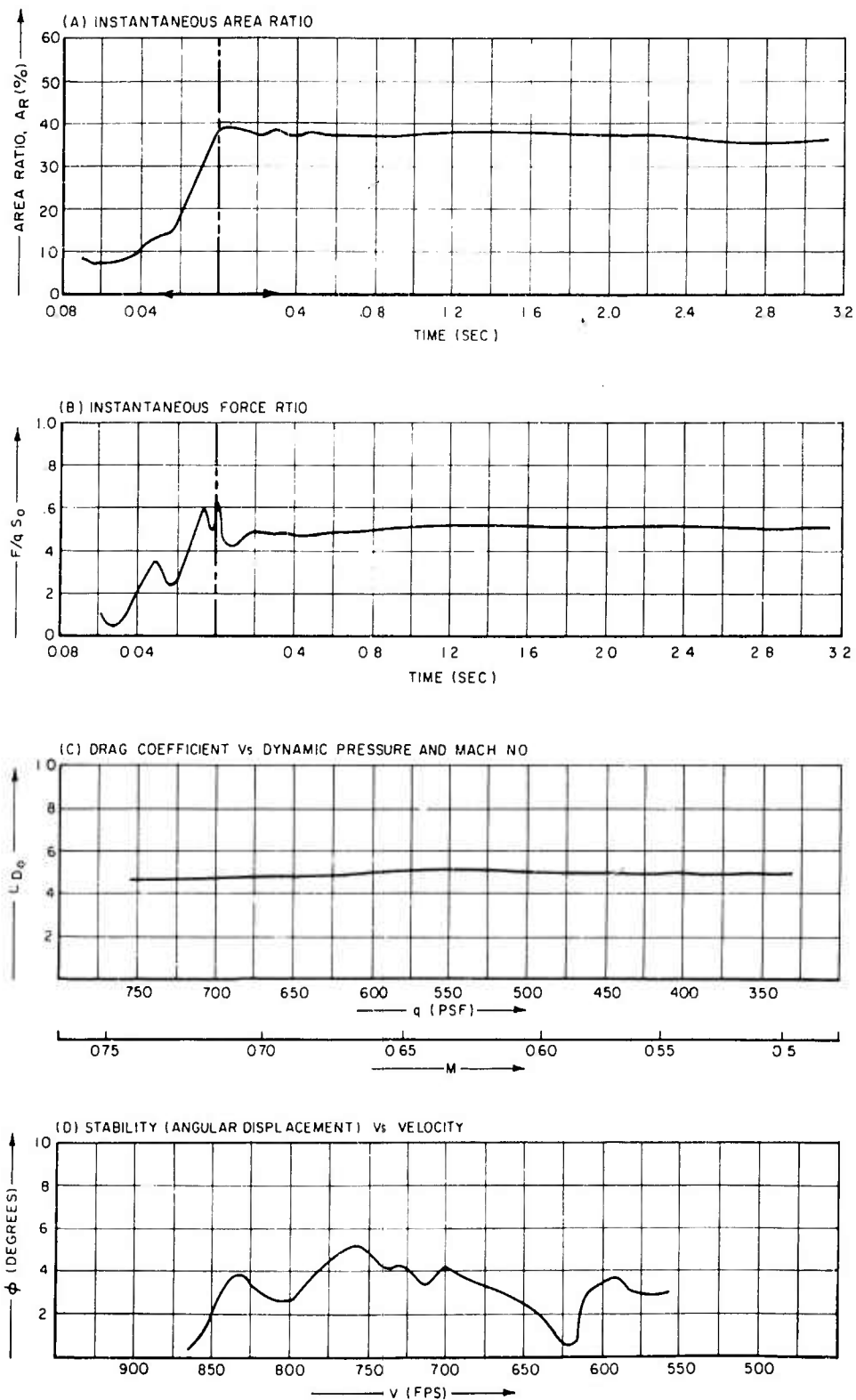


Figure 50. Performance Curves - Hemisflo Type EHR-135 Parachute

Figure 51 shows this parachute in operation shortly after deployment. The opening shock factor for the parachute on this test was 1.23. Since it represents only one test, it cannot be established as an average for the Hemisflo design. The average steady state drag coefficient was 0.51. General stability of the parachute on this test was good. The mean displacement averaged approximately three degrees. Oscillatory deviations from this mean were approximately plus or minus two degrees.

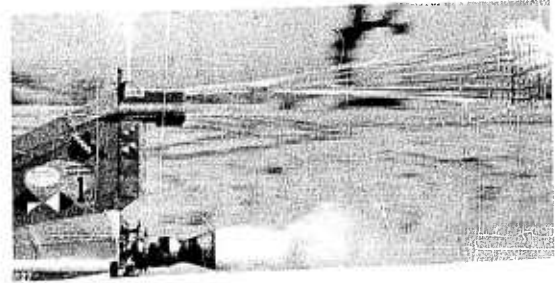


Figure 51. Hemisflo Type EHR-135 Parachute in Operation - Test No. 27

APPENDIX I

PARACHUTE DEPLOYMENT AND RELEASE SYSTEMS

A. Deployment System

All of the parachutes which were tested in this program were deployed directly aft from the test vehicle with a gun initiated pilot parachute deployment system. The gun projectile was used to remove the compartment cover by its initial rearward movement in the gun barrel. Continuing its rearward movement, the projectile and cover assembly pulled the pilot parachute bag away from the negative pressure region immediately behind the parachute compartment and into the air stream aft of the test vehicle. As the rearward travel was stopped, the inertia of the cover assembly removed the bag from the pilot parachute allowing it to inflate. At the same time an acceleration lock, attached to the pilot parachute riser, was released from the harness assembly holding the test parachute pack in the compartment. The pilot parachute riser, now attached to the parachute pack through a bridle of heavy webbing, pulled the test parachute pack from the compartment and aft from the vehicle. To assure an orderly, lines first deployment, the vent of the test parachute was secured to the inside of the parachute pack by a break line attached to the vent lines of the parachute and to the pack bridle confluence point. A pictorial diagram and physical details of the components and operation of the gun-pilot parachute deployment system is shown in Figure 52. Figure 53 shows the components of the system prior to packing and assembly in the test vehicle.

Although there was some variation in the physical shape of the parachute compartments on the two test vehicles which were used during the program, general compartment size, cover arrangement, and gun deployment system were the same. The compartment on the Tomahawk test vehicle, used on test Nos. 1 through 17, is shown in Figure 54. The solid metal cover was fabricated from 0.064-2024 aluminum sheet with an aluminum channel locking bar riveted to the vertical centerline of the cover.

To position the cover and restrict its movement, the locking bar fits into a grooved tab on the lower edge of the compartment. The upper edge of the cover was fitted with an angle which mated with the upper inside surface of the compartment when the cover was in place. This fitting was secured with cover attachment shear screws which further restricted the cover assembly against longitudinal or lateral movement. The locking bar also extended above the top of the compartment directly in line with the gun assembly. This permitted the gun projectile to be connected to the bar through a U-bolt arrangement attached to the bar.

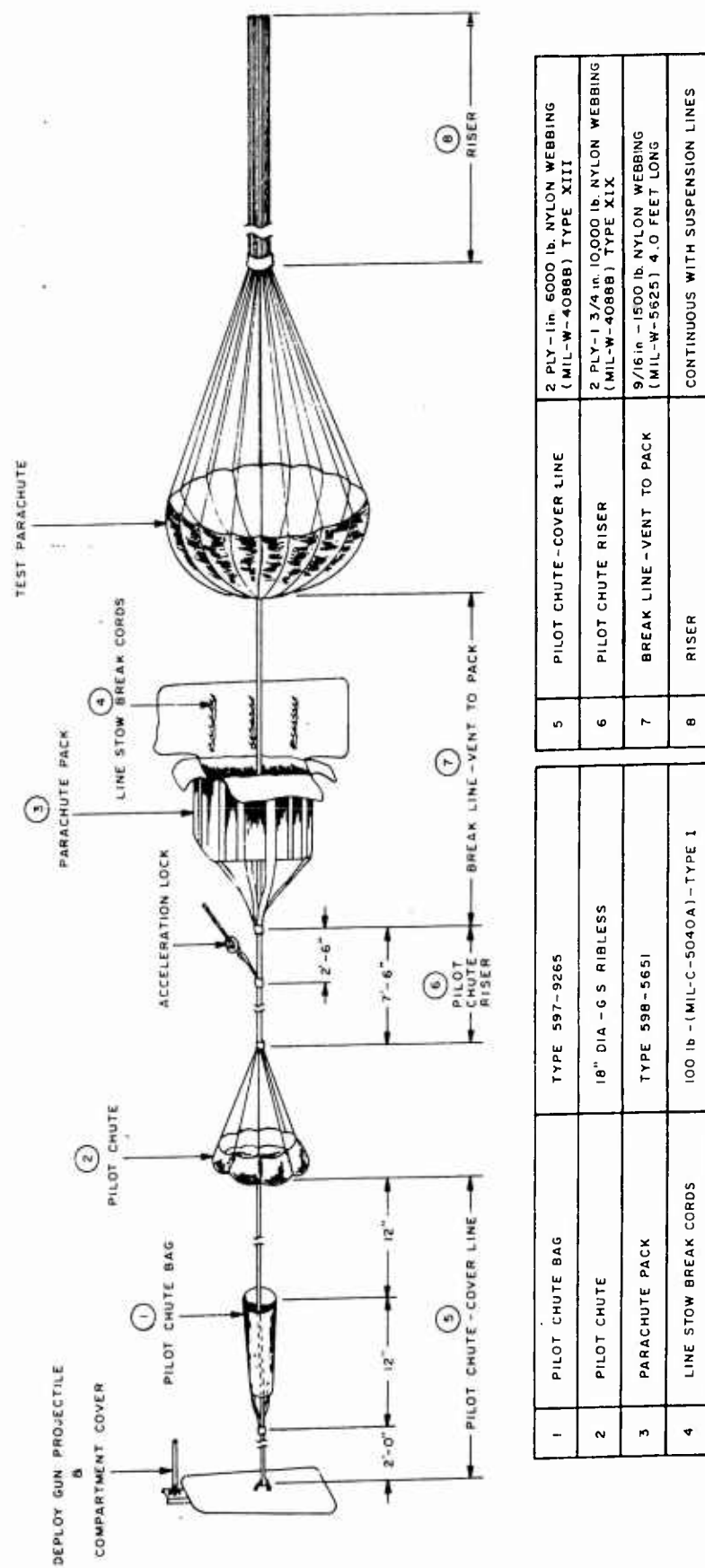


Figure 52. Pictorial Diagram of Deployment System

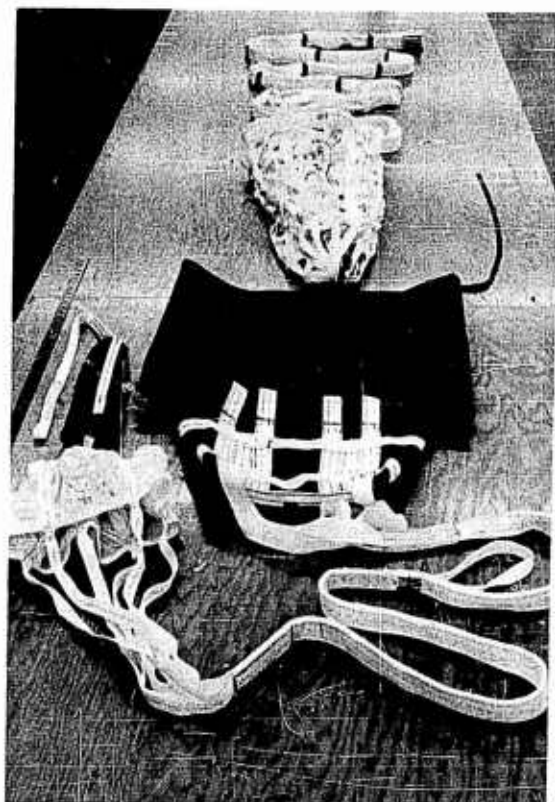


Figure 53. Components of Deployment System on Table Prior to Packing

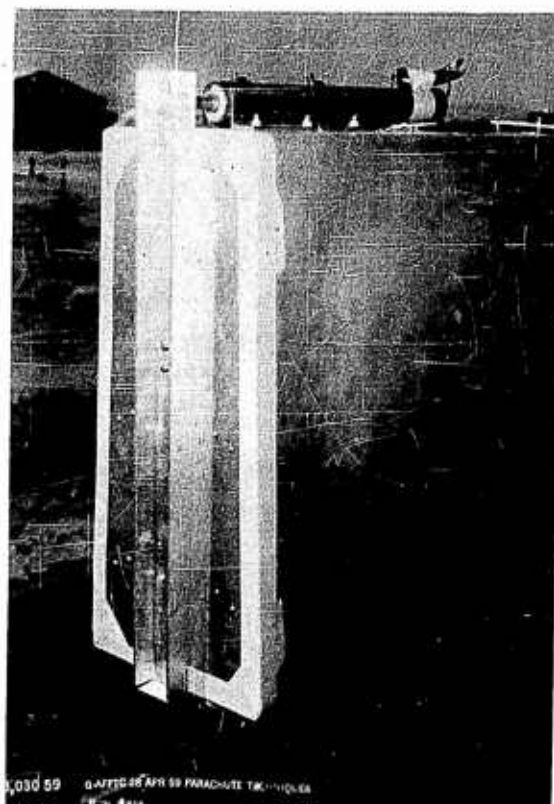


Figure 54. Parachute Compartment - Tomahawk Sled

Except for the location of the deployment gun, a similar arrangement for securing the cover to the compartment of the LOX-I test vehicle was used on test Nos. 18 through 27. As shown in Figure 55, the deployment gun on this vehicle was installed on the underside of the compartment.

Details of a deployment gun, typical of that used in all of the tests in this series, are shown in Figure 56. The cartridge for the gun was developed by Cook Research Laboratories for this particular application and contained a two gram charge of 80/20 mixture of bulk smokeless/black powder propellant. Ignition was accomplished by dual DuPont type S-65 electric fireworks squibs.

A flat rectangular type parachute pack was used on all tests conducted on

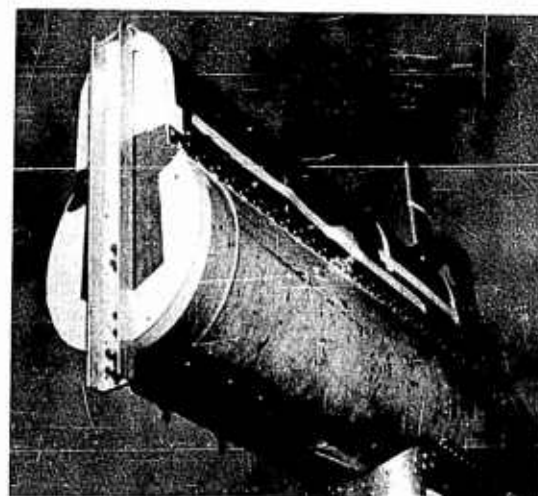


Figure 55. Parachute Compartment - LOX-I Sled

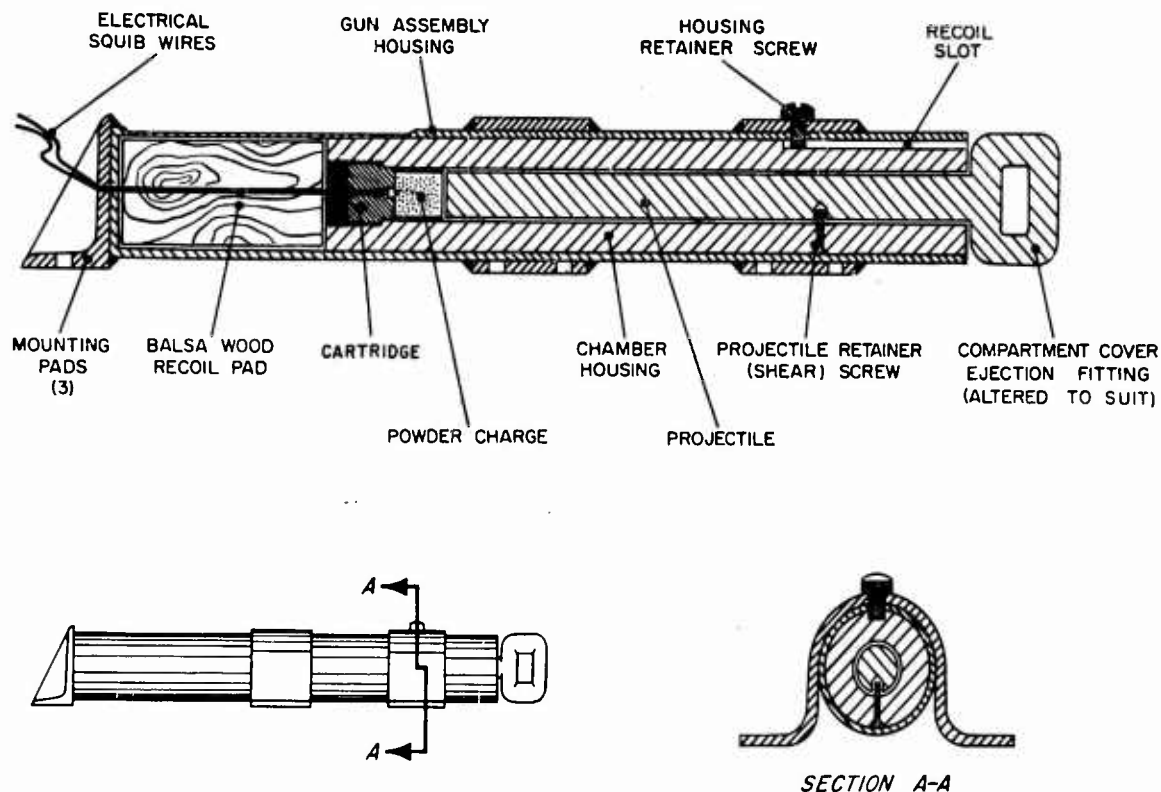


Figure 56. Deployment Gun Details

this program. The pertinent details of a typical pack of this type can be seen in the photograph in Figure 53 showing the deployment system components. The parachute canopy was contained within the pack by means of closure stows, a combination of locking loops and line stows for the suspension lines coming from the closed pack. The rest of the lines and risers were systematically tied to the long flap with break ties. The flap was then folded over the pack and secured with appropriate break cord. This arrangement provided a controlled deployment by paying out the lines as the pack separated from the test vehicle. The closure stow arrangement assures that the suspension lines and risers have been stretched taut before the parachute canopy is released from the pack. For additional assurance that the canopy will also be released properly from the pack, a break line is secured between the vent lines of the parachute and the pack.

This type of deployment pack was used, with appropriate size variations, with all of the parachutes tested in the program. The performance of the pack was very satisfactory in all tests.

Retention of the parachute pack within the test vehicle compartment during periods of high acceleration was accomplished with a unique system consisting of a pinned locking strap arrangement. Figure 57 shows this



Figure 57. Acceleration Lock and Stowage Strap Arrangement

acceleration lock in position on a test parachute pack in the compartment of the LOX-I sled. The locking pin was connected to the riser of the pilot parachute (Figure 52) and required that the pilot parachute develop significant drag force before the pin was pulled and the pack released. No failures were attributed to this system in the 27 tests which were conducted.

B. Release System

In a program of parachute testing, a reliable parachute release system is an important part of the over-all vehicle consideration. Release of the test parachute prior to stopping of the vehicle is required so that proper evaluation of operational damage to the parachute can be made. If release is not initiated before the test vehicle brakes to a halt, the parachute will droop behind the vehicle and become damaged on the track protuberances.

The parachute release system which was used on all of the tests in this program was a half-ring type attachment and severance device designed by Cook Research Laboratories for this particular application. The basic unit consists of three main components; the vehicle attachment, the parachute line attachment, and the half-rings. A typical attachment and severance device of this type is illustrated in Figure 58.

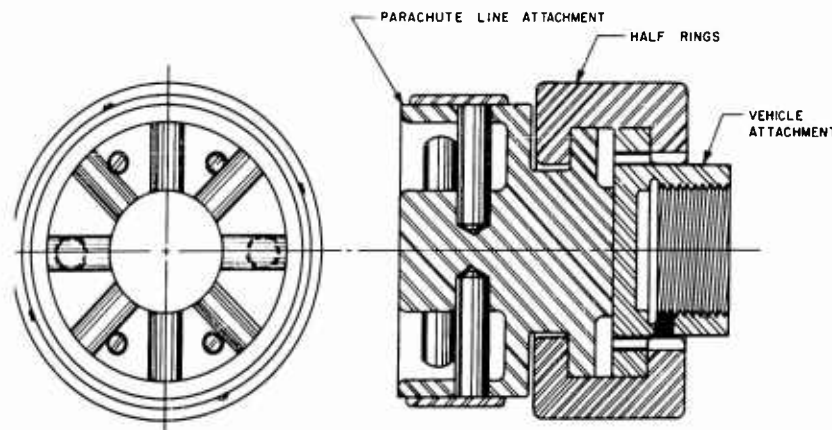


Figure 58. Parachute Attachment and Release Device

The vehicle attachment end is tied into the vehicle structure, through the load recording tensiometer and a flexible link assembly. This part remains with the vehicle after the separation is initiated.

The parachute line attachment end mates with the face of the vehicle attachment and has provision for connecting and securing the parachute line loops. The face of this part is recessed on opposite sides to accept electric blasting cap charges.

The half-rings are installed over the blasting caps and mating attachment ends in such a manner that the assembly is effectively locked together. Small shear screws are also inserted to hold the assembly firmly together until separation is initiated.

Separation is accomplished by energizing the blasting caps. Sufficient force is exerted to shear the screws and blow the half-rings from the assembly. The two attachment ends are then free to separate.

In all of the tests which were conducted on this system of parachute release the separations were initiated within the parachute compartments. No significant damage to the compartment or components within the compartment ever resulted. This also eliminated the danger of the half-rings flying into an occupied area.

Operation of this separation device was consistent, and functional reliability excellent throughout the test program. At no time was a separation failure attributed to a malfunction in this separation system.

C. Deployment and Release System Circuitry

Figure 59 is a block diagram of the circuits used on both the Tomahawk and LOX-I sleds for parachute deployment and release. Figure 60 is a simplified sketch of the knife electrodes and screen box arrangement used to supply the firing impulses.

As will be noted in the block diagram, two separate and independent circuits were employed to deploy the parachute. Squib No. 1 and Squib No. 2 were both imbedded in the powder charge which initiated the deployment sequence. Either squib could explode the charge.

The third firing circuit shown on the diagram was employed for release of the parachute from the sled. This function took place just before the sled came to rest after a test run. It was done to avoid dragging the parachutes behind the sled as it slowed down.

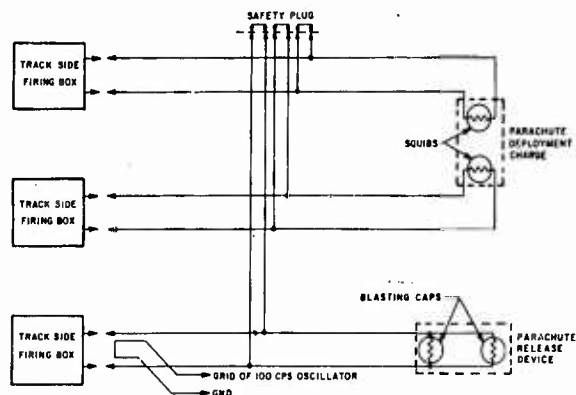


Figure 59. Schematic Diagram -
Deployment and Release
System

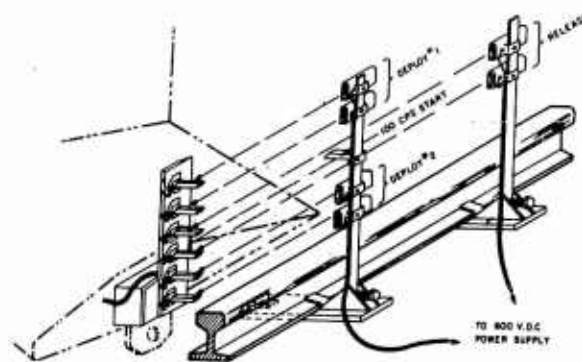


Figure 60. Pictorial Sketch of Knife
Electrodes and Screen
Box Arrangements

Only one firing circuit was employed for this function. Two firing devices (blasting caps) were used, however, and either could trigger the release.

Knife electrodes mounted on the sled, as shown in Figure 61, were used to pick up firing voltage from track side firing boxes. The arrangement was that high voltage from a condenser power supply was applied to screen boxes, as shown in Figure 62. As the sled moved along the track, the electrodes

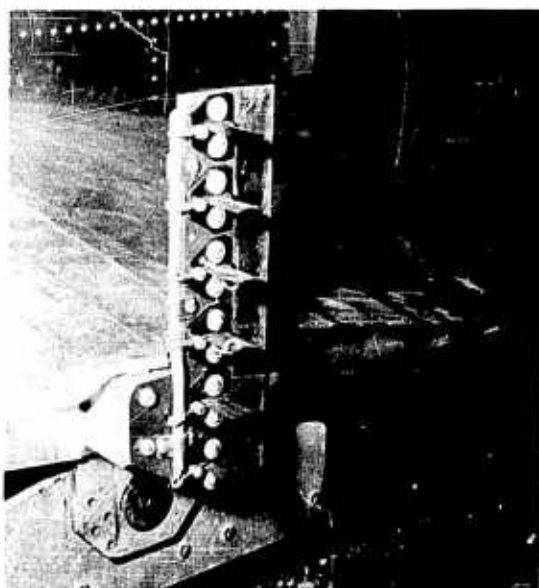


Figure 61. Knife Electrodes Mounted
on Tomahawk Sled

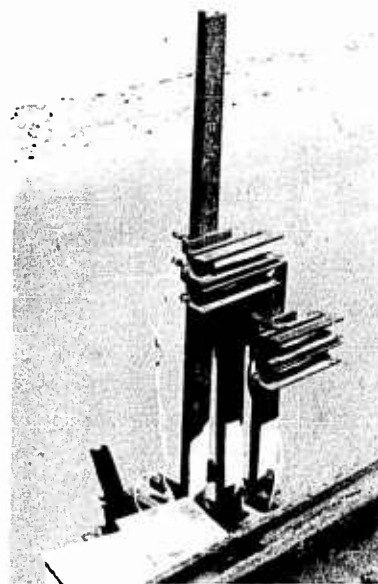


Figure 62. Screen Boxes
Attached to
Track

knifed through the screen thereby applying firing voltage to the squibs. The screen boxes were positioned along the track at locations at which the particular events were to occur.

It will also be noted that a safety-plug which short circuited all explosive devices was provided. This plug was kept in place throughout all pre-launch preparation of the sled to insure the safety of operating personnel.

APPENDIX II

TEST VEHICLES

Two parachute test vehicles were used to conduct the 27 test runs from which the data in this report were gathered.

The first 17 tests were conducted with the Tomahawk sled, a solid fuel rocket powered test vehicle designed for operation as either a single stage vehicle, or with a suitable pusher sled as a double stage vehicle. Carrying up to eight 2.2 KS-11,000 rockets, the sled was capable of developing a total of approximately 90,000 pounds of thrust for a duration of 2.2 seconds. In this configuration, the initial weight of 5,050 pounds could be accelerated to approximately Mach 1.2 at rocket engine burnout. Burnout weight was approximately 3,900 pounds. Empty weight was 2,985 pounds. With the addition of the X-15 first stage pusher vehicle containing 14 of the 2.2 KS-11,000 rocket motors, a test velocity of approximately Mach 1.60 was attained in two stage operation. All of the supersonic tests conducted on this program were made with the Tomahawk test vehicle, X-15 pusher sled combination.

Table XXIX lists the vehicles, propulsion units, and Mach numbers attained on each test conducted with these vehicles during the program.

Figure 63 shows two views of the sled and pusher on the track prior to a supersonic test. A three-view drawing giving basic over-all dimensions of the Tomahawk test vehicle is shown in Figure 64.

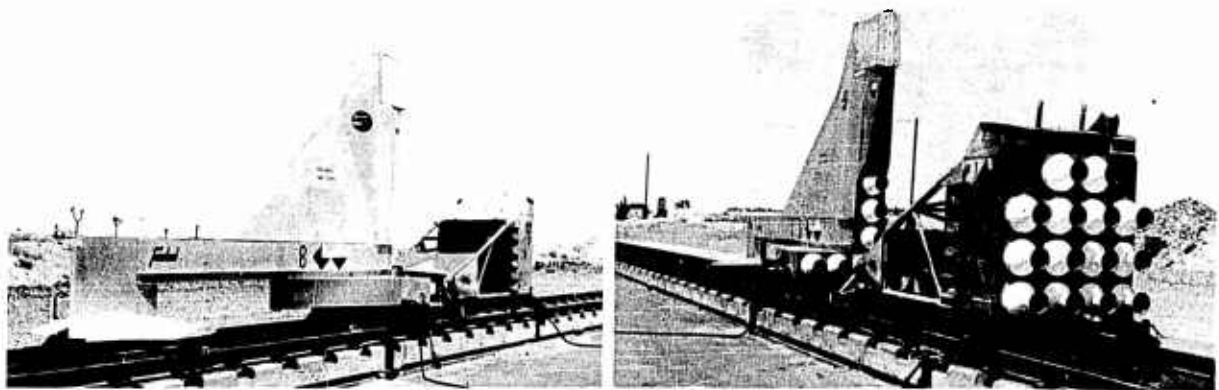


Figure 63. Tomahawk Parachute Test Vehicle with X-15 Pusher Sled

The slippers on which the sled traveled were specially designed and fabricated by Cook Research Laboratories to adapt the test vehicle to the new 171 pound rail at the Free Air Test Facility at Edwards Air Force Base.

TABLE XXIX

TEST VEHICLES, PROPULSION AND PERFORMANCE

Test No.	Test Vehicle	No. of Rockets	Pusher Vehicle	No. of Rockets	Burnout Mach No.
1	Tomahawk	8	X-15	10	1.39
2	↓	7	-	-	1.01
3	↓	8	-	-	0.96
4	↓	8	-	-	1.08
5	↓	8	-	-	1.08
6	↓	8	X-15	15	1.39
7	↓	6	-	-	0.90
8	↓	8	X-15	14	1.51
9	↓	8	X-15	14	1.47
10	↓	8	-	-	1.08
11	↓	8	X-15	14	1.55
12	↓	8	-	-	1.06
13	↓	8	X-15	14	1.34
14	↓	8	X-15	14	1.54
15	↓	8	X-15	14	1.55
16	↓	8	-	-	1.06
17	Tomahawk	8	X-15	14	1.59
18	LOX-I	Liquid Rocket Engine 50,000 lb Thrust/4.5 sec No Pusher Used			1.01
19	↓				1.00
20	↓				1.07
21	↓				1.08
22	↓	↓			1.05
23	↓				1.06
24	↓				1.04
25	↓				1.09
26	↓	"			0.80
27	LOX-I				0.81

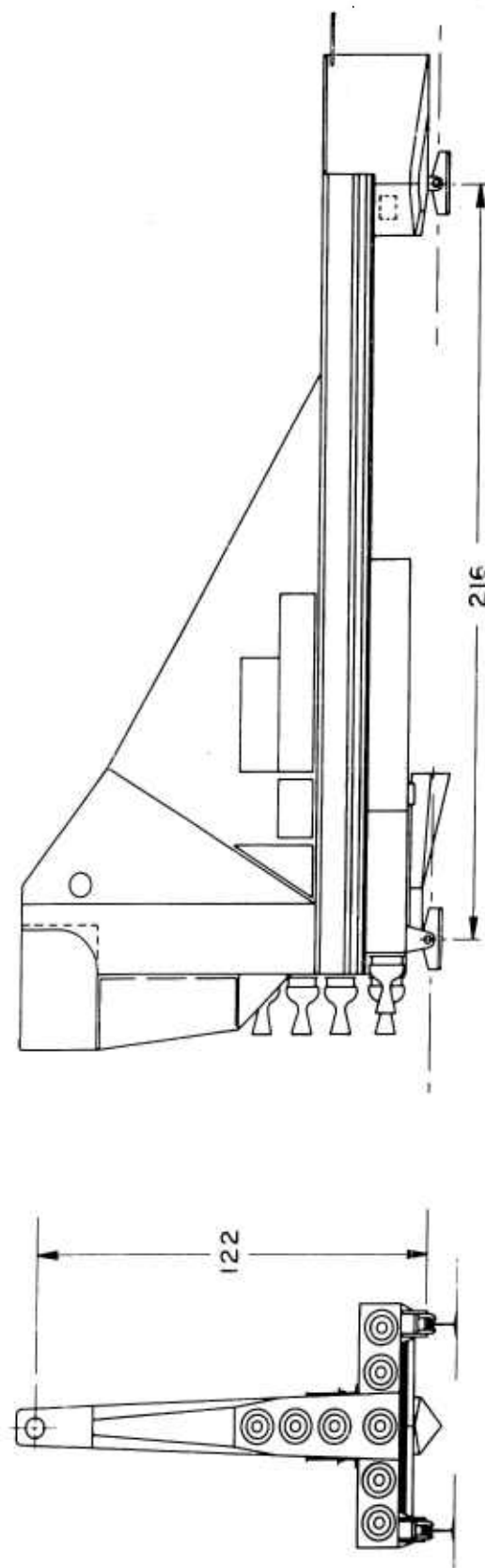


Figure 64. Basic Dimensions (3 view) of Tomahawk Parachute Test Vehicle

Dimensions and tolerances were such that standard Edwards Air Force Base stainless steel inserts could be used with the slippers.

Deceleration at the end of a test was accomplished by a water brake system consisting of a horizontal momentum exchange brake on the test vehicle and a water trough installed between the rails on the last 4,000 feet of track. The water brake, designated as Type HME-3 brake by the Air Force Test Test Facility and used there as standard equipment for many years was originally developed by Cook Research Laboratories for rocket sled application in connection with Contract AF 33(038)-10653, an earlier parachute study program at lower test velocities (Reference 2).

In the braking area, the track rails slope two inches per 1,000 feet of length. As the sled entered this portion of the track, the water brake, mounted on the aft underside of the vehicle, scooped up the water and directed it - through ducting in the brake - to discharge ports on both sides of the vehicle where it was discharged in a relative forward velocity. The energy thus imparted to the water provided a braking force as a reaction on the test vehicle.

The drag area of the Tomahawk test vehicle was approximately nine square feet in the subsonic region and 20 square feet in the supersonic region.

Magnetic tape recording instrumentation and high speed motion picture cameras were carried in the test vehicle to obtain permanent performance data on the parachutes being tested. A complete description of the sled borne and associated instrumentation used in the test program is presented in Appendix III.

The Tomahawk parachute test vehicle was designed and fabricated by Cook Research Laboratories for the Parachute Branch, Aeronautical Accessories Laboratory, Wright Air Development Division, Wright-Patterson Air Force Base, under Contract AF 33(616)-3409.

On test No. 17, at a velocity of approximately Mach 1.6, a small bird impacted with the front fairing of the test vehicle. This caused the fairing to rupture and sever immediately from the test vehicle. A portion of the top cap of the main beam was also torn off and significant damage to the vertical fin structure resulted from impact with the debris as it was torn from the front of the vehicle. Figure 65 shows the damage to the test vehicle which resulted from this incident.

Evaluation of the damage indicated that a major repair effort would be required to get the vehicle back to operational shape. Initial estimates of the time required to accomplish the repair job suggested that another vehicle be used in the interim. As it turned out, the test program was concluded before

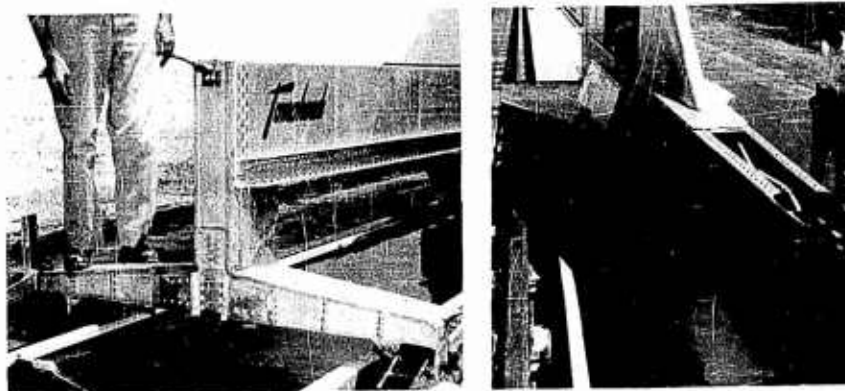


Figure 65. Damage to Tomahawk Sled - Test No. 17

the Tomahawk vehicle was returned to service.

After the damage to the Tomahawk test vehicle, preparations were made to continue the program with the LOX-I sled, a liquid propellant rocket powered parachute test vehicle. This sled, used on tests 18 through 27 in the current program had been designed and developed by Cook Research Laboratories for a series of transonic tests conducted under Contract No. AF 33(038)-10653 and had been retained at the Air Force Test Facility at Edwards Air Force Base for use on other programs.

The LOX-I sled was powered by a gas pressurized alcohol-liquid oxygen rocket engine. Maximum design capability of the engine and propellant system was a thrust of 50,000 pounds for a duration of 4.5 seconds. With a gross firing weight of approximately 5,000 pounds the maximum test velocity which could be attained was between Mach 1.10 and 1.20.

Figure 66 shows the LOX-I test vehicle as it was used on this program. A three-view drawing giving basic vehicle dimensions is illustrated in Figure 67.

The slippers which were used on the LOX-I sled were of standard Edwards Air Force Base configuration with multiple stainless steel inserts as the wearing surfaces. The water brake and braking method were identical to that used on the Tomahawk sled. Instrumentation from the Tomahawk sled was retrofitted to the LOX-I sled where it was operated to the end of the program.



Figure 66. LOX-I Parachute Test Vehicle

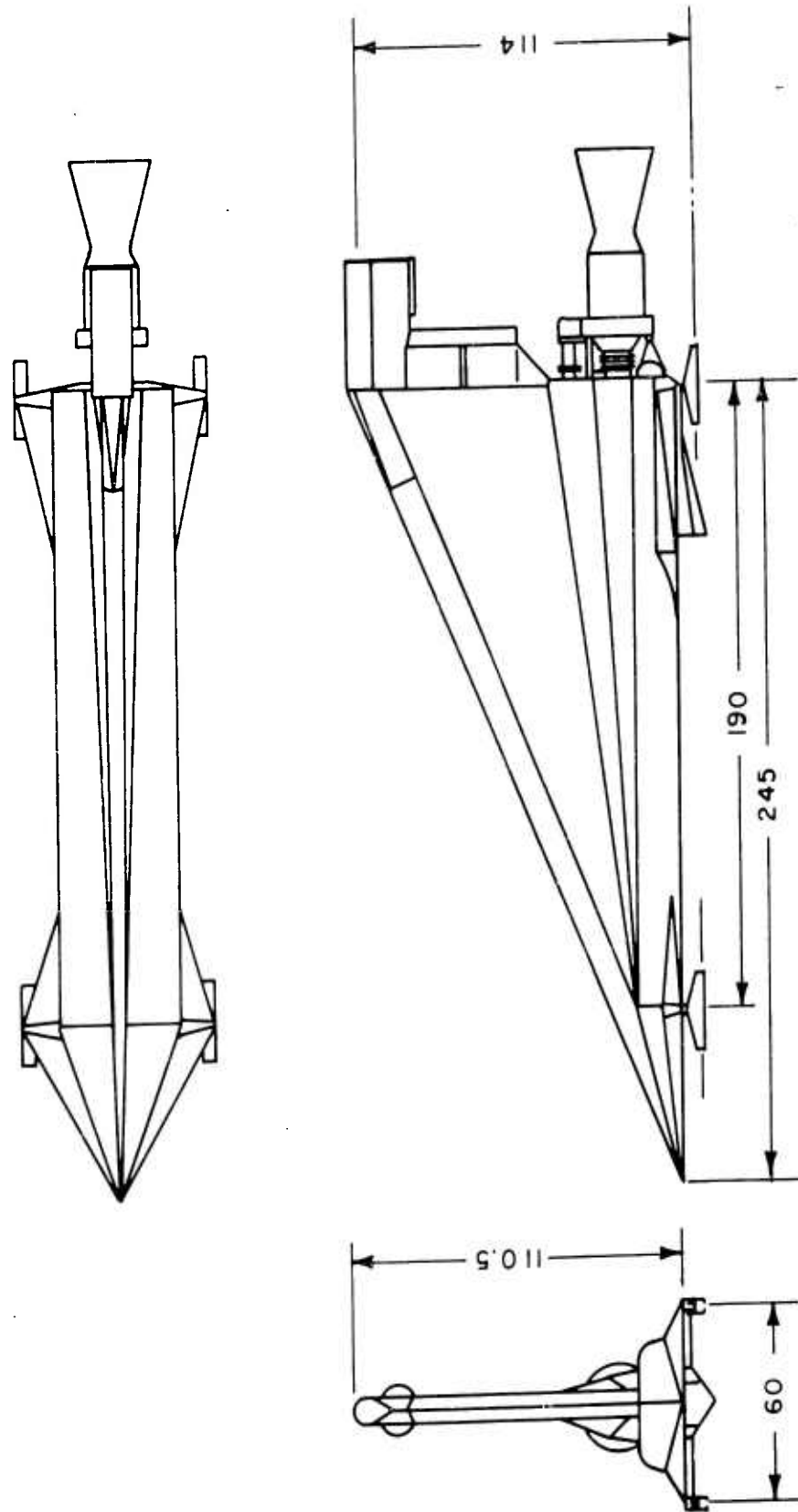


Figure 67. Basic Dimensions (3 view) of LOX-1 Parachute Test Vehicle

APPENDIX III

INSTRUMENTATION

A. Recording System

A Cook Research Laboratories six channel magnetic tape recording system and two high speed motion picture cameras comprise the instrumentation system employed on this program. Drag force measurements on the parachute and test vehicle performance information were obtained by the tape recording system. Opening characteristics and stability of the parachute were recorded by the cameras. Time correlation between tape and film was provided by recording, on both tape and film, time pulses from a common time base oscillator and track position pulses which were generated as the test vehicle passed over fixed marker stations along the track.

The instrumentation equipment was initially installed in the Tomahawk sled. When this test vehicle was damaged in test No. 17, it was transferred to the LOX-I sled and employed there for the remainder of the program.

A block diagram of the instrumentation system is shown in Figure 68. As may be seen, an eight track tape recorder (CRL model MR-31-A) was employed to record the six data channels plus two reference channels. The reference channels (two for increased reliability) placed a stable 10 kilocycle frequency on the tape which was used to control the speed of the playback tape transport during the playback process and also to compensate the data channels for errors due to tape speed irregularities.

Snatch and drag forces exerted by the parachutes were measured by a tensiometer device which formed part of the linkage by which the parachutes were attached to the test vehicle. Conventional strain gages connected in bridge configuration were employed as the sensing element in the tensiometer. Two such bridges were employed in each unit.

Linear acceleration of the test vehicle was measured by a Statham type A5A accelerometer. Impact pressure on the test vehicle was measured by a Statham type P-96 pressure transducer. Both these instruments employ resistive strain-bridge sensing elements.

A four kilocycle carrier voltage, derived from a governed motor alternator device, was employed as excitation for all strain gage instruments. Physical input to the instruments produced suppressed carrier type modulation of the four kilocycle carrier. In the signal converters this signal was rectified and filtered and the resulting dc signal used to control the frequency of an oscillator. Thus, an FM signal which was recorded on the magnetic tape was produced.

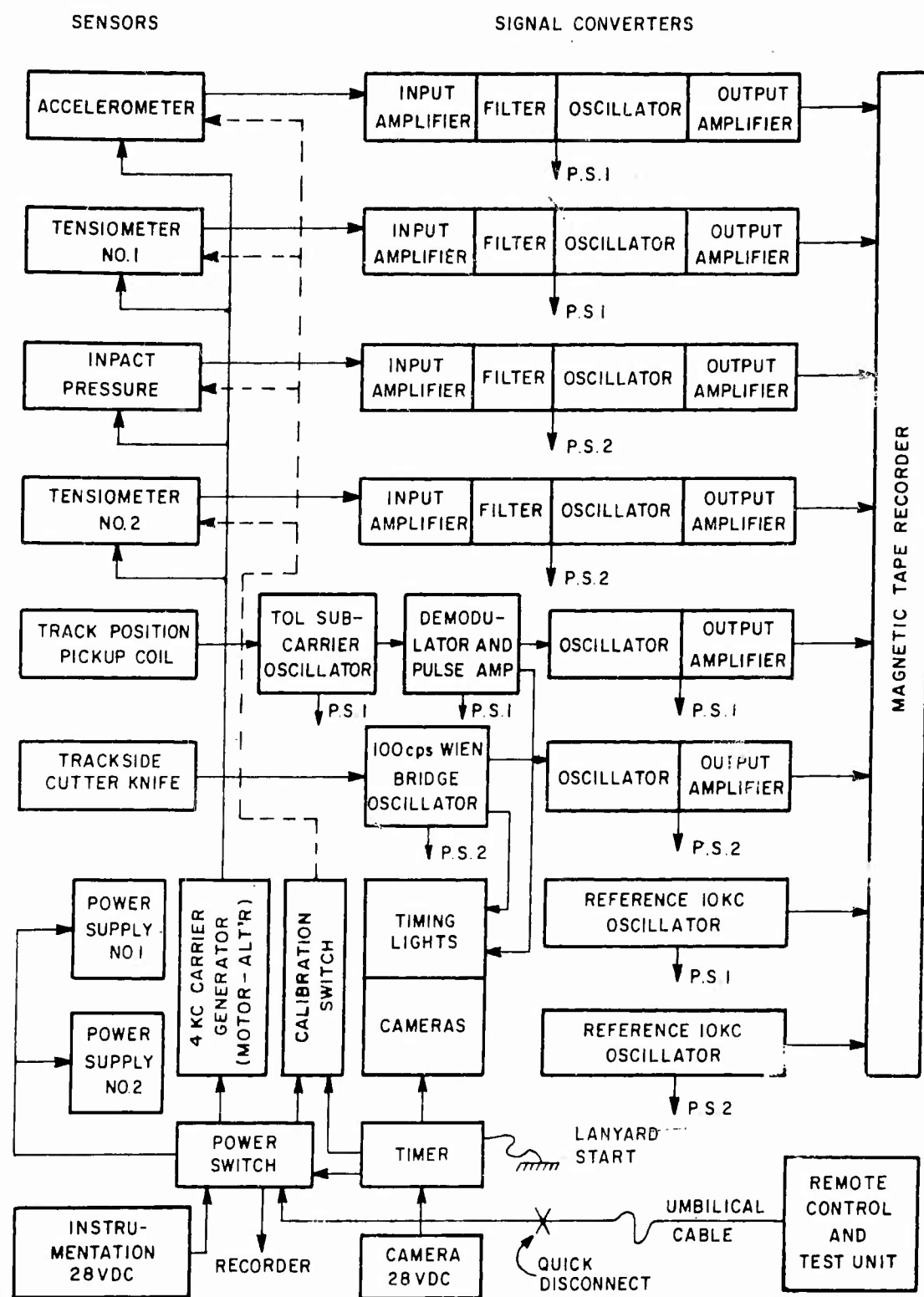


Figure 68. Block Diagram of Instrumentation System

The signal converters operated at a frequency of 12 kilocycles for no signal input and varied to approximately 16 kilocycles at full scale. Flat response to data frequencies from 0 to about 750 cycles per second was provided.

Space-time history on each sled run was obtained by both the Experimental Track Branch and the onboard recording system. It is standard procedure at Edwards Air Force Base to provide this information on all sled runs. The system employed consists of permanently located pickup coil boxes, spaced at 60 foot intervals along the track, which are connected by land lines to a central recording unit. A permanent magnet is mounted on the test vehicle (Figure 69) such that it passes near these boxes as the sled

travels down the track. Impulses generated as the magnet passes the pickup coils are recorded against an accurate time base at the central station, thereby providing the desired space-time history for the run.

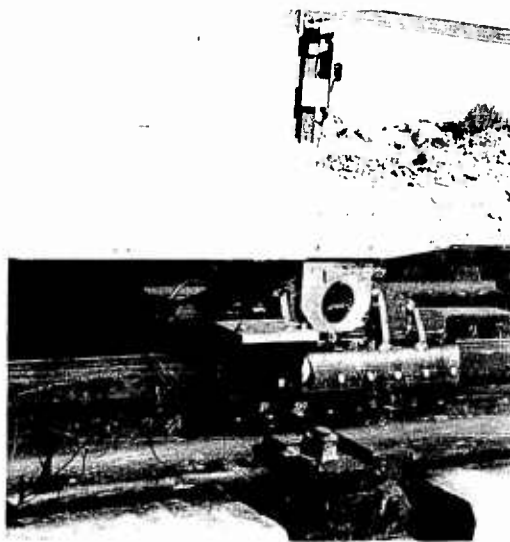


Figure 69. Sled Mounted Space-Time Magnet

The onboard system worked in a similar manner. Impulses, generated as the sled passed the coil boxes, were recorded on the magnetic tape and, in this case, also on the motion picture cameras. The principle of operation was slightly different, however. Since no magnet which might generate a signal in a sled mounted pickup coil existed in the coil boxes, some other means of generating the impulse was required. The system which was employed utilized a conventional inductance-controlled subcarrier oscillator (Bendix TOL), the inductance coil

for which was positioned on the sled such that it passed near the track side coil boxes (Figure 70). An appreciable effect on both the frequency and the amplitude of the TOL output was obtained. A simple diode detector was therefore employed to recover the amplitude modulated pulses from the output of the TOL. These pulses were then fed to the oscillator of a signal converter and the output recorded on the tape in the same manner as the other channels. Simultaneously the pulses were fed to the timing lights circuits for the motion picture cameras. Space-time correlation between tape and film was thereby provided. Special marker stations were included with the regular coil boxes at several points along the track. The marker pulse received from these boxes provided additional correlation of track position stations.

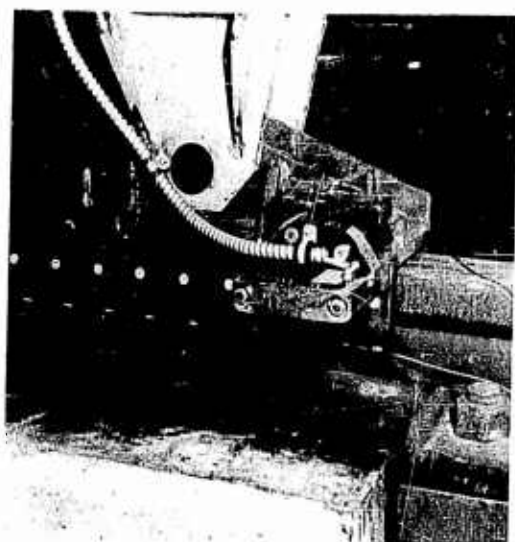


Figure 70. Sled Mounted Space-Time Inductance Coil

The time base against which the track position pulses were recorded in the sled system was obtained from a 100 cycle per second Wien-bridge oscillator. Pulses derived from this source were fed simultaneously to the recorder and to the camera timing lights.

The start of these timing pulses was made to coincide with the time of parachute deployment to positively fix the time of this event on the tape and film. This was accomplished by grounding the 100 cycle per second oscillator through a wire which was cut by a knife mounted with the deployment firing box at track side.

A timer was employed in the instrumentation system to control camera operation and to perform automatic post run calibration and power shutdown. This timer was started by a lanyard-operated switch as the sled was fired. The lower speed camera was started immediately and covered the entire test run. The high speed camera start had to be delayed in order to cover the period of parachute operation within available film time. The post run calibration was performed as a check on instrumentation performance, and power shutdown was performed to conserve power and to decrease chances of damaging the tape or film by permitting the recorder and cameras to continue running.

As will be noted in the block diagram, two independent power supplies were employed in this system. Division of the recorder channels between the two enhanced reliability.

Sealed nickel-cadmium type batteries were employed as the primary 28 volt dc power source for the system. This type battery was also used in the camera power pack.

Remote control and prefiring checkout of the system from the blockhouse was provided by a special test unit. An umbilical cable was attached to the test vehicle through a lanyard-actuated quick-disconnect connector which released upon firing of the sled. In practice, the instrumentation was turned on sufficiently ahead of firing time to provide adequate warmup. Just before firing a quick check of the operation of all channels was made. Immediately before firing the tape recorder was turned on and a calibration placed on the tape. The recorder then continued to run until shut down by the timer at the end of the run.

In addition to the sled mounted motion picture cameras, a number of track side motion picture, sequence, and still cameras were employed on each test. On a typical test this included several individually panned cameras loaded with color film and operating at a frame speed of 128 frames per second. These were located on the camera road approximately 400 feet from the track. A series of stationary high speed motion picture cameras loaded with black and white film and operating at a frame speed of approximately 1,000 frames per second was located alongside the track and oriented nearly parallel to the track to cover deployment and inflation sequences from stationary sources. A hand operated sequence camera was used to obtain still photography of the parachute deployment. Other still photography as deemed necessary was provided before and after each test.

B. Playback System

The equipment upon which the tapes from the test runs were played back was the DI-5 Playback Equipment developed by Cook Research Laboratories. This system is illustrated by block diagram in Figure 71.

Three data channels could be played back simultaneously, with a reference channel providing speed control of the drive mechanism and electronic compensation of the data channels. Also, the 10 kilocycle reference frequency was divided down into 100 cycle per second timing pulses which controlled the timing mark lights in the oscillograph.

The DI-5 was of conventional design. The data frequencies taken off the tape were preamplified, then demodulated and filtered to obtain a varying dc signal from the frequency modulated signal. This signal was then amplified and fed to a galvanometer of the recording oscillograph.

The reference channel was identical to the data channels with the exception that its output signal was inverted in phase and added to the outputs of the data channels. Thus, any error signal common to both data and reference channels, such as would result from recorder tape speed variations, was eliminated.

On typical playback of a test record, each of the data channels was played back against the track position channel and the 100 cycle per second timing channel. Space-time information was therefore displayed simultaneously with each data trace.

C. Sled Borne Camera Calibration

The two motion picture cameras were calibrated as follows. A graduated cross pole was positioned behind the sled at a distance corresponding to the

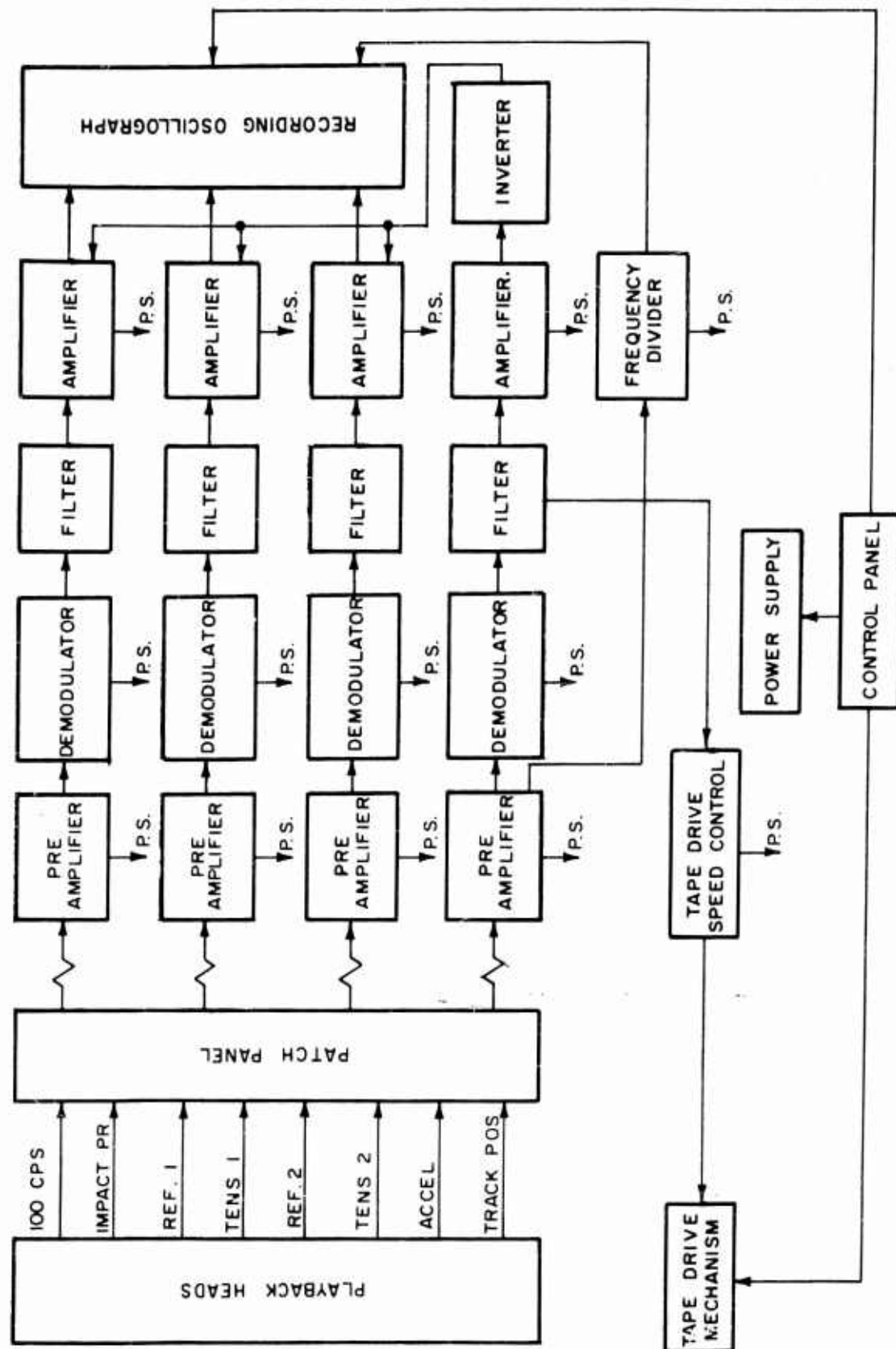


Figure 71. Block Diagram of Playback System

length of the parachute suspension system, and centered on its axis. The cameras were aimed such that the cross-pole was centered in the field of view. A calibration film was then made for each camera. The graduations on the pole permitted calibration of the viewing screen of any projector system which might be used for data reduction. Stability and opening characteristics of test parachutes could therefore be precisely described.

REFERENCES

1. United States Air Force Parachute Handbook, WADC Technical Report 55-265, December 1956
2. Cook Research Laboratories, Recovery Systems for Missiles and Target Aircraft, Air Force Technical Report 5853, Vols. I, II, and III
3. Cook Research Laboratories, Interim Progress Report PR 146-1 through PR 146-14
4. Military Specification, Parachute, FIST Ribbon, General Specification for Construction of, MIL-P-6635A (ASG)

Applicable reports and specifications not referenced by number.

Knacke, T., Design, Use and Construction of FIST Type Parachute, AMC, Engineering Division, Report No. MCREXE-672-19LL, Wright-Patterson Air Force Base, Ohio, June 1948

Heinrich, Dr. H. G., Guide Surface Parachutes, AMC, Engineering Division, Report No. MCREXE-672-25F, Wright-Patterson Air Force Base, Ohio, February 1948

MIL-W-4088B (USAF)	Webbing, Textile, Woven, Nylon
MIL-W-5625	Webbing, Nylon Tubular
MIL-R-5608B	Ribbon, Nylon, Parachute
MIL-C-8021A	Cloth, Nylon, Drag Parachute
MIL-T-5038	Tape, Nylon, Reinforcing
MIL-T-8363 (USAF)	Tape, Textile, Woven, Nylon
MIL-C-7215 (USAF)	Cord, Nylon, Coreless
MIL-T-7807	Thread, Nylon